Master's Degree Thesis
ISRN: BTH-AMT-EX--2013/D-02--SE

Statistical Assessment of Uncertainties Pertaining to Uniaxial Vibration Testing and Required Test Margin for Fatigue Life

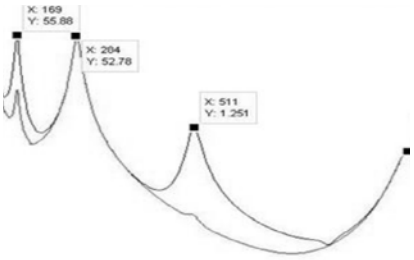

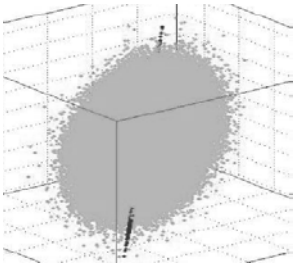

Davood Dehgan Banadaki[1]

Sunay Sami Durmush[1]

Sharif Zahiri[2]

1-Department of Mechanical Engineering
2-Department of Mathematics and Science
Blekinge Institute of Technology
Karlskrona, Sweden

Supervisors: Martin Olofsson and Tatiana Smirnova, Volvo Trucks AB
Ansel Berghuvud and Claes Jogréus, BTH

Statistical Assessment of Uncertainties Pertaining to Uniaxial Vibration Testing and Required Test Margin for Fatigue Life Verification

Davood Dehgan Banadaki[1]

Sunay Sami Durmush[1]

Sharif Zahiri[2]

1-Department of Mechanical Engineering

2-Department of Mathematics and Science

Blekinge Institute of Technology

Karlskrona, Sweden

2013

Thesis submitted for completion of

Master of Science in Mechanical Engineering with emphasis on Structural Mechanics at the Department of Mechanical Engineering,

Master of Science in Mathematical Modeling and Simulation at the Department of Mathematics and Science,

Blekinge Institute of Technology, Karlskrona, Sweden.

Abstract:

In the automotive industry uniaxial vibration testing is a common method used to predict the lifetime of components. In reality truck components work under multiaxial loads meaning that the excitation is multiaxial. A common method to account for the multiaxial effect is to apply a safety margin to the uniaxial test results. The aim of this work is to find a safety margin between the uniaxial and multiaxial testing by means of virtual vibration testing and statistical methods. Additionally to the safety margin the effect of the fixture's stiffness on the resulting stress in components has been also investigated.

Keywords:

Vibration Testing, FEA, Natural Frequency, Deterministic and Random Vibrations, Fatigue.

Acknowledgements

This thesis work has been carried out in co-ordination between Blekinge Institute of Technology, Karlskrona and Volvo Trucks, Gothenburg.

We wish to express our sincere appreciation and gratitude to our supervisors Tech. Lic. Martin Olofsson and Dr. Tatiana Smirnova at Volvo Trucks and Dr. Ansel Berghuvud and Dr. Claes Jogréus at Blekinge Institute of Technology for their professional guidance.

We also want to thank to M.Sc. Fredrik Öijer , M.Sc. Andreas Emilsson and M.Sc. Johan Gustafsson from Volvo Trucks for their valuable suggestions.

Gothenburg, March 2013

Davood Dehgan Banadaki

Sunay Sami Durmush

Sharif Zahiri

Table of Contents

1 NOTATION

E	Young's modulus
df	Frequency Resolution
f	Frequency
G	Power Spectral Density
Gvm	PSD Estimate of the Equivalent von Mises Stress
$H(\sigma)$	Frequency Response Function of Stress Component
H	Frequency Response Function
K	Safety margin quotient
S_{xr}	Real part of FRF of Stress Component
S_{xi}	Imaginary part of FRF of Stress Component
θ	Angle
$\Delta\varphi$	Phase difference
ν	Poison's ratio
ξ	Damping
ρ	Density
σvm	von Mises Stress
σ	Normal Stress Component
τ	Shear Stress Component

Abbreviations:

E.V.S	Equivalent von Mises Stress
FEA	Finite Element Analysis
FRA	Frequency Response Analysis
FRF	Frequency Response Function
M.P.S	Maximum Principal Stress
PSD	Power Spectral Density
CPSD	Cross Power Spectral Density
RMS	Root Mean Square

2 INTRODUCTION

The importance of durability of products used in the automotive industry has been increased rapidly during the recent years. The main goal is that a product should survive enough time under working conditions, the so called durability life. In order to foresee a lifetime for a product damaging factors should be known. A common damaging factor is fatigue. Fatigue is present when a component is loaded with cycling loads and vibrations. Most of the cracks seen in components are the result of fatigue damage. Fatigue causes initiation and propagation of a crack on the outer surface of components under cycling loading. This means that product life highly depends on fatigue damage. Being aware of this, product developers try to estimate a lifetime for their products. In order to achieve this, physical testing is a common way. An arising question here is that in what extend physical testing represents the real case. A physical testing has its own shortages. For instance the most widely used vibration tests in the automotive industry are uniaxial tests in which the component under testing is excited only in one direction at a time. Vibration types used are sinusoidal, with *Sweeping Frequency*, or *Stationary Random* [1]. In real case components are usually excited multiaxially and most of the time the loads will be non-stationary random or mixture of periodic and random. Taking into account these shortages, during a uniaxial test most of the time over testing of components is necessary.

The goal of this thesis work is to investigate what kinds of uncertainties are present in uniaxial testing and to find a safety margin between uniaxial loading case and multiaxial loading case. For this purpose virtual testing has been used as a main tool. Swept sinusoidal and random testing has been simulated in computer environment using different components mounted to a truck.

Comparison has been made based on the resulting stress. Random excitation causes rotation of the principal stresses therefore it is not straight forward to quantify the resulting stress using traditional measures like maximum principal stress present on the component. For this reason The

Equivalent von Mises stress suggested by Pitoiset and Preumont [2] has been used to quantify the resulting stress from random testing in the frequency domain. Since there is no rotation of principal stresses, in swept sinusoidal excitation the resulting stress can be quantified easily by using the well known von Mises formula [2].

In both testing cases excitations are applied uniaxially in three orthogonal directions sequentially and multiaxially and the resulting stress values are compared. In multiaxial *swept sinusoidal* test different phase combinations of the input signals has been considered and the results are compared. In multiaxial *random* case two different scenarios have been investigated, first when all excitation signals are independent uncorrelated signals and second when signals are correlated with known correlation coefficient. One investigation in the correlated case is to find the dominant direction by evaluating the combination of any 3-dimensional description of measured vibration. It has been shown that the obtained dominant direction gives closer results to the multiaxial case in some cases.

It will be good to mention that the literature written on the optimum test directions for vibration testing is rare. One such investigation has been done by Moon et al. [3].

Another investigation included in the work is the effect of the fixture stiffness on the stress occurred in the component under testing. In this part components attached to fixtures with different stiffness values have been analyzed.

Introduction to Vibration Testing

Vibration testing is a common tool used to predict the lifetime of components used in the truck manufacturing and automotive industry. Vibration testing can be defined as exciting components in certain directions by means of a shaking device such as shaker table. A successful vibration test should help to predict with high probability a lifetime for a product. Figure 2.1 shows simple vibration test equipment.

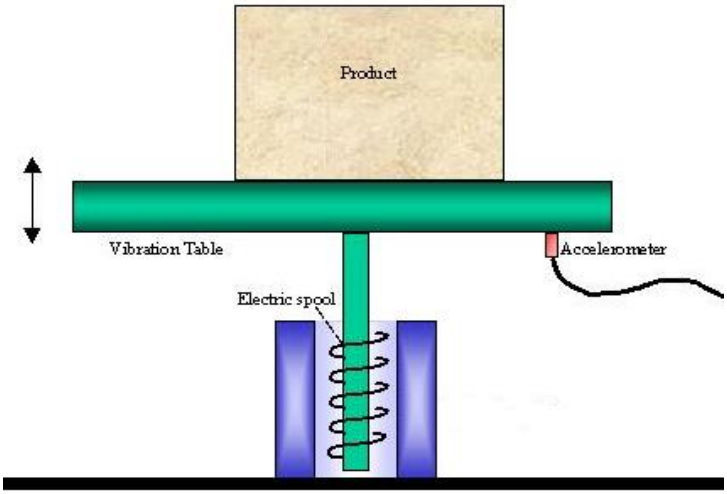

Figure 2.1 *Vibration test equipment.*[1]

As it is shown in Figure 2.1 main parts of vibration test equipment are the power unit and the shaker table.

The most widely used vibration test in the automotive industry is uniaxial in nature. This means that the component under testing is excited only in one direction at a time. The vibration types used are swept sinusoidal and stationary random. However in real case truck components are excited most of the time by multiaxial non-stationary random and periodic vibrations. This means that uniaxial testing does not fully represent the real case. In order to fill this gap most of the time components are over tested or testing is performed using higher excitation levels. As a result resource usage is increasing as well as the testing time. If the most damaging uniaxial direction is known it is possible to get closer results to the real case by exciting the component in this specific direction.

[1] Reference for the figure, http://www.opti-pack.org/10700,4

2.1 Scope

The conclusion that one would like to make from a successful vibration test is that the component will endure a truck lifetime, with a certain, high probability. Currently, primarily because of the uncertainty about multiaxial excitation effect, almost all vibration tests are performed with exaggerated vibration levels. Otherwise the mentioned probability of making the correct conclusion will be too low. For this reason a safety margin is required to fill the gap between uniaxial testing and multiaxial excitation effects which is the case in reality. The safety margin can be obtained by simulating vibration testing using finite element analysis. The ratio between the quantified stress obtained from uniaxial testing and multiaxial testing will give the safety margin.

Safety Margin = Stress present in multiaxial testing/Stress present in uniaxial testing

The obtained safety margin helps to determine how successful a uniaxial test is. Smaller safety margin means that uniaxial testing gives closer results to multiaxial testing or in other words it represents better the real working conditions. It has been seen that the safety margin depends on the direction of excitation in uniaxial testing. For this reason most of the time one need to optimize the test directions but this is not possible without looking at the structure itself. This means that the structure and the direction to which it is sensitive to should be investigated. This investigation can be done by simulating vibration testing in computer environment as it has been done in the present work.

3 ANALYSIS METHODS

3.1 Swept Sinusoidal Excitations

This testing type consists of exciting the test component by sinusoidal signals with sweeping frequency. Figure 3.1 shows a swept sine signal in the time domain.

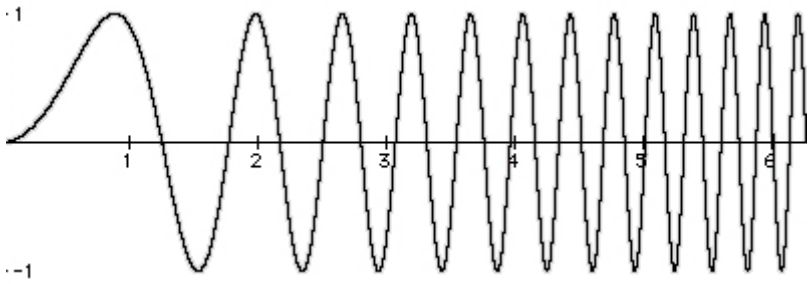

Figure 3.1 *Swept sinusoidal acceleration signal in the time domain.*

Figure 3.2 shows resulting stress on a component due to swept sine input in the frequency domain.

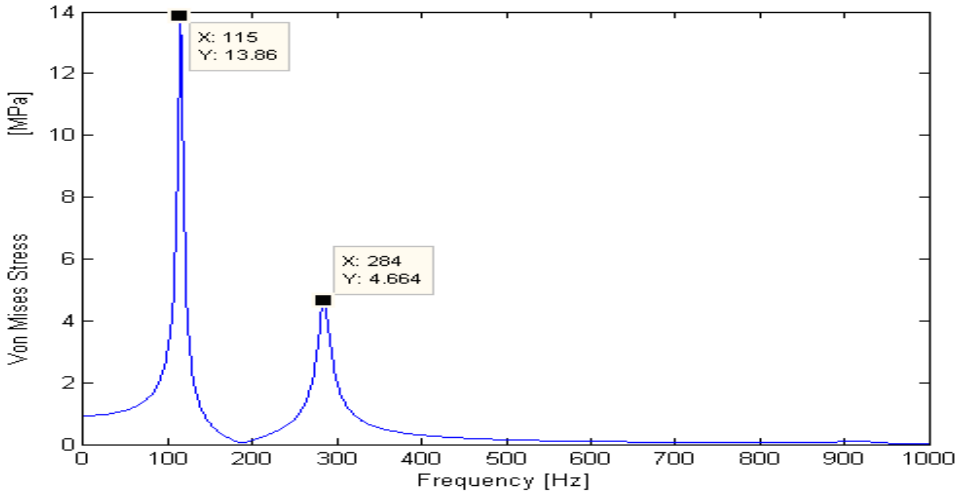

Figure 3.2 *The von Mises stress in the frequency domain.*

In the present work swept sine test has been simulated in computer environment using finite element analysis. Frequency domain analysis has been used. In order to quantify the resulting stress, the maximum peak value at the turning point of vibrations as it is shown in Figure 3.2 has been considered.

Vibration tests can be simulated in the computer environment using finite element analysis. Analysis can be performed both in the frequency and in the time domain [4]. In the present work Nastran has been used as FEA solver and part of the calculations has been done in Matlab. The general steps when performing vibration simulation in Nastran and Matlab using the frequency domain are given below.

For swept sinusoidal test the following routine has been used,

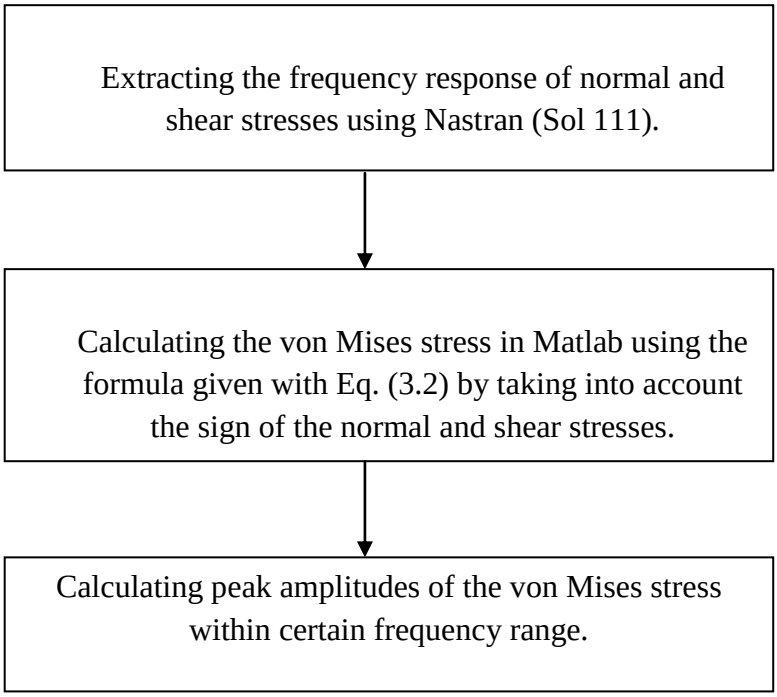

Since fatigue damage often is present on the component's outer surface the stress state on the surface has been considered. This means that two

normal and one shear stress have been used when calculating the von Mises stress. Biaxial stress components have been shown in Figure 3.3.

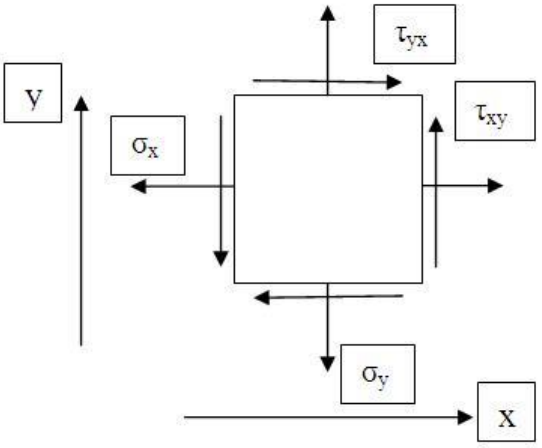

Figure 3.3 *Biaxial stress components.*

The two dimensional stress tensor containing the biaxial stress components is given below,

$$\sigma = \begin{bmatrix} \sigma x & \tau xy \\ \tau xy & \sigma y \end{bmatrix} \tag{3.1}$$

The following formula has been used to calculate the von Mises stress for swept sinusoidal input and for biaxial stress state,

$$\sigma_{vm}^2(f) = \sigma_x{}^2(f) + \sigma_y{}^2(f) - \sigma_x(f) \times \sigma_y(f) + 3 \times \tau_{xy}{}^2(f) \tag{3.2}$$

Where,

$\sigma_{vm}(f)$, is the von Mises stress at frequency *f*.

$\sigma_x(f), \sigma_y(f)$ *and* $\tau_{xy}(f)$ are the normal and shear stresses at frequency *f*.

When calculating the von Mises stress using Eq. (3.2) the sign of the normal and shear stresses should be taken into account. The sign can be extracted considering the phase relationship between biaxial stress tensor components at the turning points of vibration i.e. at the resonance peaks.

In swept sinusoidal testing we call FRF’s scaled since the input sinusoidal acceleration signal has peak amplitude of 1g=9810 mm/s^2.

3.2 Random Excitations

Regardless of the type of excitation and that if it is uniaxial random or multiaxial random, the stress response of components can be either uniaxial or multiaxial. The multiaxial nature of the stress state makes it difficult to quantify the stress level. In order to quantify the stress, it is required to use a proper scalar. Several methods have been studied in this work to quantify the stress.

One alternative method that may be suggested is to use the PSD estimate of the maximum principal stress. This alternative is based on the iterative procedure to project the stress state on a surface to transform the stress in different directions. Then, based on the maximum RMS value, the 'overall maximum principal' stress is chosen. However, principal stress in different modes of vibration may have different directions. When this is the case, the stress state is multiaxial non-proportional [5]. The main cause, for multiaxial, non-proportional stress response is when vibrations in different eigenmodes interact in a hot-spot stress and the corresponding modal stresses happen to have different principal stress directions. Hence, the true principal direction no longer exists. Thus, this iterative procedure was rejected for the *Equivalent von Mises stress* due to the following reasons:

- Easier calculation when multiaxiality doesn't imply concern for directivity.

- The alternative 'overall principal stress' doesn't take any account of possible multiaxiality.

This complexity itself causes to look for a scalar to quantify the stress response on a given component and then evaluate the uniaxial direction of excitation that provides the same damage as multiaxial excitation.

The selected scalar in this project is PSD estimate of the *Equivalent von Mises stress* which is independent of the direction of the principal stress [2]. This scalar has zero mean value and Gaussian distribution. In fact, it

reduces the multiaxial stress state to a uniaxial scalar which is suitable to calculate the uniaxial fatigue damage and to compare the impact from different excitations through the PSD and RMS value of the Equivalent von Mises stress respectively.

All above mentioned statement about random vibration will be discussed in detail in this chapter. Thus, in the first subsection of this chapter the short description about random vibration characteristics will be discussed. Then, the multiaxiality phenomena will be shown in detail. Then, the Equivalent von Mises stress will be presented and finally the results will be compared with those of overall principal stresses.

3.2.1 Random Vibration Characteristics

In this type of vibration testing components are excited by random signals. In the frequency domain this kind of signals are represented by power spectral densities (PSD). In order to quantify the resulting stress, the root mean square value (RMS) of the estimated PSD function of resulting stress should be calculated [6].

3.2.2 Multiaxial Stress Response

As it was mentioned in the introduction section, different excitations may cause multiaxial stress response on components. This is an obstacle in quantifying the response of different excitations. As a result, the Equivalent von Mises stress has been found as a suitable scalar to quantify the response.

The stress response of structures can be categorized as the following [5];

1. Uniaxial response; it can be assumed as simple plane stress.

2. Proportional multiaxial response; it is a multiaxial stress field where stress tensor elements increase and decrease proportionally.

3. Non-proportional multiaxial response; it is a multiaxial stress field where stress tensor elements do not increase and decrease proportionally and the principal stress direction changes with time.

In the first two cases the direction of the principal stress is stationary. In order to analyze this type of vibration, either principal stress or the Equivalent von Mises stress can be used. The amount of deviation from uniaxial response can be obtained by the *Biaxiality* ratio [7]. The biaxiality ratio is the ratio of the smaller to the larger in-plane principal stresses. This ratio varies between -1 and 1. The zero value shows the uniaxial stress state. The stress state variations on a certain hot spot in a component with high stress, can deviate from uniaxial stress conditions. It can be shown by evaluating the following items [5]:

1) The biaxiality ratio is nonzero (zero value means uniaxial response).

2) The orientation of the principal stress may vary with time.

Therefore, it is important to know what has caused the rotation of the principal stresses. In general the principal stresses rotate at the following circumstances:

1. Rotation caused by different damping of the structure.

2. Rotation caused by exciting the vibration modes.

3. Rotation caused by multiaxial loading.

For components with a constant damping distribution, there would be no rotation of principals regarding to the damping effect. However, rotation of the principals by the last two reasons has been studied and verified by considering more elements on different components.

Based on the above statement, some steps have been considered to perform random vibration analysis and observing the rotation of the principal stresses when using uniaxial and multiaxial excitations. The output of the

analysis is the PSD estimate of the stress components, the maximum principal stress and the Equivalent von Mises stress. The maximum principal stress is calculated to verify the Equivalent von Mises stress. The analysis consists of the following steps:

- Setting up the component for computer simulation in Ansa.
- Performing Normal Modes analysis in MD-Nastran.
- Determining the hot spots using Metapost.
- Performing the Modal Frequency Response Analysis in MD-Nastran
- Calculating the maximum principal stress and its direction
- Calculating the Equivalent von Mises stress
- Calculating the stress quantity, E.V.S or M.P.S, in Multiaxial excitations
- Statistical analysis and determining the safety margin

3.2.2.1 Setting up the Component for Computer Simulation in Ansa

The component under consideration is a bracket which should be attached to a chassis by two connecting bolts. So, the holes of the bracket should be constrained and also excited by a white noise random vibration. As discussed before, the crack propagates on the surface of the element so the shell mesh should be applied in order to obtain the biaxial stress response. However for simplicity, the bracket was meshed using CTETRA volume elements and the stress response at the center of the element was requested. It has been seen that using volume elements gives fair results compared to using shell elements. The number of elements was selected such that the result converged to a unique value. The input load is the PSD estimate of

acceleration with unit (g^2/Hz) .The PSD estimates of the stress tensor components, $\sigma_x, \sigma_y, \sigma_z, \tau_{xy}, \tau_{yz}, \tau_{xz}$, have been obtained as the output of the analysis. The following table demonstrates the bracket and the way it has been constrained.

Table 3.1 Initial set up of the Component.

Quantities	Properties	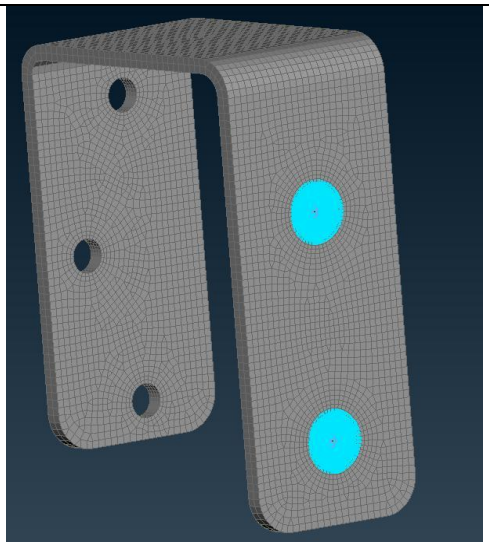
Material	Steel	
Density	7850 kg/m^3	
Young Modulus	210 G Pa	
Poisson's ratio	0.3	
Damping Ratio	0.05	Damping of the component.
Boundary Condition	Connecting Bolts	Two holes are constraint by rigid body elements (RBE2).
Input	PSD acceleration	Level 1 (G^2/Hz) within the frequency Forcing Frequency of base: 1-1000 Hz, G=9810 (mm/s^2) .
Output of Nastran	Modal Analysis and Complex Stress tensor	1) Modal analysis. 2) The FRF of 6 stress components.

3.2.2.2 Performing Modal Analysis in MD-Nastran

At the second step, in order to find the natural frequencies and mode shapes of the bracket, modal analysis of the bracket has been performed. In this case, the Lanczos method has been selected to extract the natural frequencies in MD Nastran. The Lanczos method is the ideal method for many medium- to large-sized components, since it has a performance advantage over other methods [8]. This step should be performed in Random as well as Swept Sinusoidal vibration analyses. As an example the calculated natural frequencies for the component shown in Table 3.1 are presented in Table 3.2 and the results associated with the figures of the mode shapes will be demonstrated in the result section.

Table 3.2 Natural Frequencies of the Bracket.

Bracket 1	Natural Frequencies				
	1^{st}	2^{nd}	3^{rd}	4^{th}	5^{th}
Values (Hz)	115	169	284	510	924

It is apparent from the table that the fourth and fifth natural frequencies are very high and the trucks aren't usually subjected to such forcing frequency excitations. Therefore, only the first two or three modes are usually considered for the rest of the calculations and the other modes are presented to show the influence of high natural frequency on the lower ones.

3.2.2.3 Determining the Hot Spots Using Metapost

Hot spots are those critical points, elements, which have maximum von Mises or Principal Stress values at each natural frequency. They are

obtained at mode of vibration. By using Metapost software and selecting a criterion like the von Mises stress or the maximum principal stress, the hot spots can be easily distinguished. The important point at extracting the hot spots is that to avoid singularity in order not to have rigid body modes (or mechanism Modes [4]). In this sense, the hot spots which show singularity, i.e. the elements at the boundary conditions of the component, should be eliminated from the FRA. The following figure illustrates the hot spots at the second natural frequency which shows singularity. In this case, it is required to use other elements which are located in the areas of stress gradients of a particular eigenmode. Figure 3.5 shows the element which has been selected to avoid singularity and it is also subjected to considerable stress. The values of natural frequencies have been also listed at the left hand side of the following figure.

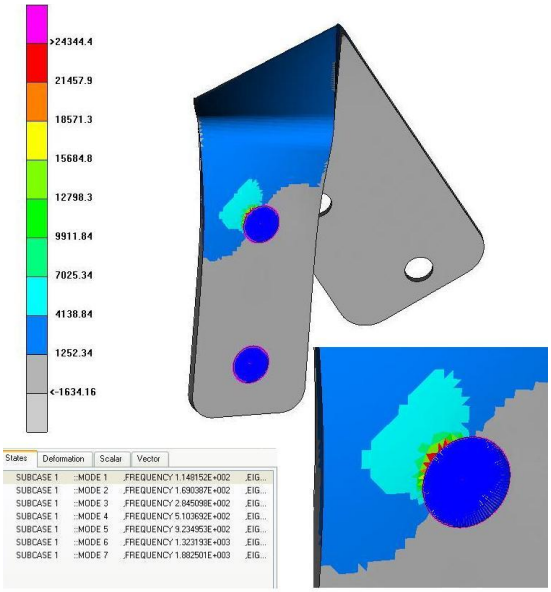

Figure 3.4 *Demonstration of hot spots by Metapost-Showing Singularity.*

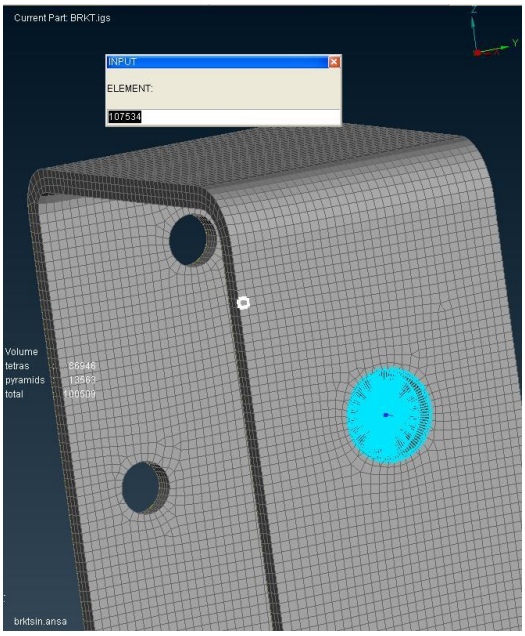

Figure 3.5 *Hot spot selected to avoid singularity.*

The hot spot shown in Figure 3.5, element 107534, which is selected for the first analysis throughout this chapter, is the hot spot at the outer side of the bracket and far from the boundary conditions to avoid singularity.

In total, seventeen different hot spots were studied on the shown bracket to prove the accuracy of the selected methods which will be discussed later on in this chapter. Moreover, some elements have been selected on three more components in order to make statistical analysis to find the relation between the uniaxial and the multiaxial excitation cases. Only the shown element on the first bracket will be discussed in this chapter to provide the method chosen to deal with the excitations of the bracket. The other components will be used for statistical purposes and the results will be shown at the corresponding chapter.

3.2.2.4 Performing Modal Frequency Response Analysis

After determining the hot spots at different modes and corresponding elements of a certain component, frequency response analysis, SOL 111 in MD-Nastran, should be performed to request the stress response at those elements. In fact, in this type of analysis, the bracket is excited by one uniaxial direction; X, Y, Z, and the frequency response functions (FRF) of the stress tensor at the hot spots are requested as the output of the analysis. The outputs will be imported to Matlab in order to obtain the PSD estimate for each stress component and plot them for each excitation and compare the results.

The following equations implemented in Matlab, shows how to calculate the PSD of a stress component, normal X stress for example, by using its FRF obtained in MD-Nastran;

$$H(\sigma_x) = s_{xr} + j s_{xi} \tag{3.3}$$

$$PSD(\sigma_x) = G \times H(\sigma_x) \times H(\sigma_x)^* \tag{3.4}$$

Where $s_{xr}\ and\ s_{xi}$ stands for two outputs of MD-Nastran, for real and imaginary parts of the stress response respectively. G is the PSD estimate of the input acceleration, $H(\sigma_x)$ is the calculated FRF for normal X stress and $PSD(\sigma_x)$ is the power spectral density of the normal X stress.

The following figure represents comparing the normal X stress component, σ_x, for all three uniaxial excitations.

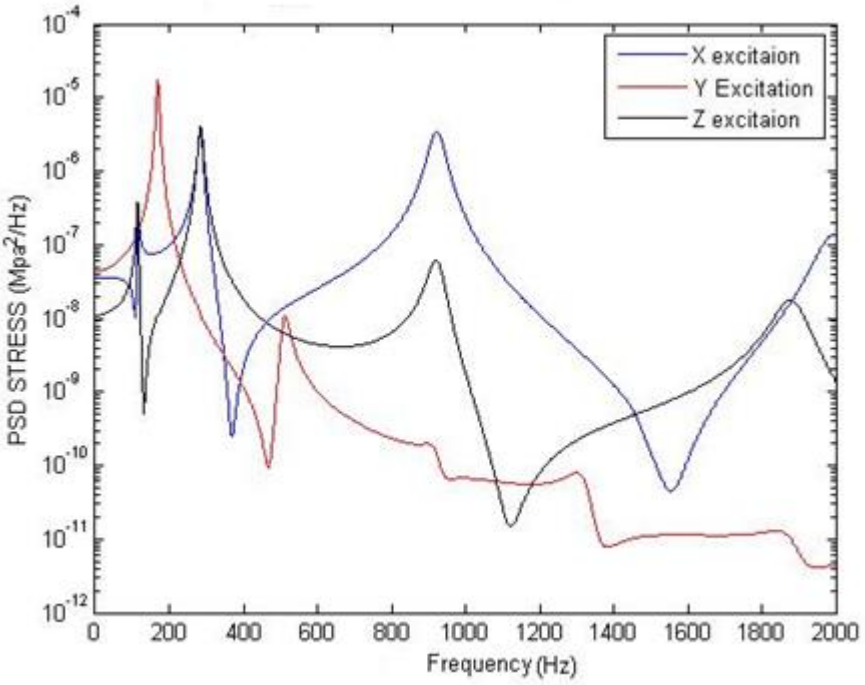

Figure 3.6 *Comparing the PSD estimates of σ_x for uniaxial excitations - element 107534.*

A comparison similar to the one shown in Figure 3.6 can be produced for all 6 components of the stress tensor. The PSD estimates for each component of the stress tensor obtained using three uniaxial excitations are utilized for further steps to calculate the maximum principals as well as the Equivalent von Mises stress which are explained at the next sections.

3.2.2.5 Calculating the Maximum Principal Stress and its Direction

In the present work, for each excitation, the maximum principal stress on a surface of an element and its corresponding direction have been calculated by two methods: using the static formula of transformation of the stress tensor in Matlab, and transformation in Ansa and MD-Nastran by changing the local coordinate system for each analysis. These methods have been presented in the Appendix in detail. As it was explained at the introduction

of this chapter, the aim of the discussion concerning the maximum principal stress is to identify the rotation of the principal stress at different modes as well as different excitations. The following figure demonstrates the rotation in the direction of the maximum principal stress present on an element. This figure has been obtained for element 107534 which is located at the YZ plane and the results are obtained for multiaxial excitation.

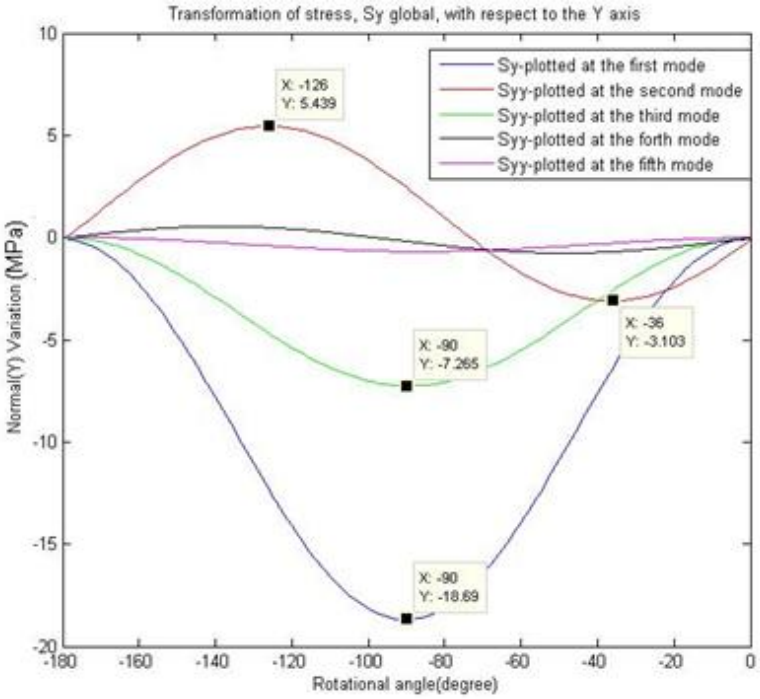

Figure 3.7 *Rotation present in the direction of the maximum principal stress.*

As it can be seen from Figure 3.7 the direction of the maximum principal stress (Syy in the figure) is not constant. For the first mode we have the maximum principal stress present at 90 degrees (counted counterclockwise) with respect to the Y axis (the horizontal axis) while for the second mode

the maximum principal stress is present at 126 degrees with respect to the Y axis.

Taking into account this phenomenon, it is clear that the maximum principal stress is not a sufficient measure to quantify the resulting stress caused by random excitations.

3.2.2.6 Calculating the Equivalent von Mises Stress

According to the previous section, the maximum principal stress within an element may change with time and frequency when different excitations are subjected to the bracket. However, in order to compare the stress response of different uniaxial excitations with the multiaxial one on a certain element it is required to utilize a quantity which is independent of the direction of the local coordinate system of the element. The Equivalent von Mises stress is a suitable tool to fulfill this requirement.

Using *the von Mises stress in the time* domain instead of *the Equivalent von Mises stress in the frequency* domain brings several problems. The problems are due to the quadratic nature of this time domain relationship between the von Mises stress and its stress components [2]:

- The von Mises stress is neither Gaussian, nor zero mean.
- The von Mises stress in the time domain is positive and it cannot be reduced to the applied alternative stress in uniaxial excitations.
- Its frequency content is not consistent with that of the stress components. Moreover, the peak of the PSD estimate of the von Mises stress doesn't show the natural frequency of the structure.

Using the Equivalent von Mises stress in the frequency domain solves all the above problems. The Equivalent von Mises stress by its construction is defined as Gaussian with zero mean. Moreover, its frequency content encapsulates the frequency contents of the stress tensor components. This is

a reason to apply the PSD estimate of the Equivalent von Mises stress in quantifying the stress in the case of multiaxial stress response.

In the present work MD-Nastran has been used as FEA solver and some parts of the calculations have been done in Matlab.

The general steps when performing vibration simulation by using frequency domain analysis in MD-Nastran and Matlab are given below. The following routine has been used for random vibration excitations.

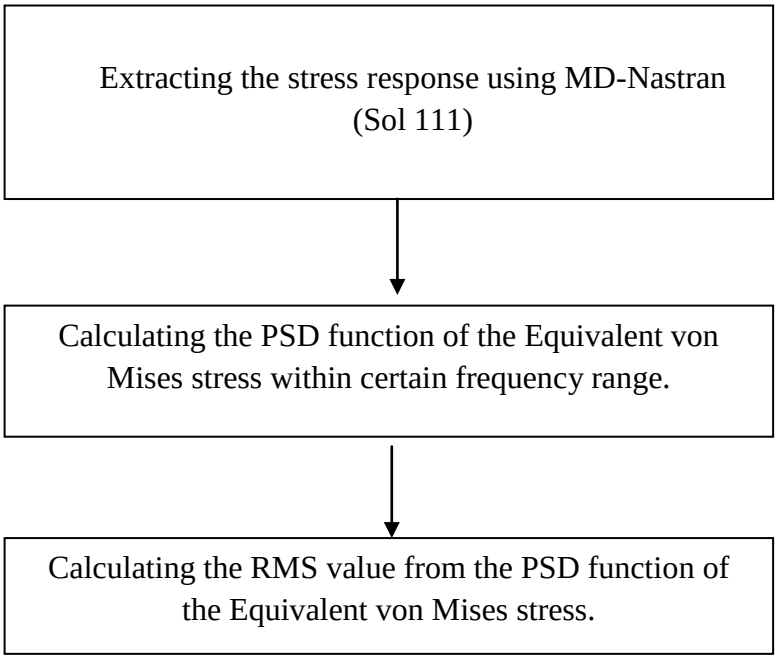

As it is apparent from the above flowchart, the RMS value of the Equivalent von Mises stress in the frequency domain is the quantity which is used to compare different excitations despite it gives no information about the rotations in the directions of the principal stresses at different modes of vibration. However, the results can be compared with RMS values of the maximum principal stress. In order to calculate the RMS value of the PSD function of the Equivalent von Mises stress and the maximum principal stress the following formula has been used [6].

$$RMS = \sqrt{\sum_{k=1}^{k=n} (PSD(f_k) * df)} \tag{3.5}$$

Where, *PSD* is the value of the PSD estimate at each frequency f_k, *df* is the frequency resolution (frequency increment) which is 1 throughout this report and *n* is the total number of frequencies.

The physical meaning of Eq. (3.5) is that it is the square root of the area under the PSD function's curve.

Since fatigue damage is often present on the component's outer surface the stress state on the surface has been considered. Therefore the stress state is biaxial and there are two normal stresses and one shear stress on the plane of a finite element. This stress state is used when calculating the Equivalent von Mises stress. The stress tensor is calculated by MD-Nastran. Thereafter the outputs are used in Matlab to calculate the Equivalent von Mises stress. In order to calculate the Equivalent von Misses stress from random testing the following equation suggested by Pitoiset and Preumont [2] has been used,

$$Gvm\ (f) = trace\ ([A] \times [G\ (f)]) \tag{3.6}$$

Where, *Gvm(f)* is the PSD value of the Equivalent von Mises stress at frequency *f*.

$$[\mathrm{A}] = \begin{bmatrix} 1 & -0.5 & 0 \\ -0.5 & 1 & 0 \\ 0 & 0 & 3 \end{bmatrix} \tag{3.7}$$

$$G(f) = \begin{bmatrix} G_{\sigma x \sigma x}(f) & G_{\sigma x \sigma y}(f) & G_{\sigma x \tau xy}(f) \\ G^{*}_{\sigma x \sigma y}(f) & G_{\sigma y \sigma y}(f) & G_{\sigma y \tau xy}(f) \\ G^{*}_{\sigma x, \tau xy}(f) & G^{*}_{\sigma y, \tau xy}(f) & G_{\tau xy \tau xy}(f) \end{bmatrix} \quad (3.8)$$

$G_{\sigma x \sigma x}$, $G_{\sigma y \sigma y}$ and $G_{\tau xy \tau xy}$ are the auto PSD's of the stress components and the rest are the cross-spectral densities. The star sign shows the complex conjugate of the cross-spectral densities.

Here the subscripts σ_x, σ_y and τ_{xy} are the components of the biaxial stress tensor given in Eq. (3.1).

The auto PSD's and the cross PSD's can be calculated by multiplying the FRF's by the input load's PSD values. The equation given below formulates this routine,

$$G_{\sigma i \sigma i}(f) = H_{ij}(f) * G_{jj}(f) * conj(H_{ij}(f)) \quad (3.9)$$

Where, $G_{\sigma i \sigma i}(f)$ is the auto PSD of component σ_i at frequency *f*.

$G_{jj}(f)$ is the input's PSD.

$H_{ij}(f)$ is the FRF's between the output and the input.

Since in this work the input is white noise the input PSD's are constant for the frequency range used. In the present work the input PSD function has the amplitude of 1g^2 (g=9810 mm/s^2) in each frequency. The amplitude scaling of the outputs have been done in Matlab as it is given with Eq. (3.9)

It is good to mention that input loads not necessarily have to be in the form of white noise. They could have different amplitude values in each frequency. In the present work white noise has been used for its simplicity.

Considering the selected hot spot, element 107534, and the above description of the Equivalent von Mises stress, this quantity can be

calculated and plotted for each excitation. Figure 3.8 demonstrates the Equivalent von Mises stress for X excitation of the bracket and compares it with the maximum principal stress at the angle in which it's RMS value is maximum. The results for the other excitations as well as the RMS value of each excitation will be shown in the Result chapter.

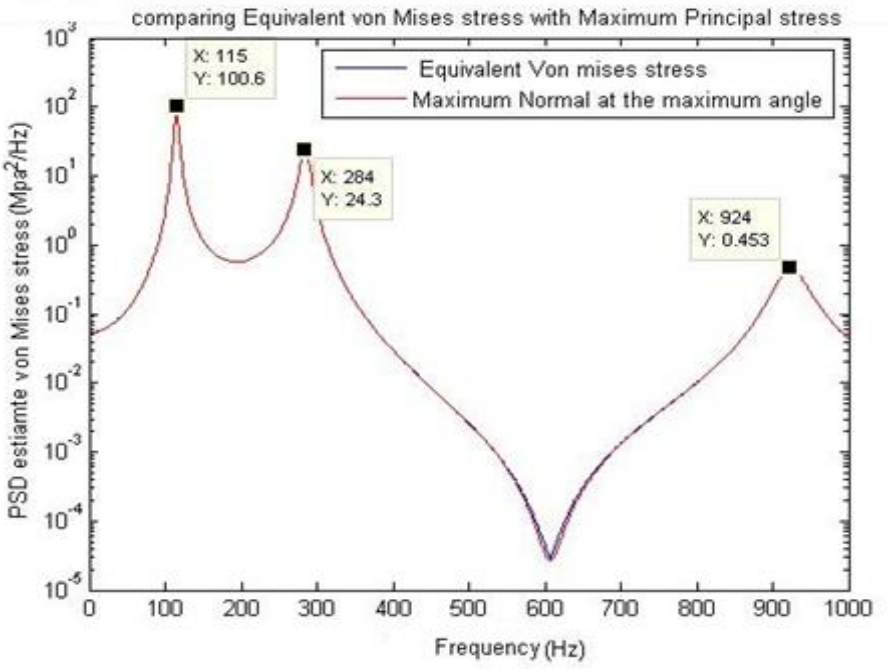

Figure 3.8 *Comparing the Equivalent von Mises stress and the maximum principal stress.*

3.2.2.7 Calculating Stress Modulus in Multiaxial Excitations

In order to quantify the stress modulus for both the Equivalent von Mises stress and the maximum principal stress, in uniaxial excitation the formula given with Eq.(3.9) has been used. When it comes to multiaxial excitations one useful approach to consider the multiaxial loading is to linearly superpose *multiple uncorrelated inputs* [9]. Based on this assumption, the following formula is used to consider all three orthogonal excitations, X, Y, Z, at the same time;

$$G_{\sigma j \sigma j}(f) = \left|H_{jx}(f)\right|^2 G_{xx}(f) + \left|H_{jy}(f)\right|^2 G_{yy}(f) + \left|H_{jz}(f)\right|^2 G_{zz}(f) \qquad (3.10)$$

In other words, if the sources are statistically independent then the PSD of the total response is the sum of the PSD estimate of the responses due to individual sources. The PSD inputs are set to be 1g^2/Hz for all three excitations, thus according to this formula, in order to calculate the multiaxial loading it is required to sum the squared FRF's generated by each excitation multiplied by input's PSD's. By using this assumption it is possible to calculate the Equivalent von Mises stress as well as the maximum principal stress for multiaxial excitations for the element under consideration. The following figures demonstrate the transformed stress when all three orthogonal excitations are applied to the bracket, RMS value of normal X and the comparison between the Equivalent von Mises stress and the maximum principal stress.

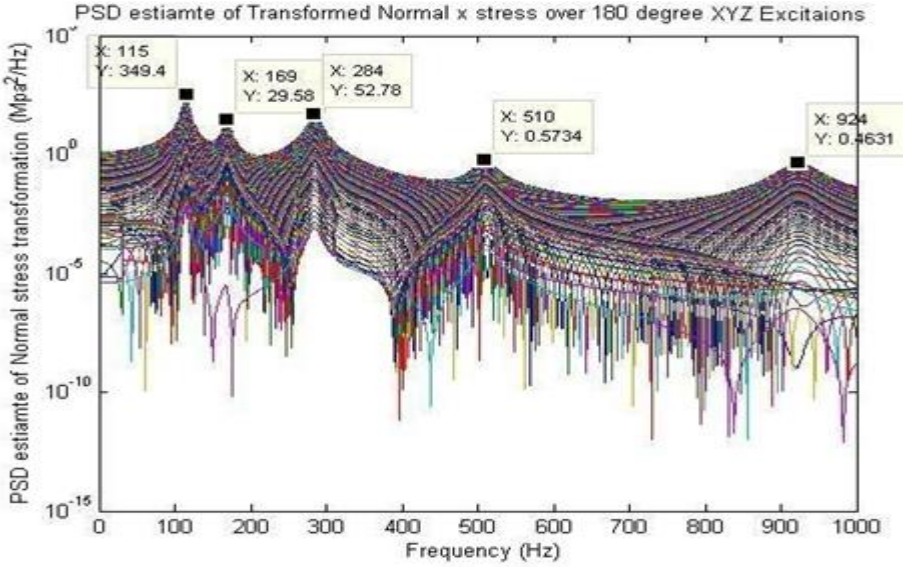

Figure 3.9 *Transformed PSD estimate of stress in multiaxial excitation.*

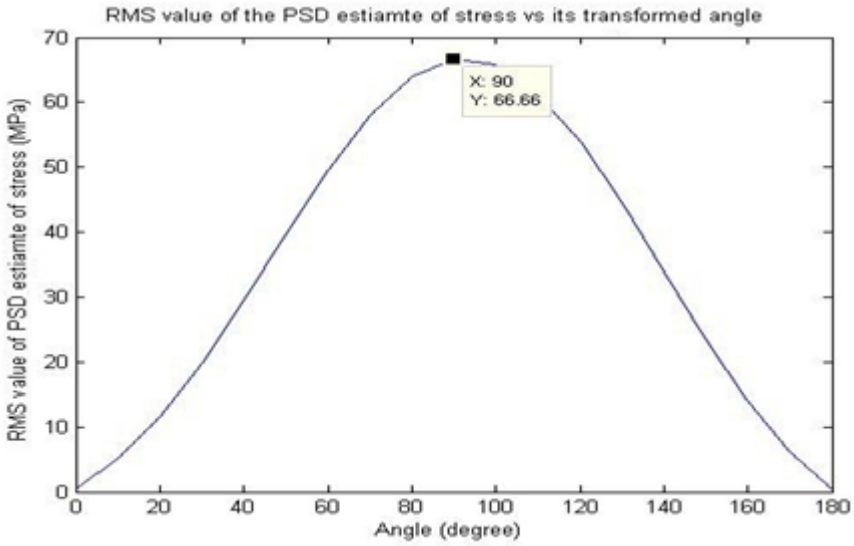

Figure 3.10 *RMS value of transformed stress versus angle for multiaxial loading.*

The above figures show the results for normal X stress component for multiaxial excitation for the first hot spot, element 107534.

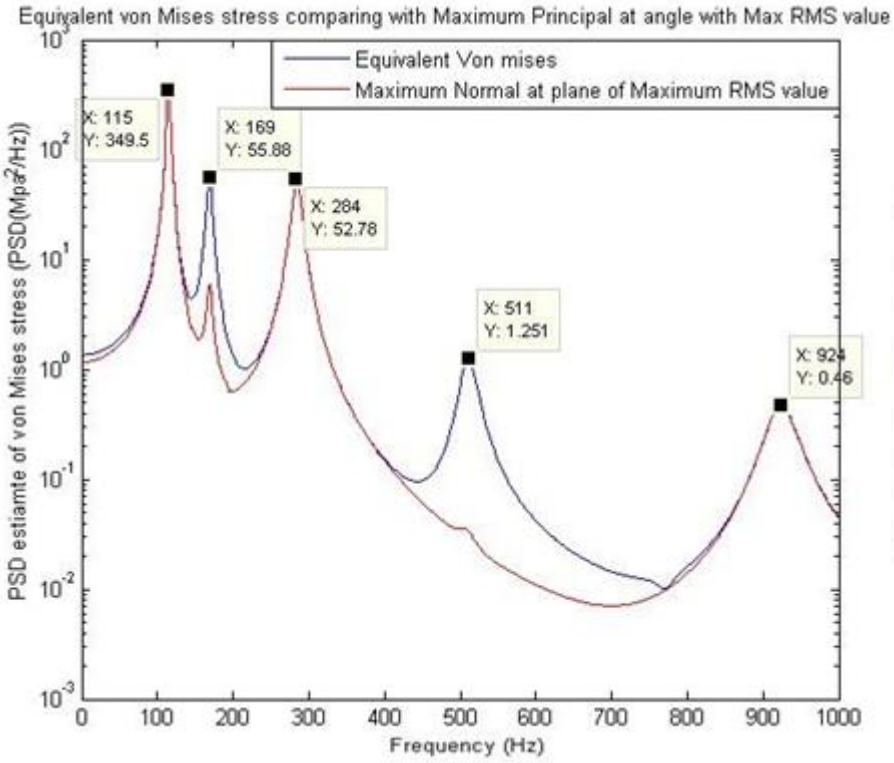

Figure 3.11 *Comparing the Equivalent von Mises stress and the maximum principal stress in multiaxial excitation.*

As it is apparent from Figure 3.11, the maximum principal stress doesn't completely follow the Equivalent von Mises stress despite the fact that in uniaxial excitation, i.e. X direction excitation in Figure 3.8, they quite coincide with each other.

The reason of such a difference is that there is no rotation of the direction of the maximum principal stress when exciting the bracket in X direction. However, in multiaxial excitation the direction of the maximum principal stress rotates and prompts the illustrated difference.

3.2.2.8 Statistical Analysis and Determining the Safety Margin

At this step, the quotient between stress response under uniaxial and multiaxial loading is obtained for all hot spots. Studying the quotients makes it possible to assess the direction of excitation in which the bracket is sensitive to. In order to do so, for each element under consideration, the quotient between the RMS of the Equivalent von Mises stress under multiaxial excitation and each of uniaxial excitations is calculated and compared to find the value close to unity.

Safety margin K as defined in Eq. (3.11) is the quotient of the stress response obtained under multiaxial excitation divided by the stress responses obtained under uniaxial excitation. So for each uniaxial excitation in each direction there will be a safety margin quotient. The safety margin value close to unity indicates that the contribution of the uniaxial excitation to the stress response is similar to the multiaxial excitation's contribution.

$$K = \frac{Stress\ response\ from\ multiaxial\ excitation}{Stress\ response\ from\ uniaxial\ excitation} \tag{3.11}$$

Using the statistical analysis over the obtained quotients makes it possible to find some parameters for the component such as the sensitive direction of vibration, safety margin and test specification for the test considering one uniaxial excitation such that resulting damage is closer to the damage that component experiences under multiaxial excitation. The results of quotient calculations are shown in Results and Conclusion sections.

3.3 Correlation in Vibration Fatigue Analysis

As it was discussed in the Introduction section a component mounted on a truck is generally subjected to a set of loads directed differently in space. The loads acting on the component can be both correlated and uncorrelated. It is of interest to investigate how the correlation between the loads affects the stress state of the component.

In durability analysis traditionally loads are represented as time dependent variables and resulting responses are also calculated in the time domain. In the time domain the dependencies between the loads are presented as correlation matrices or as phase differences or time lags between the loads which is especially important in periodic loads such as swept sinusoidal loads. The frequency domain representation of the load signals has its own advantages such as modal information, or distribution of the power and it is time efficient regarding calculations, but analyzing correlation and phase difference in the frequency domain requires dealing with complex numbers and can be cumbersome to implement in FEA solution codes.

In real test environment loads are measured by mounting sensors on components of a truck and measuring specific parameters, mostly acceleration, in different directions during the testing time. It is predictable that there will be correlation and phase difference between loads measured at different positions on the truck. These loads will be transferred trough truck's structure to its components. Phase difference effect in this case has been investigated. In this thesis work we will consider resulting loads on each component and analyze the correlation between loads components in three orthogonal directions.

Accelerations measured in three orthogonal directions on a specific point of a component might be correlated and this relation will affect the direction of the resulting acceleration at that point. For instance, if three of the accelerations in three directions are 100% correlated and have the same magnitude, the resulting acceleration will act along a line in 3-D space which is inclined with an angle to the original orthogonal direction and all

three orthogonal accelerations can be substituted by one uniaxial acceleration in that diagonal direction.

In computer simulation one can generate arbitrary loads such as load having different signal types or loads with desired correlation between them, and more over one have the freedom to apply several loads simultaneously in different directions on a component. Having this characteristics computer simulation is the most suitable tool for correlation analysis.

3.3.1 Correlation in Random Vibration

In real world a component of a truck will be exposed to multi-directional acceleration loads which are originated from the forces applied to the wheels and transferred trough the body and structure of the truck to the component. In general acceleration experienced by the component, caused by road depends on several factors such as component's location and mounting situation, road structure and condition or speed of the truck etc., and most of the time the resulting acceleration has random nature. It shows randomness in both magnitude and direction. So acceleration in each time instant can be represented as a random vector in the three dimensional space. In road test this acceleration is measured in three orthogonal directions at the connection points of the component to its fixture. In laboratory test or computer simulation of that component, an imitation of the acceleration signal will be applied to the connection points of the component to simulate the real acceleration excitation which the component will be encountering during its service life.

In computer simulation environment the random acceleration load's vector or in other words multiaxial acceleration can be defined by a vector having components that are normally distributed. In Figure 3.12 each point represents ending point of random acceleration vectors where, vector components are normally distributed with same mean and variance for X, Y and Z directions. As it is apparent from the figure directions of such a set will be evenly spread in space.

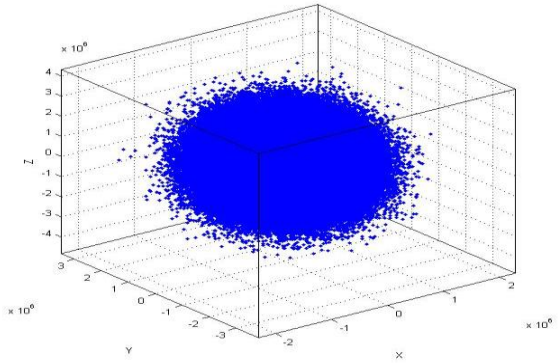

Figure 3.12 *Uncorrelated random multi axial acceleration with Gaussian distribution where the expected value vector* $\boldsymbol{M} = [\boldsymbol{\mu_X}, \boldsymbol{\mu_Y}, \boldsymbol{\mu_Z}] = [\mathbf{0}, \mathbf{0}, \mathbf{0}]$ *and correlation matrix* $\boldsymbol{C} = \begin{bmatrix} \mathbf{1} & \mathbf{0} & \mathbf{0} \\ \mathbf{0} & \mathbf{1} & \mathbf{0} \\ \mathbf{0} & \mathbf{0} & \mathbf{1} \end{bmatrix}$.

Each component of the acceleration vector can be considered as a uniaxial vibration excitation in corresponding direction. The acceleration vector components can be correlated or uncorrelated. If acceleration vectors component have no correlation between them it means that the direction of the accelerations are evenly distributed in 3-dimentional space, see Figure 3.12. If vector components are correlated depending on the correlation rate between each pair of directions X, Y or Z, resulting point cloud will be skewed towards one direction. For instance in Figure 3.13 set of acceleration vectors with correlation matrix $\mathbf{C} = \begin{bmatrix} 1 & 0.2 & 0{,}8 \\ 0.2 & 1 & 0.5 \\ 0.8 & 0.5 & 1 \end{bmatrix}$ and their skewed direction is presented. Generating correlated random loads has been presented in the Appendix.

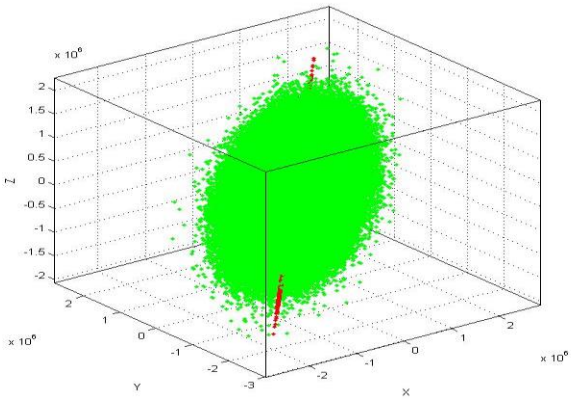

Figure 3.13 *Correlated random multi axial acceleration with Gaussian distribution where the expected value vector* $\boldsymbol{M} = [\boldsymbol{\mu_X}, \boldsymbol{\mu_Y}, \boldsymbol{\mu_Z}] = [\mathbf{0}, \mathbf{0}, \mathbf{0}]$ *and correlation matrix* $\boldsymbol{C} = \begin{bmatrix} 1 & 0.2 & 0{,}8 \\ 0.2 & 1 & 0.5 \\ 0.8 & 0.5 & 1 \end{bmatrix}$.

Skewness in acceleration distribution implies that the effective loads acting on a component during the time interval are mostly oriented in a certain direction. In the case of correlated accelerations probability of direction is not the same and one or few of the directions have higher probability than the others. In Figure 3.14 cumulative acceleration magnitude has been illustrated on the upper half of the unite sphere for the same load as in Figure 3.13.

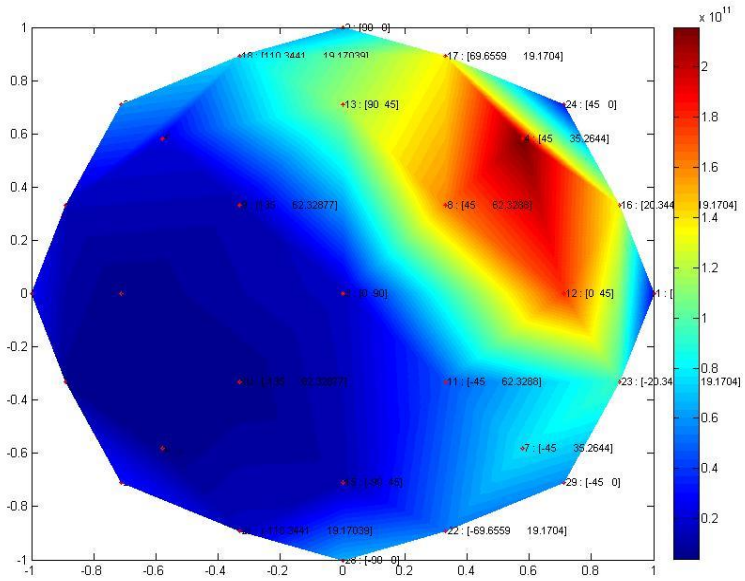

Figure 3.14 *Cumulative acceleration magnitude for acceleration load with* $\boldsymbol{M} = [\mathbf{0}, \mathbf{0}, \mathbf{0}]$ *and* $\boldsymbol{C} = \begin{bmatrix} 1 & 0.2 & 0{,}8 \\ 0.2 & 1 & 0.5 \\ 0.8 & 0.5 & 1 \end{bmatrix}$.

The results presented in Figure 3.14 are obtained considering 29 evenly distributed directions on the upper half of the unit sphere. Thereafter accelerations with less than 30 degrees deviation from each of the considered directions are projected on the closest considered direction. Resulting magnitudes are summed as the representative magnitude of that direction.

The load and its multiaxial characteristics have been discussed so far. However, the aim of the analysis is to simulate the multiaxial vibration load and find a corresponding uniaxial load such that it produces as similar impact as possible to multiaxial vibration. But the response of the component is more dependent on the structural dynamic properties of the component rather than load's characteristics as it is discussed in detail in Section 3.3. Therefore even if one succeed to produce the most similar uniaxial load to a multiaxial load in terms of load characteristics it does not

guarantee that the component will respond to that uniaxial load in the same way as it responds to the multiaxial one.

The response of the component will always be higher in multiaxial random load compared to any uniaxial random load.

Considering the modal characteristic and geometry of a component it may have highest stress response to a uniaxial load in a certain direction. If a component has the same sensitivity in all directions, it is likely to have the highest stress response in effective direction of the random multiaxial load, since it receives excitation loads in that direction more often than the other directions. But if the component has higher sensitivity to a vibration load in a certain direction rather than the others, it will have the highest stress response in that direction regardless of the effective direction of the random multiaxial load. In Table 3.3 results of random load analysis for a component is presented. It shows that the component has higher sensitivity in Y direction rather than X or Z and it has higher stress response in this direction when the random load is uncorrelated and it has the same probability in all directions.

Table 3.3 Random Analysis Results for an Element.

Element number 12666	X-direction excitation	Y-direction excitation	Z-direction excitation	Multiaxial excitation load
Equivalent von Mises RMS (MPa)	46.700	**91.330**	52.420	**115.190**
Safety factor K	2.47	**1.26**	2.20	

3.3.2 Correlation in Swept Sinusoidal Vibration

Correlation between sinusoidal signals can be illustrated considering one sinusoidal signal and its copy with introduced phase difference. As a measure of correlation the correlation coefficient is used. If signals have no phase difference ($\Delta\varphi = 0$) they are correlated with correlation

coefficient $r_p = +1$, by introducing phase difference the correlation coefficient will decrease and if there is a phase difference of $\Delta\varphi = \pi$ then they are correlated with correlation coefficient $r_p = -1$. In Figure 3.15 correlation coefficient of two signals versus phase difference between them has been illustrated.

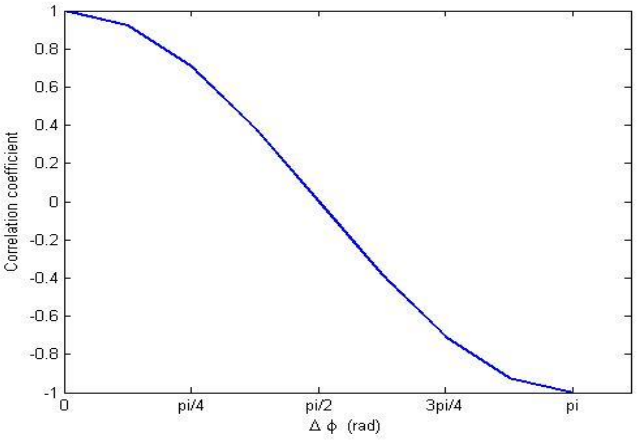

Figure 3.15 *Correlation coefficient versus phase difference between a sinusoidal signal and its copy with a phase difference.*

There is an infinite number of possible phase difference combinations for three signals. For sake of simplicity, the correlation coefficients matrix has been summarized as a vector $C = [C_{xy}, C_{xz}, C_{yz}]$, and the following four extreme combinations will be considered;

1) $C = [+1, +1, +1]$, 2) $C = [-1, +1, +1]$,

3) $C = [+1, -1, +1]$, 4) $C = [+1, +1, -1]$.

Here in case 1) there is no phase difference between acceleration signals ($\Delta\varphi = 0$).

In case 2), 3) and 4) respectively the signal in X-direction, the signal in Y-direction and the signal in Z-direction has 180 degrees phase difference with respect to the other two signals ($\Delta\varphi = \pi$).

Table 3.4 is a sample of the maximum von Mises stress comparison for one element of a component under uniaxial and different multiaxial combination loads of swept sinusoidal type.

Table 3.4. Table of results from Swept sinusoidal safety factor analysis for element number 12666 of component 4. This element located in a x-z plane and the maximum von Mises stress for multiaxial combinations is $V_m = 85.03\ MPa$ *and it is observed in* $C = (1, -1, 1)$ *combination and frequency* $f = 31\ Hz$*. The highest uniaxial stress response is observed in Y direction excitation and in frequency* $f = 31\ Hz$ *with a von Mises value of* $V_m = 56\ MPa$*. According to these observations safety factor for this component will be* $K = 1.52$.

$C = (C_{xy}, C_{xz}, C_{yz})$			(1,1,1)	(-1,1,1)	(1,-1,1)	(1,1,-1)
El no.12666(x-z)		Max. von Mises Stress (MPa)	26,97	45,54	85,03	66,48
Uniaxial excitation direction	Max. von Mises Stress (MPa)	Frequency (Hz)	31	31	31	31
X-direction	15,07	107	1,79	3,02	5,64	4,41
Y-direction	56	31	0,48	0,81	**1,52**	1,19
Z-direction	19,76	31	1,36	2,30	4,30	3,36

It has been observed that in some cases there is a magnification effect and in some other cases there is a cancelation effect between combined multiaxial loads compared to uniaxial loads. For instance, two first combinations of multiaxial load in Table 3.4 produce less stress responses than uniaxial load in the Y direction. It means that adding two other load signals in two orthogonal directions to a load in the Y direction even reduces the stress response.

3.4 Fixture Assembly Analysis

In real situation the bracket under consideration is installed on another component and this component itself may be mounted on the frame of the truck or etc. It means that the bracket is excited by the accelerations experienced by the component it is attached to. In test analysis of the bracket, the bracket should be mounted on another component, let's say a fixture, in order to be ready to be excited by the shaker. The following analysis is performed to study the influence of the fixture on a bracket under consideration.

The same analysis as described in Random Excitation section is performed for an assembly of the bracket and the fixture. The analysis shows how a flexible fixture affects the natural frequency of the bracket and its sensitive direction regarding to a certain excitation. All steps taken in random vibrations analysis should be also applied for this analysis in addition to some more steps due to the presence of the fixture.

The material properties of the fixture have been selected so that its low resonance frequencies are in the same range as resonance frequencies of the bracket. The properties of the selected fixture are given in Table 3.5.

Table 3.5 Material properties of the bracket and main analysis steps.

Quantities	Properties	
Material	Lead	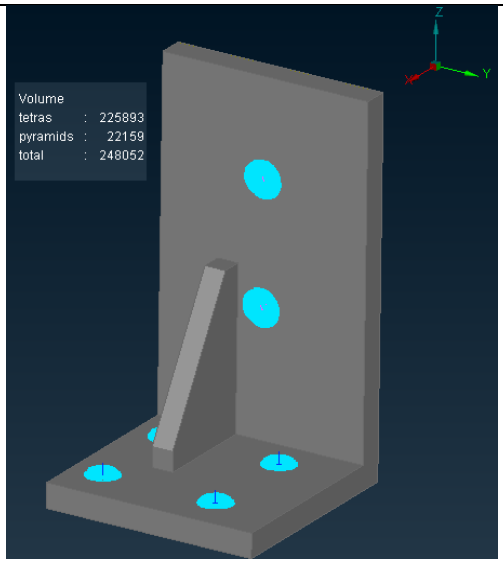
Density	2850 kg/m^3	
Young Modulus	30 GPa	
Poisson's ration	0.35	
Boundary Condition	Bolts at the base	Four holes are constraint by rigid body elements (RBE2).
Damping ratio	0.05	The damping of the fixture.
Input	PSD acceleration	Level 1 (G^2/Hz) for each excitation within the frequency range: 1-1000 Hz, G=9810 (mm/s^2) .
Output of MD-Nastran	Modal Analysis and Complex Stress tensor	1) Modal analysis of fixture. 2) Modal analysis of assembly. 3) FRA of assembly.

As it is apparent from Table 3.5, the first step is to perform a modal analysis of the fixture.

After calculating the natural frequencies of the fixture, the next step is to combine the two components in order to form an assembly to be able to obtain the natural frequencies of the assembly. To do so, the components are connected through two screws at the holes of the bracket. The element type of the connecting screws is CBAR and has the following material properties.

Table 3.6 Material properties of the connecting screws.

Quantities	Properties	
Material	Steel	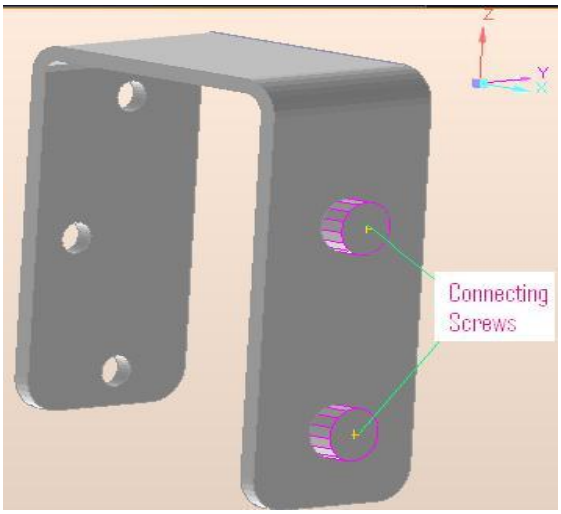
Density	7850 kg/m^3	
Young Modulus	210 GPa	
Poisson's ration	0.30	

The connection is fairly rigid so that its flexibility doesn't have any significant influence on the bracket and the analysis itself. The next step is to calculate the natural frequencies of the assembly. The results of the modal analysis have been shown in the following table.

Table 3.7 Natural frequencies of the bracket and the fixture.

Values (Hz)	Natural Frequencies					
	1st	2nd	3rd	4th	5th	6th
Bracket	115	169	284	510	924	
Fixture	140	239	313	501	897	
Assembly	109	124	149	225	302	331

As it is apparent from Table 3.7, the natural frequencies of the assembly have been affected by modes of each component. The next step is to perform the FRA in order to calculate the Equivalent von Mises stress for a certain hot spot, element 106760, on the bracket.

At the first try in the fixture analysis, four holes at the base of the fixture are constrained and then excited simultaneously in different directions, X, Y, Z and multiple loading of all three excitations. Then the stress response will be requested at the specified hot spot. The following figure demonstrates the hot spot in which the frequency response analysis has been performed.

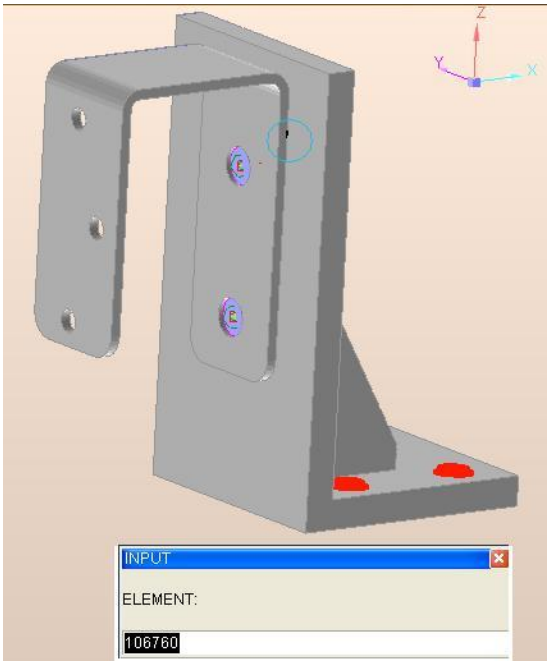

Figure 3.16 *Demonstration of the assembly analysis and the element under consideration.*

It should be mentioned that the accelerations generated at the interference of the bracket and the fixture are always in three directions. Therefore, regardless of the type of excitation of the base of the fixture, the bracket is always excited by three orthogonal accelerations generated at the connecting screws of the assembly. It is also possible to combine the stress response caused by generated accelerations at the connecting screws. However, the specified formula for combining the stress response of different excitations, Eq. (3.10), cannot be used for the current purpose. As it was mentioned in the corresponding section, Eq. (3.10) can be applied for multiaxial excitations when the inputs are fully uncorrelated, i.e. exciting the bracket only by three independent accelerations, but in the assembly the generated accelerations at the connecting joints are correlated because of the mechanical filter of the fixture itself. The following figure shows the correlated acceleration in Z direction generated at two connecting screws.

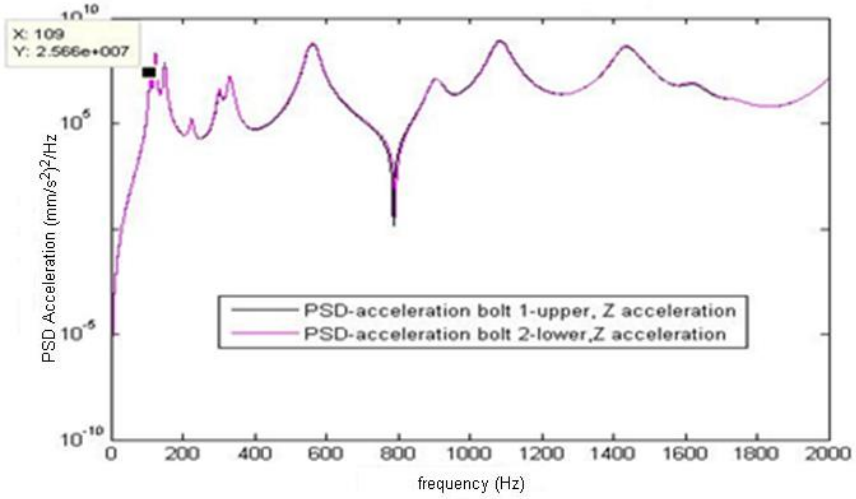

Figure 3.17 *PSD estimate of the correlated acceleration in Z direction.*

Not only the generated acceleration at two screws in specific direction is correlated, but also the accelerations in all 3 directions may be correlated due to the nature of the fixture. In this sense, fixture works as a mechanical filter that relates all accelerations at the interferences.

In order to clarify the above mentioned statement, the second analysis was performed. In this analysis, only the bracket was excited by three accelerations in different directions at the interface with the fixture which have been generated by each excitation of the base of the fixture and the stress response was requested on the same hot spot as the previous analysis, element 106760. In this sense, Eq. (3.10) was used to combine the responses of three excitations. As it was expected the result was different from that of the directly exciting the assembly.

The following figure shows the result of comparing the Equivalent von Mises stress obtained in two different analyses; a) Exciting the base of the assembly in X direction and requesting the stress on the bracket, b) Exciting only the bracket by generated accelerations at the connecting screws joining the bracket with the fixture.

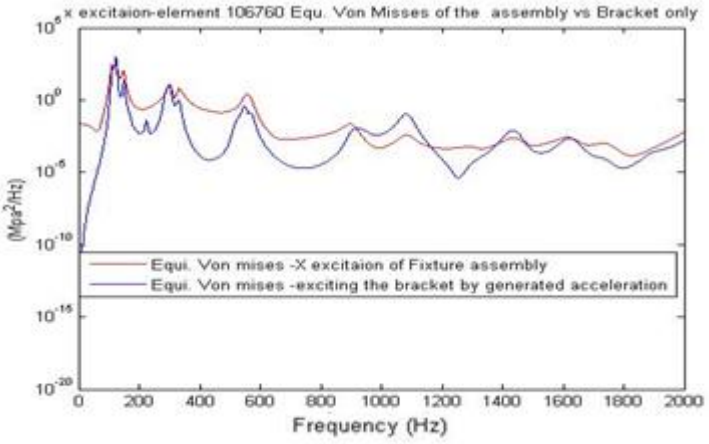

Figure 3.18 *Comparing the Equivalent Von Mises stress of two analyses obtained in X direction excitation of the base.*

As it was mentioned earlier, the reason of the difference between the two analyses is that Eq. (3.10) cannot be used when the excitations are correlated. However, in order to correct the results, when the inputs are statistically correlated, the degree of correlation should be obtained by considering the cross-spectral density. Therefore, the spectral density of the response is evaluated according to the following formula [11];

$$G_j = \sum \sum_{k=1}^{n} H_{ja}(f_k) \, . H^*_{jb}(f_k) . G_{ab}(f_k) \qquad (3.12)$$

Where, $H_{ja}(f_k)$ is the FRF between the output j and the input a, $H^*_{jb}(f_k)$ stands for the complex conjugate of the FRF between the output j and the input b and G_{ab} is the cross-power spectral density between the components a and b. The other way of considering the correlated inputs in multiaxial loading is to perform Transient Response analysis rather than Frequency Response analysis in order to keep the information of the correlation during the calculation.

4 Results

In this section results obtained from vibration simulation using swept sinusoidal and random inputs have been presented as well as results obtained from correlation analysis and fixture analysis.

For vibration simulation four different test models have been used for testing. The test models are different kinds of brackets used in trucks.

4.1 Normal Modes Analysis Results

This analysis gives an idea about the structural behavior of the component.

4.1.1 Component 1

The first model is shown in Figure 4.1. This model is a simple bracket used in trucks. It has been meshed using 100509 second order tetra elements. The material properties are: Young's modulus (E) = 210 GPa, Poison's ratio (ν) = 0.3 and density (ρ) = 7850 kg/m^3.The damping ratio ξ is 0.05.It is fixed from the holes to the truck's frame as it is shown in Figure 4.1.

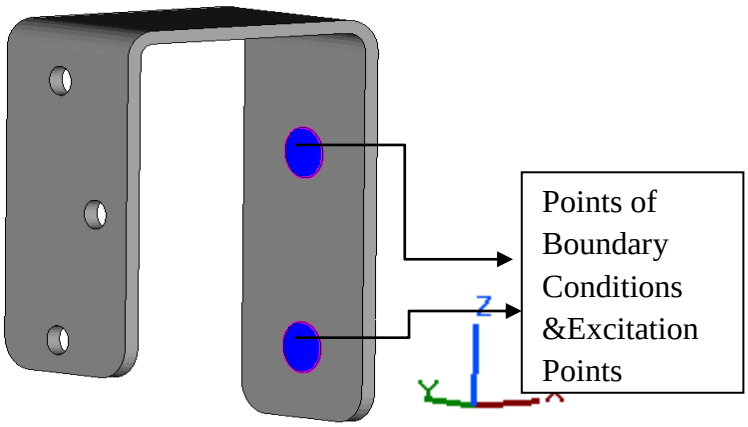

Figure 4.1 *Component 1.*

Results obtained from the normal modes analysis are given below. Table 1 shows the natural frequencies within the range 0-1000 Hz.

Table 4.1 Natural frequencies and mode types of Component 1.

Frequency [Hz]	Mode type
115	Bending
169	Torsion + Bending
285	Bending
510	Torsion + Bending
923	Bending

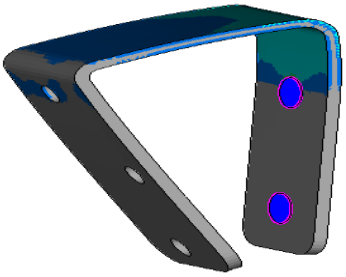

1st mode at 115 Hz

2nd mode at 169 Hz

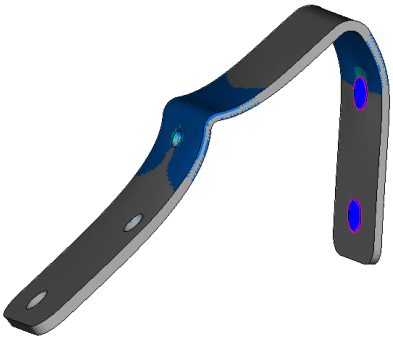

3rd mode at 285 Hz

4th mode at 510 Hz

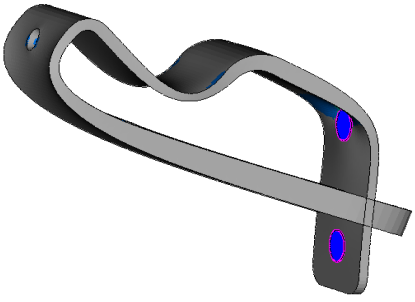

5th mode at 923 Hz

Figure 4.2 *Mode shapes of Component 1.*

4.1.2 Component 2

Model 2 is given below. This model is a bracket carrying a battery box. It has the same material properties as Component 1. The bracket is attached to the truck's frame from the holes as shown below. It has been meshed using 315832 second order tetra elements.

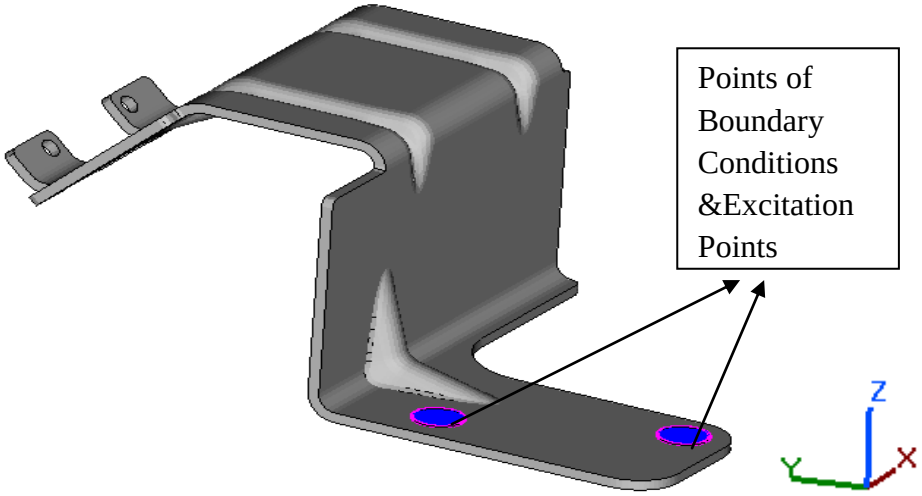

Figure 4.3 *Component 2.*

Results obtained from the normal modes analysis are given below.

Table 4.2 Natural frequencies and mode types of Component 2.

Frequency [Hz]	Mode type
97	Bending
164	Torsion + Bending
299	Torsion + Bending
368	Bending
715	Torsion + Bending

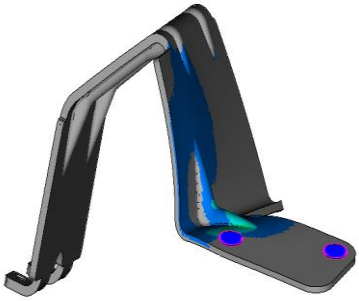

1st mode at 97 Hz

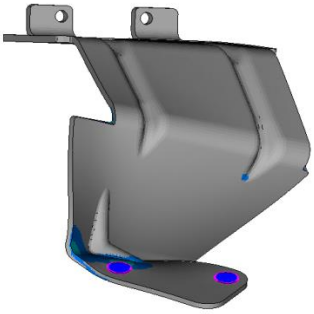

2nd mode at 164 Hz

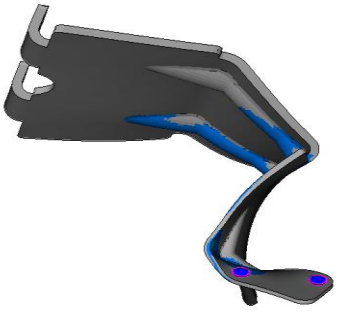

3rd mode at 299 Hz

4th mode at 368 Hz

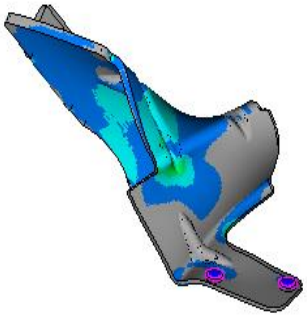

5th mode at 715 Hz

Figure 4.4 *Mode shapes of Component 2.*

4.1.3 Component 3

Model 3 is given below. This model is a bracket with concentrated mass as it is shown below. Material properties are: Young's modulus (E) = 75 GPa, Poison's ratio (ν) = 0.35 and density (ρ) = 2750 kg/m^3 and ξ = 0.05. The mesh consists of 76479 second order tetra elements.

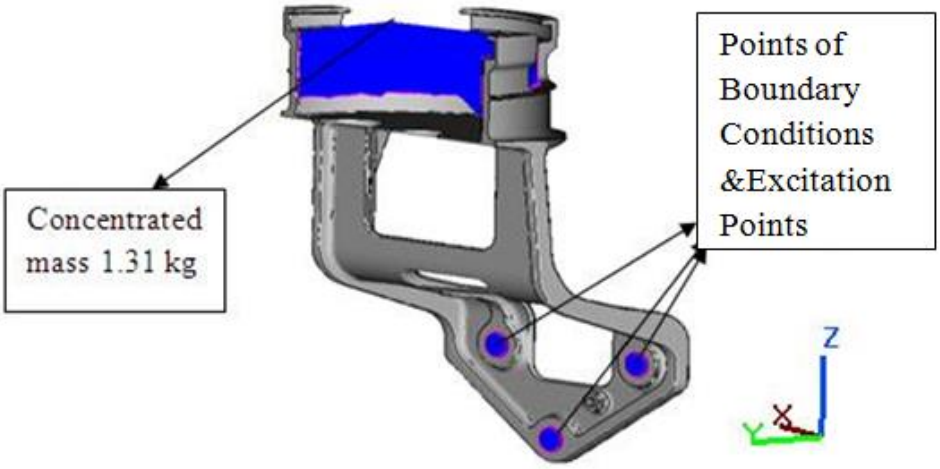

Figure 4.5 *Component 3.*

Results obtained from the normal modes analysis are given below.

Table 4.3 Natural frequencies and mode types of Component 3.

Frequency [Hz]	Mode type
35	Bending
110	Torsion + Bending
237	Bending
417	Torsion + Bending
791	Torsion + Bending
880	Torsion + Bending

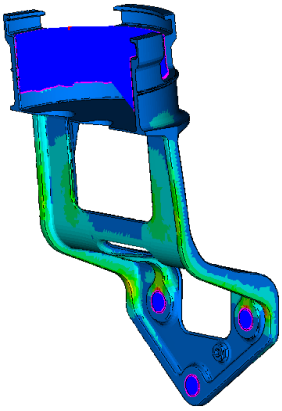

1st mode at 35 Hz

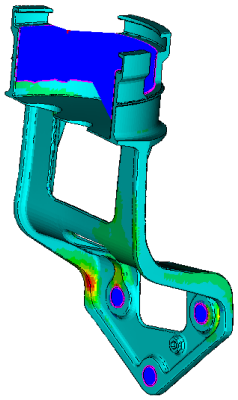

2nd mode at 110 Hz

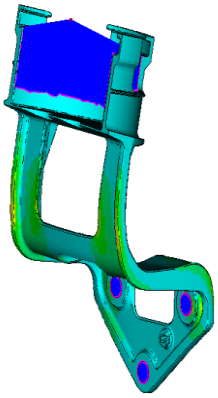

3rd mode at 237 Hz

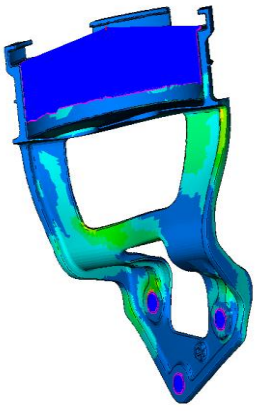

4th mode at 417 Hz

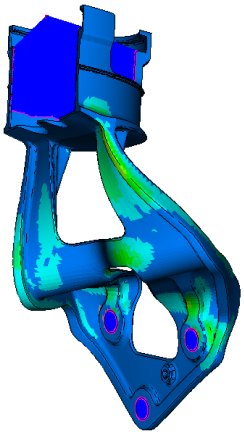

5th mode at 791 Hz

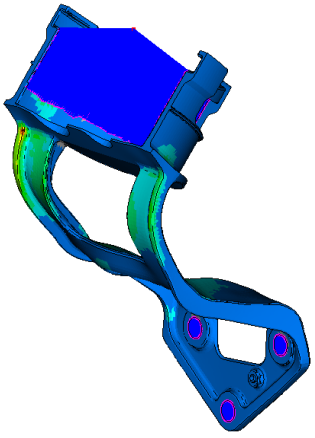

6th mode at 880 Hz

Figure 4.6 *Mode shapes of Component 3.*

4.1.4 Component 4

This model is a larger version of Component 3 with the same material properties. The mesh used consists of 157415 second order tetras.

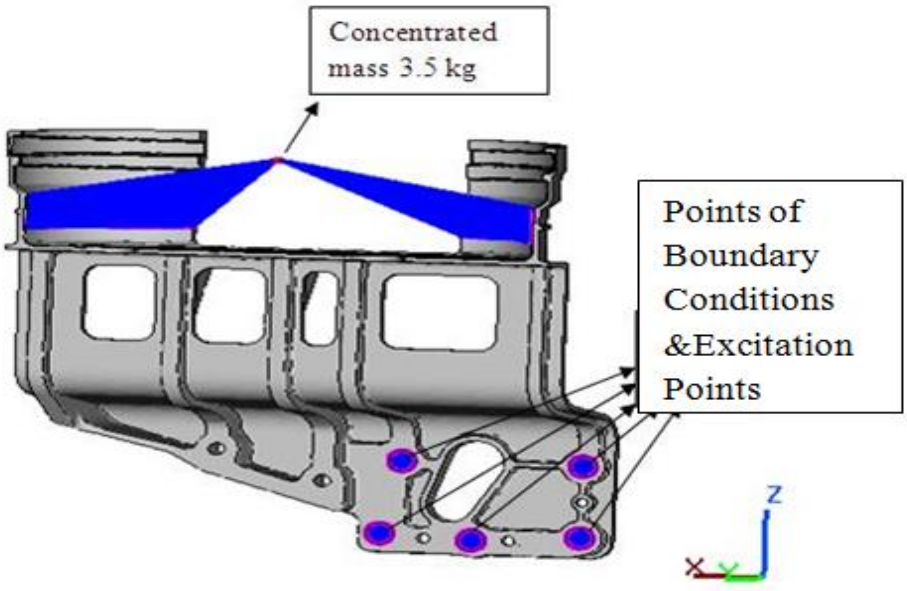

Figure 4.7 *Component 4.*

Results obtained from the normal modes analysis are given below.

Table 4.4 Natural frequencies and mode types of Component 4.

Frequency [Hz]	Mode type
31	Bending
107	Torsion + Bending
239	Bending
285	Torsion + Bending
553	Torsion + Bending
873	Torsion + Bending

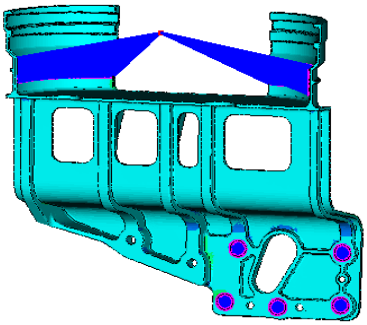

1st mode at 31 Hz

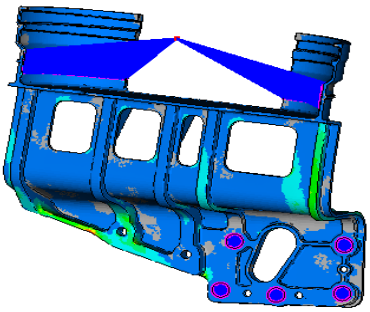

2nd mode at 107 Hz

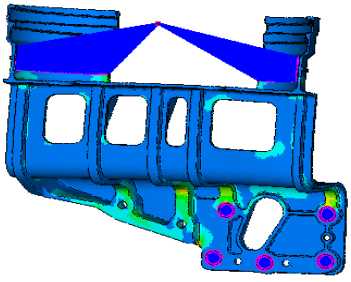

3rd mode at 239 Hz

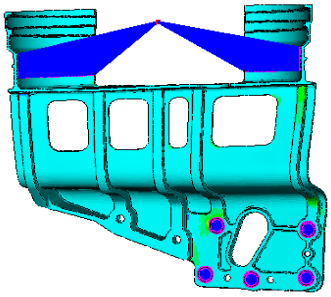

4th mode at 285 Hz

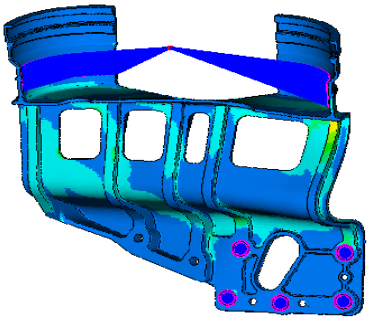

5th mode at 553 Hz

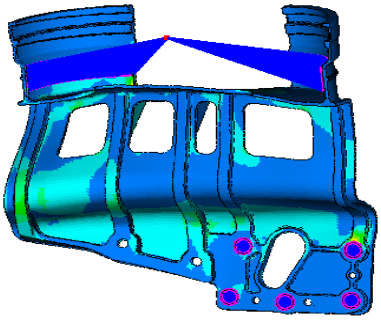

6th mode at 873 Hz

Figure 4.8 *Mode shapes of Component 4.*

4.1.5 Determining Hot Spots Using Metapost

The hot spots for the first bracket have been selected such that they are subjected to high stress at different modes of vibrations and also they are located in different planes in order to check the accuracy of the methods. The following hot spots are selected for the first component and some have already been shown in previous chapters for other components;

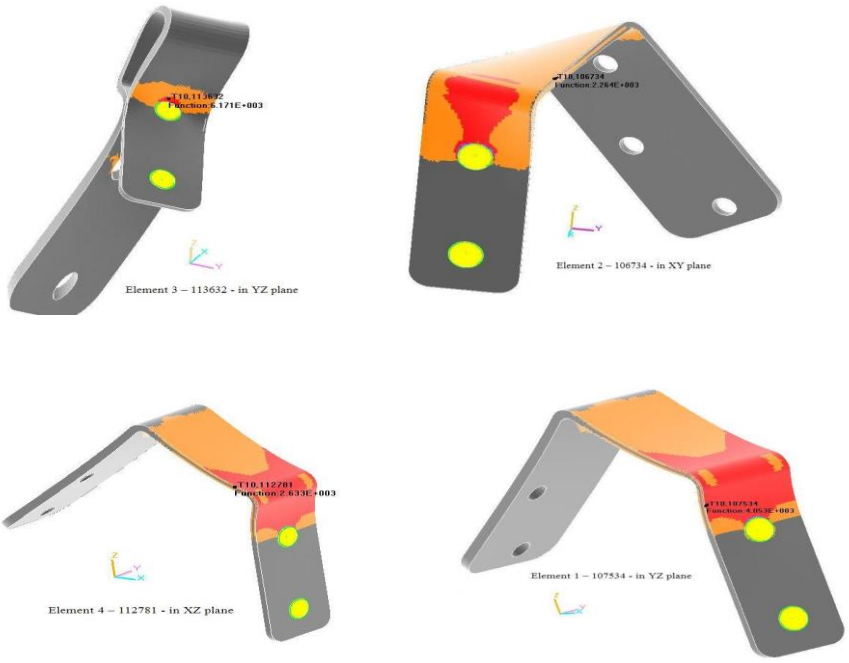

Figure 4.9 *Demonstration of four hot spots by Metapost for Component 1.*

The same analysis has been performed for all 4 components to obtain the critical points of them. Thus, the further results for Swept Sinusoidal in addition to the Random vibration analyses will be shown for such hot spots in this chapter as well as in the Appendix.

4.2 Swept Sinusoidal Simulation Results

Models have been excited with swept sinusoidal excitations uniaxially in X, Y and Z directions and multiaxially considering different phase combinations. Phase difference used is 180 degrees. The output has been requested for 10 elements located at the different parts of the brackets.

Only results for 3 elements have been given, results for the rest of the elements can be found in the appendix. Maximum peak values for uniaxial and multiaxial excitations are given in bold font.

4.2.1 Component 1

Swept sinusoidal results for Component 1 are given below.

In the tables given below the maximum peak values are presented together with the frequencies at which they occur. The quotients between the uniaxial and the multiaxial excitations are also given. These quotients give an idea about how much the uniaxial excitation is close to the multiaxial one. The most interesting quotients are the ones between the maximum uniaxial and the all multiaxial combinations.

Table 4.5 Peak values for Component 1 element no:107534.

Element No:107534 **Located at yz-plane**	**Max. Peak Amplitude**		**XYZ/X**	**X'YZ/ X**	**Y'XZ/ X**	**Z'XY/ X**
	MPa	frequency [Hz]	1.02	2.57	1.02	2.57
X-direction	10.01	115	XYZ/Y	X'YZ/Y	Y'XZ/Y	Z'XY/Y
Y-direction	7.44	169	1.38	3.46	1.38	3.46
Z-direction	**15.73**	**115**	XYZ/Z	X'YZ/Z	Y'XZ/Z	Z'XY/Z
XYZ-in-phase	10.23	284	0.65	1.64	0.65	1.64
X-out of phase, YZ-in-phase (X'YZ)	25.73	115	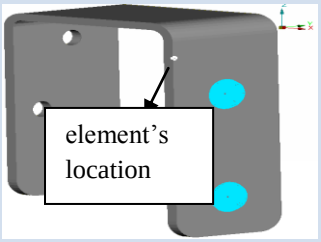			
Y-out of phase, XZ-in-phase (Y'XZ)	10.26	284				
Z-out of phase, XY-in-phase (Z'XY)	**25.75**	**115**				

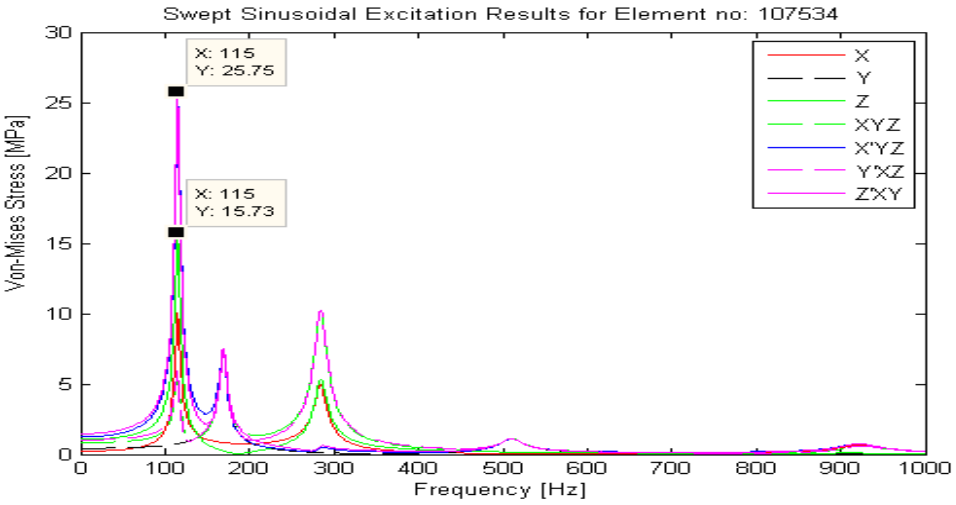

Figure 4.10 *Maximum peak values for element no: 107534.*

Table 4.6 Peak values for Component 1 element no:105337.

Element No:105337 **Located at yz-plane**	**Max. Peak Amplitude**		**XYZ/X**	**X'YZ/X**	**Y'XZ/X**	**Z'XY/X**
	MPa	frequency [Hz]	1.33	2.57	1.32	2.57
X-direction	8.82	115	XYZ/Y	X'YZ/Y	Y'XZ/Y	Z'XY/Y
Y-direction	11.67	169	1.0	1.94	1.0	1.95
Z-direction	**13.86**	**115**	XYZ/Z	X'YZ/Z	Y'XZ/Z	Z'XY/Z
XYZ-in-phase	11.71	169	0.84	1.64	0.84	1.64
X-out of phase, YZ-in-phase (X'YZ)	22.69	115	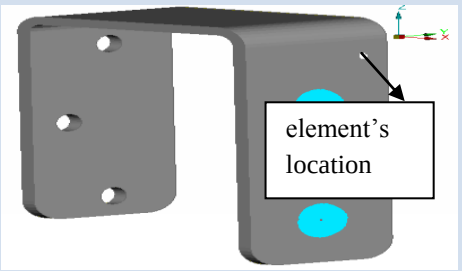			
Y-out of phase, XZ-in-phase (Y'XZ)	11.64	169				
Z-out of phase, XY-in-phase (Z'XY)	**22.71**	**115**				

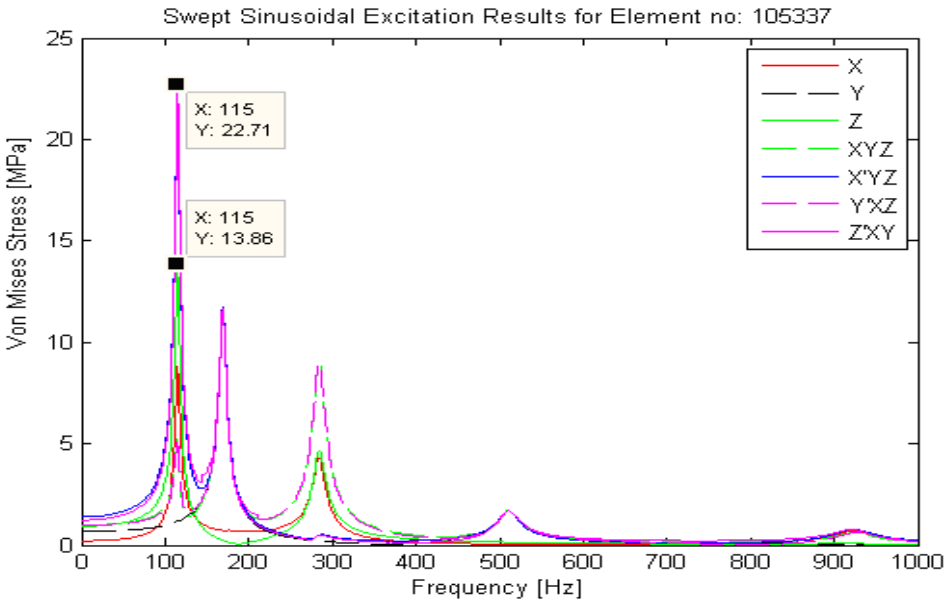

Figure 4.11 *Maximum peak values for element no: 105337.*

Table 4.7 Peak values for Component 1 element no:108891.

Element No:108891 **Located at xy-plane**	**Max. Peak Amplitude**		**XYZ/X**	**X'YZ/X**	**Y'XZ/X**	**Z'XY/X**
	MPa	frequency [Hz]	1.5	2.58	1.49	2.58
X-direction	8.56	115	XYZ/Y	X'YZ/Y	Y'XZ/Y	Z'XY/Y
Y-direction	12.77	169	1.0	1.73	1.0	1.73
Z-direction	**13.49**	**115**	XYZ/Z	X'YZ/Z	Y'XZ/Z	Z'XY/Z
XYZ-in-phase	12.8	169	0.95	1.64	0.94	1.64
X-out of phase, YZ-in-phase (X'YZ)	22.06	115	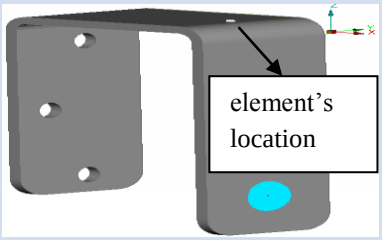			
Y-out of phase, XZ-in-phase (Y'XZ)	12.73	169				
Z-out of phase, XY-in-phase (Z'XY)	**22.09**	**115**				

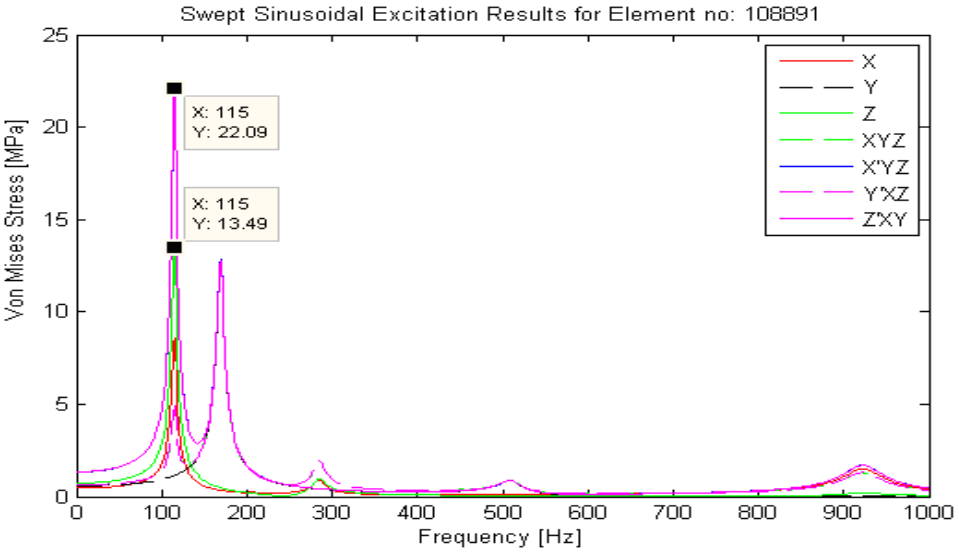

Figure 4.12 *Maximum peak values for element no: 108891.*

Looking at the tables given above and the ones given in the Appendix for Component 1 we can say that the most damaging uniaxial excitation is the one in the Z direction. It contributes to the first mode at 115 Hz. On the other hand the most effective multiaxial combination is the one in which the Z direction input is 180 degrees out of phase compared to the X and Y direction inputs (Z'XY). It also contributes to the first mode at 115 Hz. The ratio between the Z'XY excitation and Z excitation (Z'XY/Z) is 1.64. This means that if a uniaxial test is to be carried out with Z-direction excitation a safety margin of 1.64 should be used to account for the worst case real life scenario. It is good to mention that different sides of the parts are sensitive to different excitation directions. Therefore the results obtained from finite elements located at the different sides will differ. In order to make a generalization about the most effective direction the stress levels obtained from different sides can be compared. The excitation direction giving the highest stress level can be taken as the most effective one.

4.2.2 Component 2

Swept sinusoidal results for Component 2 are given below,

Table 4.8 Peak values for Component 2 element no: 95110.

Element No:95110 **Located at xy-plane**	**Max. Peak Amplitude**		**XYZ/X**	**X'YZ/X**	**Y'XZ/X**	**Z'XY/X**
	MPa	Freq [Hz]	0.35	1.65	2.56	3.2
X-direction	16.91	164	XYZ/Y	X'YZ/Y	Y'XZ/Y	Z'XY/Y
Y-direction	18.87	97	0.32	1.47	2.29	2.86
Z-direction	**29.74**	**97**	XYZ/Z	X'YZ/Z	Y'XZ/Z	Z'XY/Z
XYZ-in-phase	6.0	164	0.2	0.93	1.44	1.8
X-out of phase, YZ-in-phase (X'YZ)	27.83	164	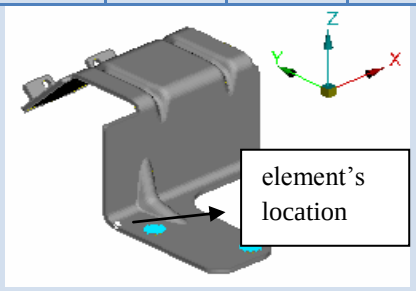			
Y-out of phase, XZ-in-phase (Y'XZ)	43.21	97				
Z-out of phase, XY-in-phase (Z'XY)	**54.03**	**97**				

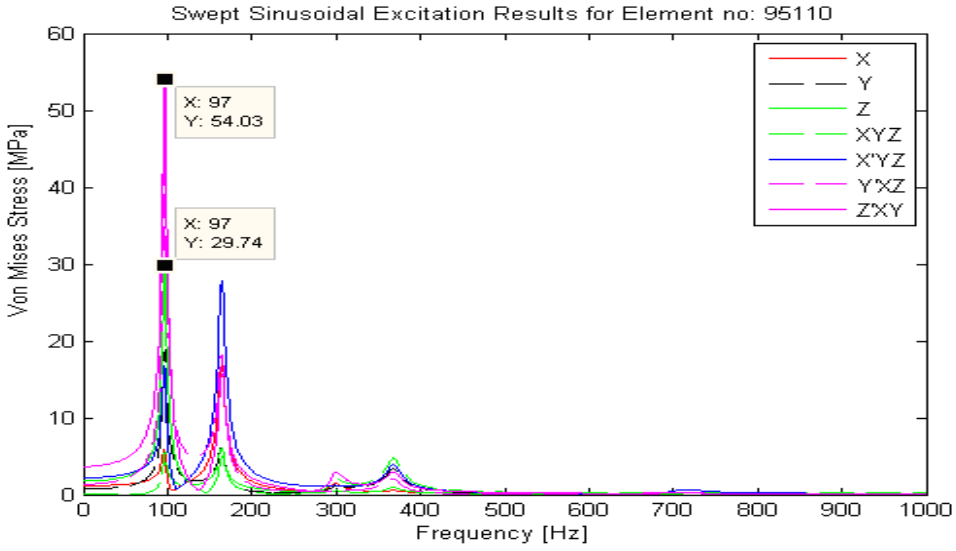

Figure 4.13 *Maximum peak values for element no: 95110.*

Table 4.9 Peak values for Component 2 element no: 87178.

Element No:87178 **Located at yz-plane**	**Max. Peak Amplitude**		**XYZ/X**	**X'YZ/X**	**Y'XZ/X**	**Z'XY/X**
	MPa	Freq [Hz]	0.42	1.65	2.47	3.07
X-direction	13.2	164	XYZ/Y	X'YZ/Y	Y'XZ/Y	Z'XY/Y
Y-direction	14.16	97	0.39	1.54	2.29	2.86
Z-direction	**22.32**	**97**	XYZ/Z	X'YZ/Z	Y'XZ/Z	Z'XY/Z
XYZ-in-phase	5.56	368	0.42	0.97	1.45	1.82
X-out of phase, YZ-in-phase (X'YZ)	21.74	164	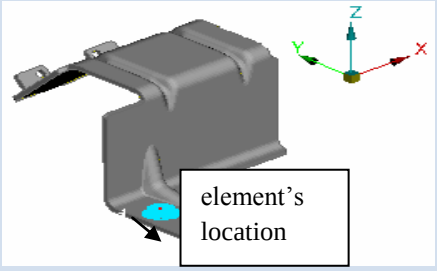			
Y-out of phase, XZ-in-phase (Y'XZ)	32.42	97				
Z-out of phase, XY-in-phase (Z'XY)	**40.55**	**97**				

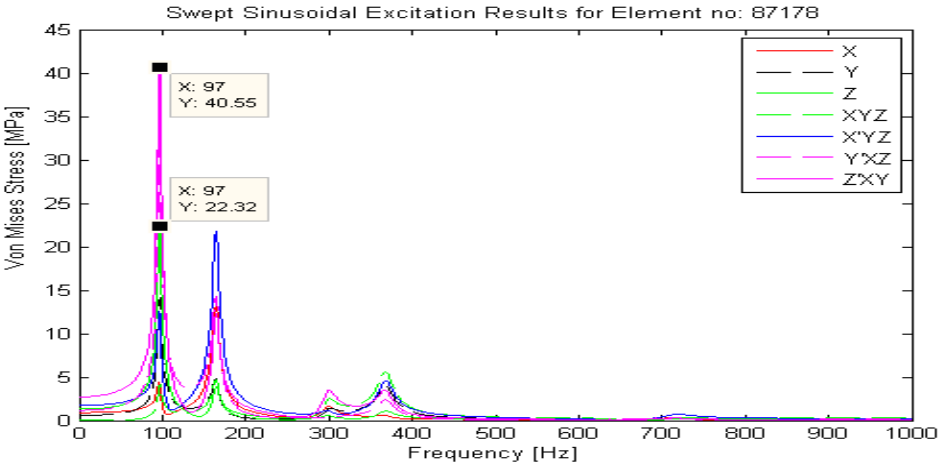

Figure 4.14 *Maximum peak values for element no:87178.*

Table 4.10 Peak values for Component 2 element no: 88125.

Element No:88125 **Located at xz-plane**	**Max. Peak Amplitude**		**XYZ/X**	**X'YZ/X**	**Y'XZ/X**	**Z'XY/X**
	MPa	Freq [Hz]	0.35	1.65	1.08	0.97
X-direction	**15.27**	**164**	XYZ/Y	X'YZ/Y	Y'XZ/Y	Z'XY/Y
Y-direction	5.53	164	0.98	4.55	2.97	2.67
Z-direction	8.12	97	XYZ/Z	X'YZ/Z	Y'XZ/Z	Z'XY/Z
XYZ-in-phase	5.4	164	0.67	3.1	2.02	1.82
X-out of phase, YZ-in-phase (X'YZ)	**25.15**	**164**	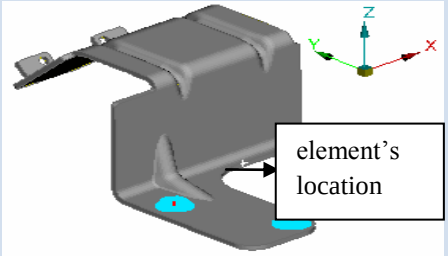			
Y-out of phase, XZ-in-phase (Y'XZ)	16.44	164				
Z-out of phase, XY-in-phase (Z'XY)	14.77	97				

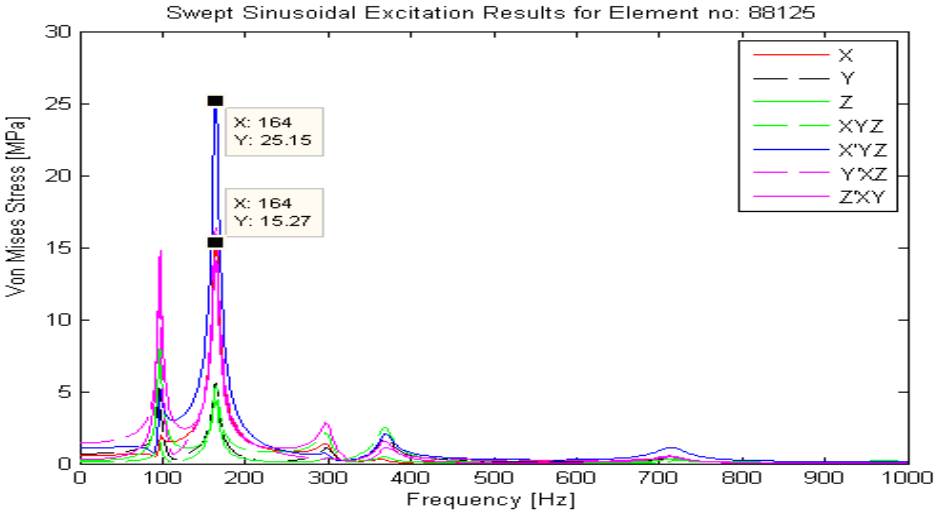

Figure 4.15 *Maximum peak values for element no: 88125.*

In this model it can be seen by looking at the results shown above and in the Appendix that elements located at the different sides of the bracket are sensitive to different directions. The highest stress level in elements 95110 and 87178 occurs at the Z direction excitation while in element 88125 we have the highest stress level at the X direction excitation. If a most damaging test direction is to be suggested it should be the Z direction since the stress level is higher. Another fact is that the Z direction excitation always contributes to the first mode at 97 Hz while the X direction excitation contributes to the second mode at 164 Hz. The Y direction excitation shows different characteristics compared to the X and Z direction excitations. It contributes for the first, second and fourth mode at 97 Hz, 164 Hz and 368 Hz respectively. For multiaxial combinations we have the worst case when the Z direction excitation is 180 degrees out of phase compared to the X and Y direction excitations (Z'XY). The safety margin between Z'XY and Z is 1.8-1.82.

4.2.3 Component 3

Swept sinusoidal results for Component 3 are given below,

Table 4.11 Peak values for Component 3 element no: 5521.

Element No:5521 **Located at xy-plane**	**Max. Peak Amplitude**		**XYZ/X**	**X'YZ/X**	**Y'XZ/X**	**Z'XY/X**
	MPa	Freq [Hz]	1.17	1.5	2.72	2.4
X-direction	4.9	110	XYZ/Y	X'YZ/Y	Y'XZ/Y	Z'XY/Y
Y-direction	**9.54**	**35**	0.6	0.77	1.4	1.23
Z-direction	3	35	XYZ/Z	X'YZ/Z	Y'XZ/Z	Z'XY/Z
XYZ-in-phase	5.75	35	1.92	2.45	4.45	3.92
X-out of phase, YZ-in-phase (X'YZ)	7.35	35	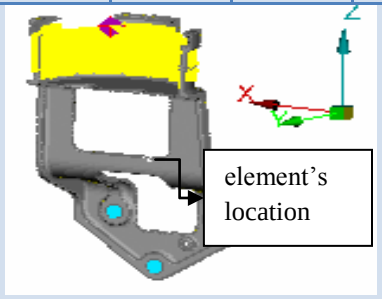			
Y-out of phase, XZ-in-phase (Y'XZ)	**13.34**	**35**				
Z-out of phase, XY-in-phase (Z'XY)	11.76	35				

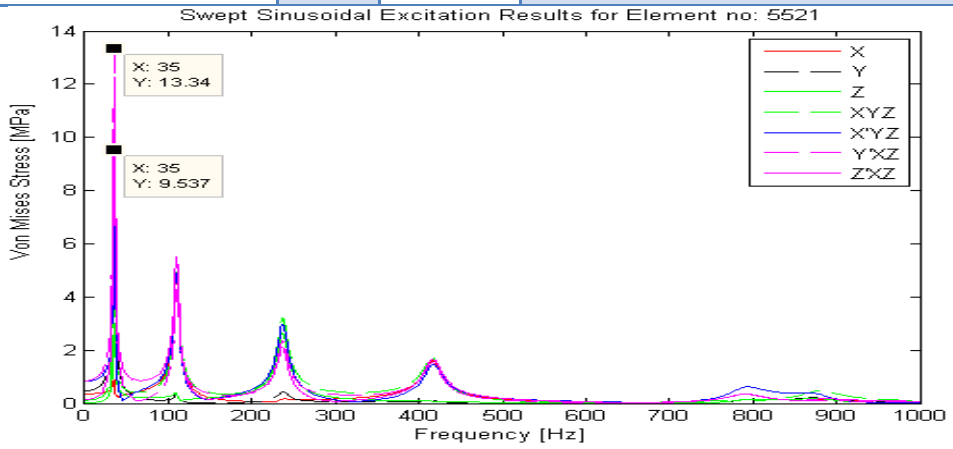

Figure 4.16 *Maximum peak values for element no: 5521.*

Table 4.12 Peak values for Component 3 element no: 28366.

Element No:28366 **Located at xz-plane**	**Max. Peak Amplitude**		**XYZ/X**	**X'YZ/X**	**Y'XZ/X**	**Z'XY/X**
	MPa	Freq [Hz]	1.42	1.8	3.3	2.92
X-direction	37.93	110	XYZ/Y	X'YZ/Y	Y'XZ/Y	Z'XY/Y
Y-direction	**89.64**	**35**	0.6	0.76	1.4	1.23
Z-direction	28.39	35	XYZ/Z	X'YZ/Z	Y'XZ/Z	Z'XY/Z
XYZ-in-phase	53.98	35	1.9	2.41	4.42	3.9
X-out of phase, YZ-in-phase (X'YZ)	68.34	35	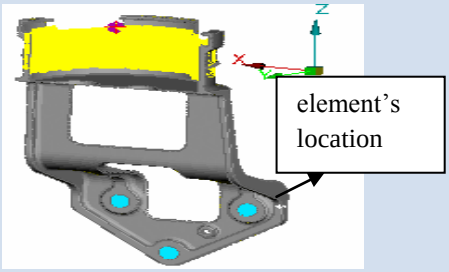			
Y-out of phase, XZ-in-phase (Y'XZ)	**125.4**	**35**				
Z-out of phase, XY-in-phase (Z'XY)	110.7	35				

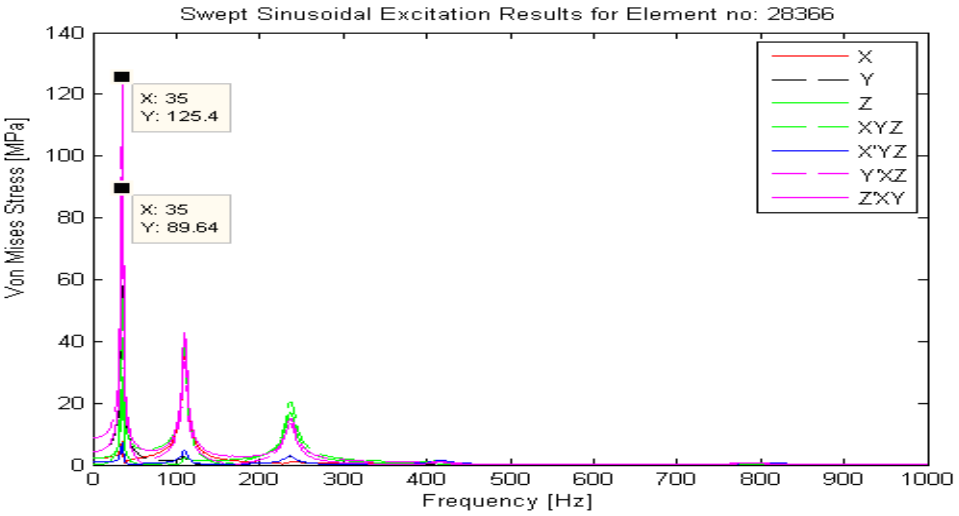

Figure 4.17 *Maximum peak values for element no: 28366.*

Table 4.13 Peak values for Component 3 element no: 25941.

Element No:25941 **Located at yz-plane**	**Max. Peak Amplitude**		**XYZ/X**	**X'YZ/X**	**Y'XZ/X**	**Z'XY/X**
	MPa	Freq [Hz]	1.52	1.92	3.51	3.12
X-direction	34.59	110	XYZ/Y	X'YZ/Y	Y'XZ/Y	Z'XY/Y
Y-direction	**87.1**	**35**	0.61	0.76	1.39	1.24
Z-direction	27.58	35	XYZ/Z	X'YZ/Z	Y'XZ/Z	Z'XY/Z
XYZ-in-phase	52.71	35	1.91	2.41	4.41	3.91
X-out of phase, YZ-in-phase (X'YZ)	66.41	35	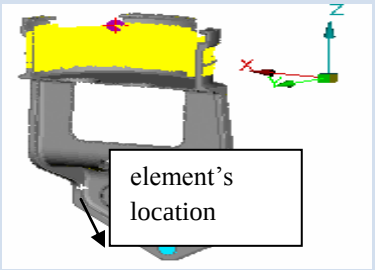			
Y-out of phase, XZ-in-phase (Y'XZ)	**121.5**	**35**				
Z-out of phase, XY-in-phase (Z'XY)	107.9	35				

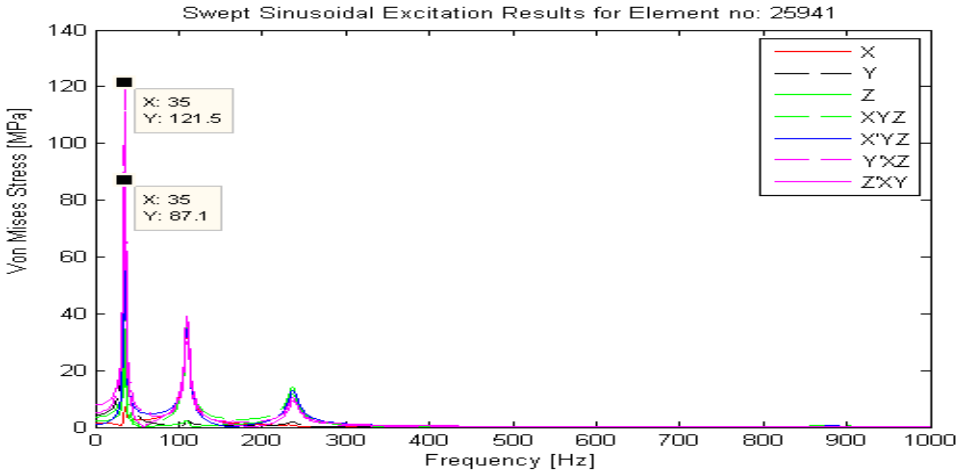

Figure 4.18 *Maximum peak values for element no: 25941.*

For this part it can be easily said that the most damaging uniaxial direction is Y and the most effective multiaxial combination is the one in which the Y direction excitation is 180 degrees out of phase compared to the X and Z direction excitations (Y'XZ). It is seen that except for the X direction excitation case the first mode at 35 Hz is active. In the X direction excitation the second mode is active at 110 Hz. The safety margin between Y'XZ and Y is 1.39-1.40.

4.2.4 Component 4

Swept sinusoidal results for Component 4 are given below.

Table 4.14 Peak values for Component 4 element no: 121014.

Element No:121014 **Located at xy-plane**	**Max. Peak Amplitude**		**XYZ/X**	**X'YZ/X**	**Y'XZ/X**	**Z'XY/X**
	MPa	Freq [Hz]	1.97	3.33	6.24	4.88
X-direction	11.66	107	XYZ/Y	X'YZ/Y	Y'XZ/Y	Z'XY/Y
Y-direction	**47.84**	**31**	0.48	0.81	1.52	1.19
Z-direction	17	31	XYZ/Z	X'YZ/Z	Y'XZ/Z	Z'XY/Z
XYZ-in-phase	22.95	31	1.35	2.28	4.28	2.48
X-out of phase, YZ-in-phase (X'YZ)	38.78	31	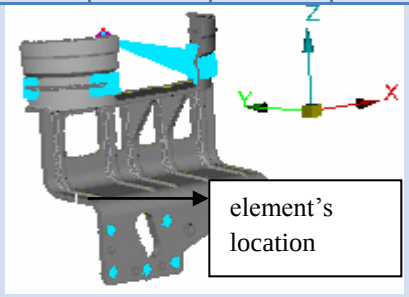			
Y-out of phase, XZ-in-phase (Y'XZ)	**72.75**	**31**				
Z-out of phase, XY-in-phase (Z'XY)	56.92	31				

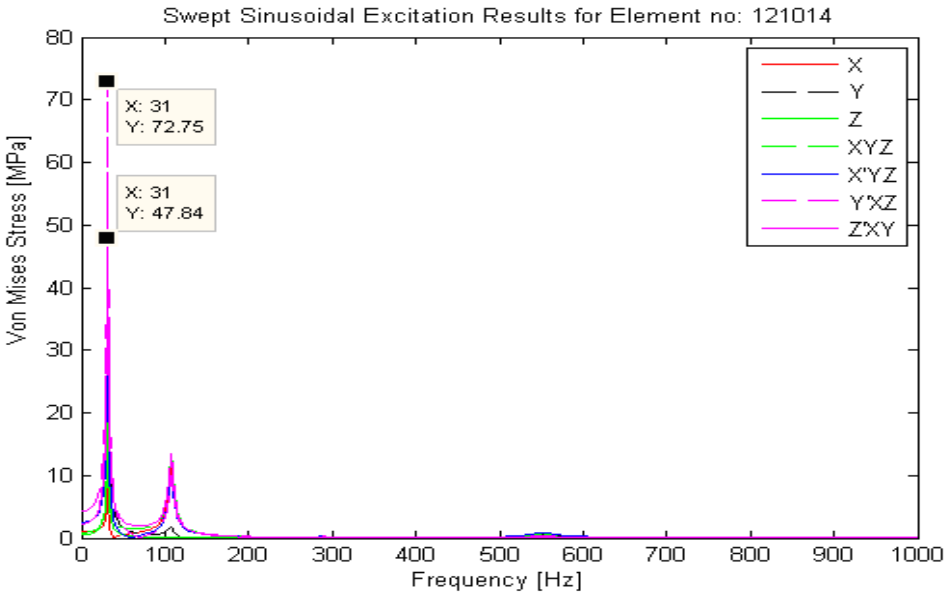

Figure 4.19 *Maximum peak values for element no: 121014.*

Table 4.15 Peak values for Component 4 element no:12666.

Element No:12666 **Located at xz-plane**	**Max. Peak Amplitude**		**XYZ/X**	**X'YZ/X**	**Y'XZ/X**	**Z'XY/X**
	MPa	Freq [Hz]	1.79	3.02	5.64	4.41
X-direction	15.07	107	XYZ/Y	X'YZ/Y	Y'XZ/Y	Z'XY/Y
Y-direction	**56**	**31**	0.48	0.81	1.52	1.19
Z-direction	19.76	31	XYZ/Z	X'YZ/Z	Y'XZ/Z	Z'XY/Z
XYZ-in-phase	26.97	31	1.36	2.3	4.3	3.36
X-out of phase, YZ-in-phase (X'YZ)	45.54	31	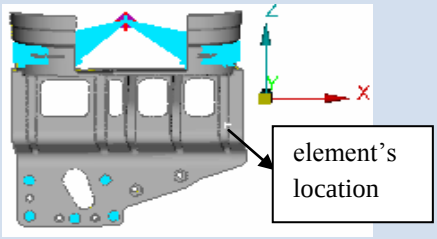			
Y-out of phase, XZ-in-phase (Y'XZ)	**85.03**	**31**				
Z-out of phase, XY-in-phase (Z'XY)	66.48	31				

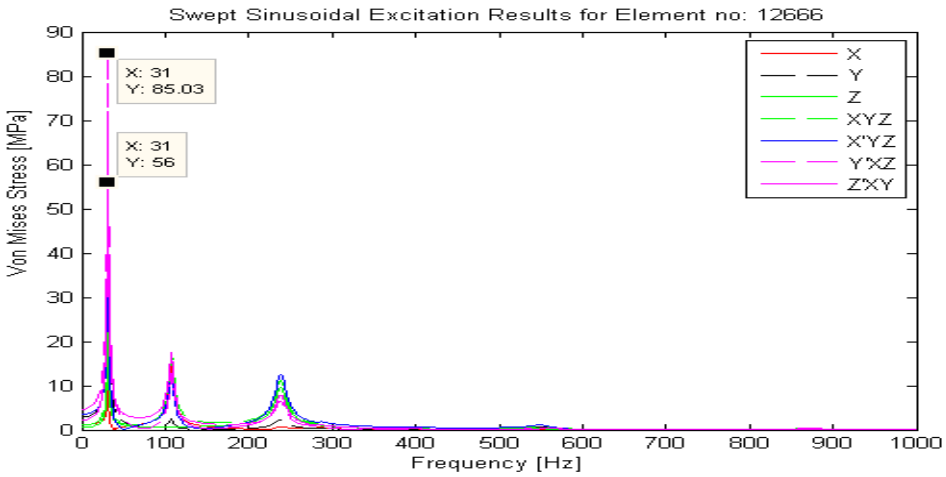

Figure 4.20 *Maximum peak values for element no: 12666.*

Table 4.16 Peak values for Component 4 element no: 33081.

Element No:33081 **Located at yz-plane**	**Max. Peak Amplitude**		**XYZ/X**	**X'YZ/X**	**Y'XZ/X**	**Z'XY/X**
	MPa	Freq [Hz]	1.67	2.82	5.27	4.12
X-direction	11.43	107	XYZ/Y	X'YZ/Y	Y'XZ/Y	Z'XY/Y
Y-direction	**39.63**	**31**	0.48	0.81	1.52	1.19
Z-direction	14	31	XYZ/Z	X'YZ/Z	Y'XZ/Z	Z'XY/Z
XYZ-in-phase	19.07	31	1.36	1.69	4.3	3.36
X-out of phase, YZ-in-phase (X'YZ)	32.23	31	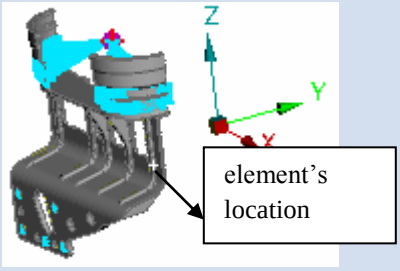			
Y-out of phase, XZ-in-phase (Y'XZ)	**60.2**	**31**				
Z-out of phase, XY-in-phase (Z'XY)	47.05	31				

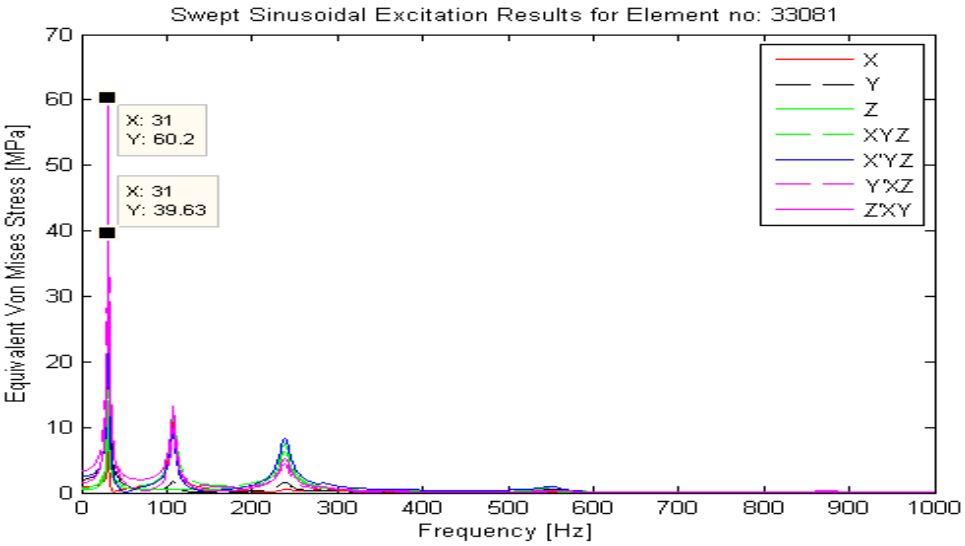

Figure 4.21 *Maximum peak values for element no: 33081.*

This part shows very similar characteristics to the previous part. Again the most effective uniaxial and multiaxial directions are Y and Y'XZ respectively. The ratio between these two is 1.5-1.53. The X direction excitation contributes to the second mode at 107 Hz while the other excitations contribute to the first mode at 31 Hz.

4.3 Random Excitations Results

In this section, the results of Random excitations for three uniaxial, X, Y and Z, excitations as well as the multiaxial loading of all excitations will be presented in detail. In Chapter 3.2 this procedure was explained by exciting the first bracket in X direction and the results for hot spot 107534 were shown in detail. In this section, the results for the excitation in other directions will be presented for the hotspots selected for the first model. Moreover, the results for the other components will be presented in tables in this chapter.

4.3.1 Performing Modal Frequency Response Analysis

According to FRA, the outputs of MD-Nastran can be PSD estimate of any stress component of a stress tensor. Before in Chapter 3.2, the figure of PSD σ_x for element 107534 which was obtained by exciting the bracket in all three uniaxial excitations, were presented. As it is apparent from Figure 4.9 this element is located in the YZ plane. Figure 4.22-Figure 4.24 show the PSD estimate of biaxial stress components,$\sigma_y,\ \sigma_z\ and\ \tau_{yz}$, regarding to all uniaxial excitations as well as the multiaxial excitation;

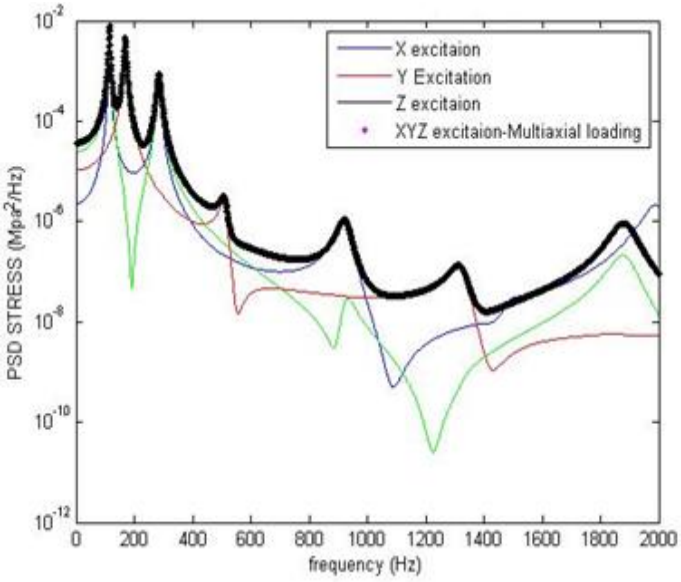

Figure 4.22 *PSD estimate of Normal Y stress, σ_y, under uniaxial and multiaxial excitation-element 107534.*

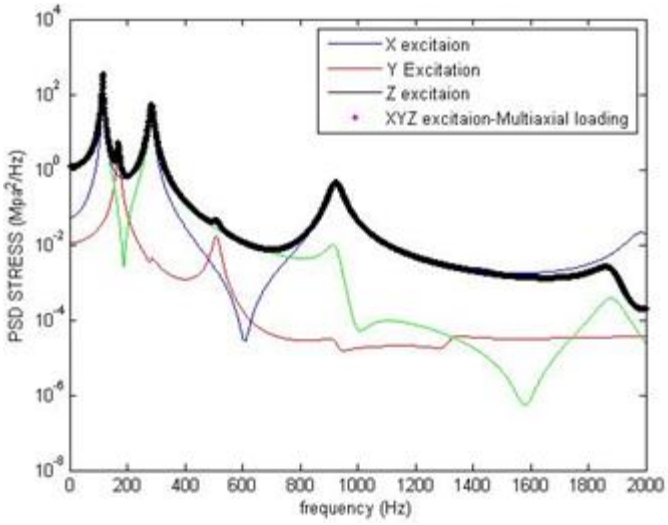

Figure 4.23 *PSD estimate of Normal Z stress, σ_z, under uniaxial and multiaxial excitation-element 107534.*

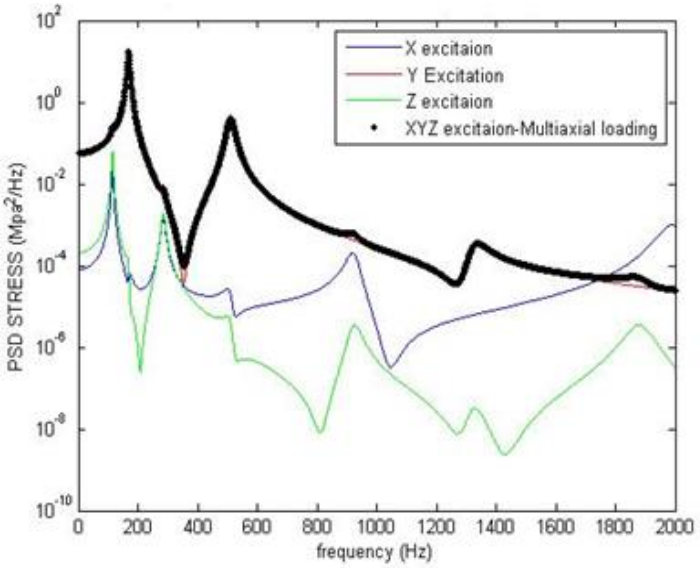

Figure 4.24 *PSD estimate of Shear stress, τ_{yz}, under uniaxial and multiaxial excitation-element 107534.*

As it is apparent from the above figures, the PSD estimates of stress tensor components under multiaxial excitation is superposed by PSD values of contributing stress components due to uniaxial excitations. Despite the fact that these results have been obtained directly by MD-Nastran, Eq. (3.10) can be used to combine the results obtained from the uniaxial excitations to get the multiaxial results.

4.3.2 Equivalent von Mises Stress Results

In this part the results of E.V.S calculations will be presented together with the results of M.P.S calculations where the stress tensor is extracted at the angle corresponding to the max RMS value.

- Calculating the Equivalent von Mises stress (E.V.S) and its verification by the maximum principal stress (M.P.S)

- Comparing the E.V.S under Different Excitations

4.3.2.1 Calculating the Equivalent von Mises Stress and its Verification by M.P.S.

The following results have been provided for the four given hot spots specified at Figure 4.9 and the results for the other hotspots are summarized within a table in the Appendix.

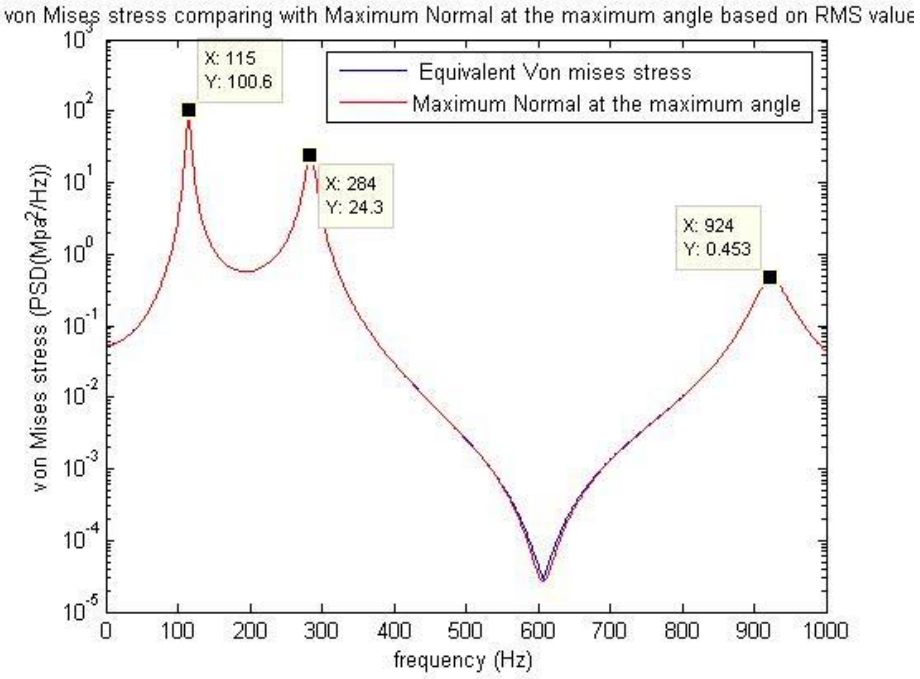

Figure 4.25 *Comparing E.V.S stress and M.P.S in element 107534 - X excitation.*

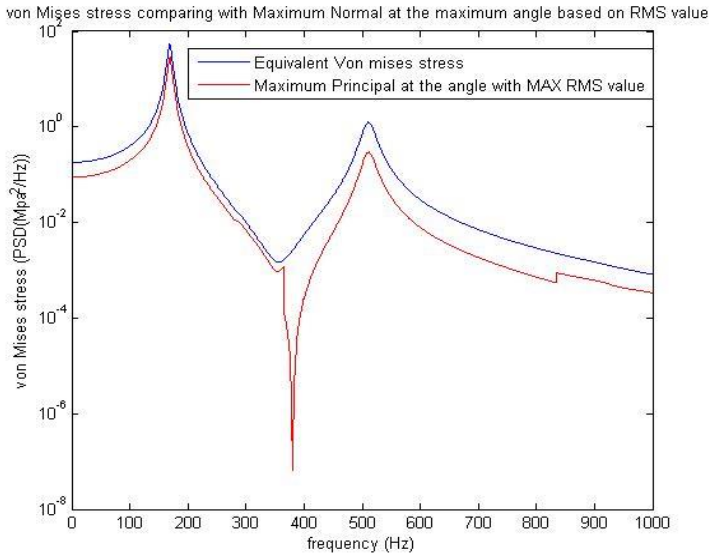

Figure 4.26 *Comparing E.V.S stress and M.P.S in element 107534 - Y excitation.*

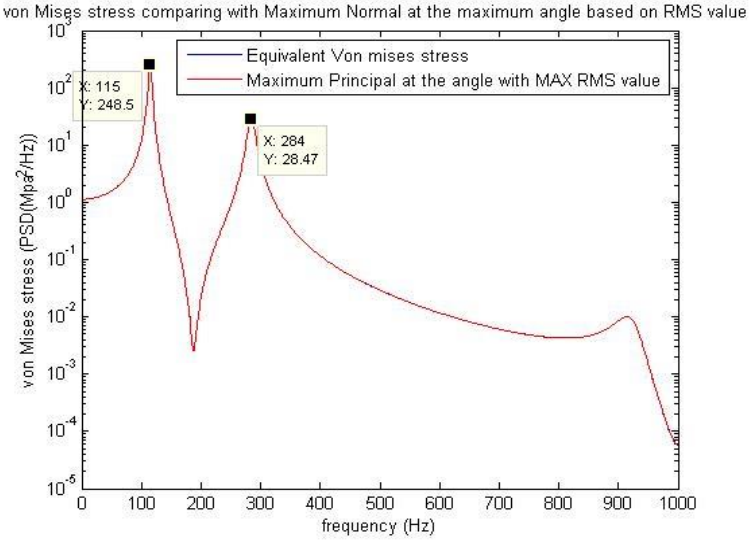

Figure 4.27 *Comparing E.V.S stress and M.P.S in element 107534 - Z excitation.*

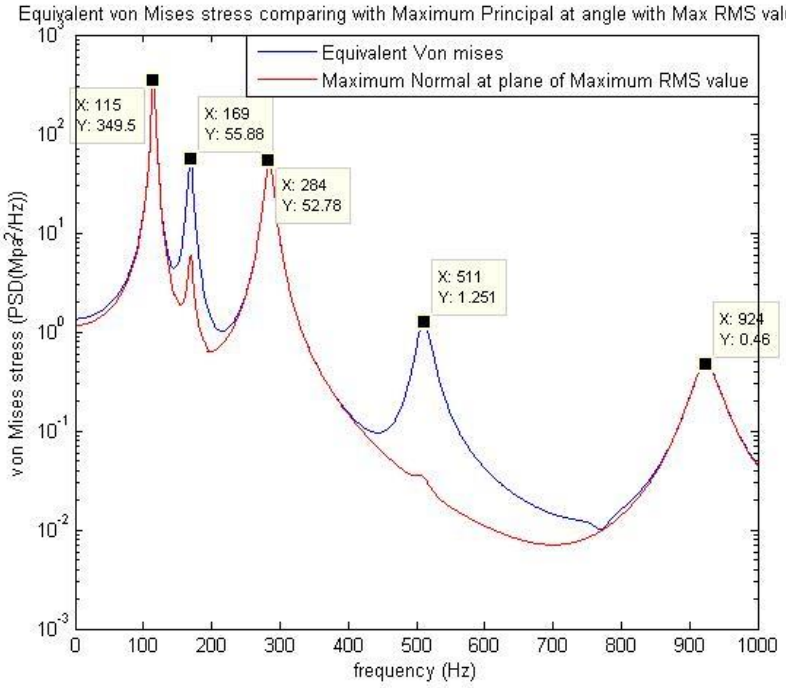

Figure 4.28 *Comparing E.V.S stress and M.P.S in element 107534 - Multiaxial excitation.*

As it is apparent from Figure 4.28, the specified peak values in multiaxial excitation are larger than all uniaxial excitations. However the figure shows some big gaps between E.V.S and M.P.S at the second and forth modes of vibration even though the peak values are quite the same. The reason is that, as it is apparent from the figure, the M.P.S in this figure has been plotted at the plane in which the RMS value is Maximum, $\theta = 90^{\circ}$, thus it doesn't take the rotation of the direction of the M.P.S at different modes into account. In order to verify the above statement, the E.V.S at the following figure has been compared with M.P.S at the planes in which the second and fourth modes have also been activated.

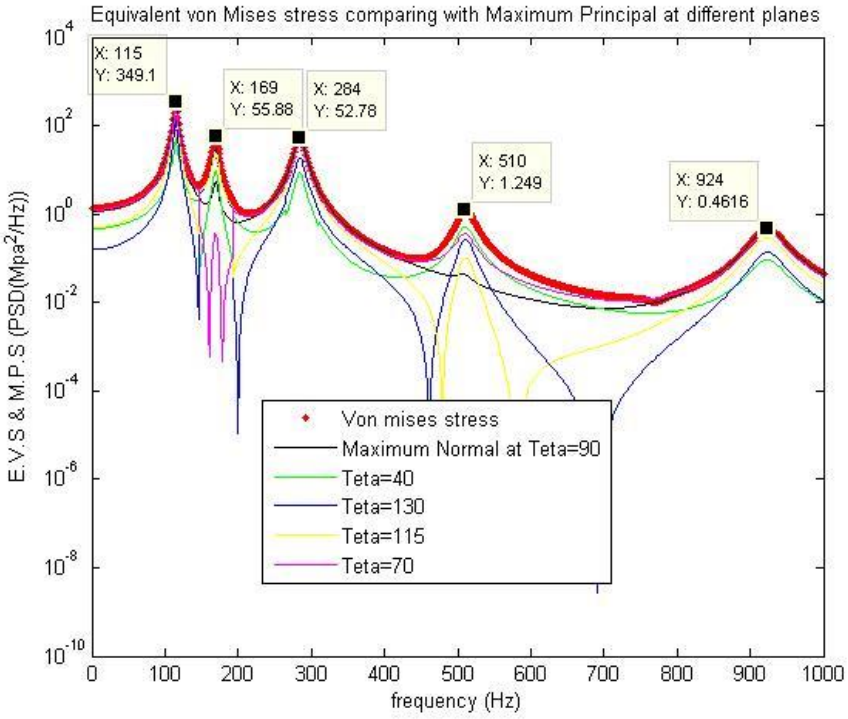

Figure 4.29 *Comparing E.V.S stress and M.P.S at several planes in element 107534 - multiaxial excitation.*

The above figure compares the E.V.S with M.P.S not only at plane in which the RMS value is maximum but also at the planes in which the second, fourth and fifth modes have been also taken into account. As it is apparent from the above figure, now the M.P.S can follow the E.V.S at second and fourth modes of vibration as well.

It is worthy of notice that the results of the M.P.S have been verified by using Metapost. The consequent results will be shown in the Appendix.

4.3.2.2 Comparing the E.V.M.S at Different Excitations

According to the above figure, dealing with the E.V.S is much simpler than M.P.S to compare the severity of different excitations because it is independent of direction. Thus, the E.V.S of all excitations can be easily

compared to the multiaxial loading. The result will be shown in the following figure:

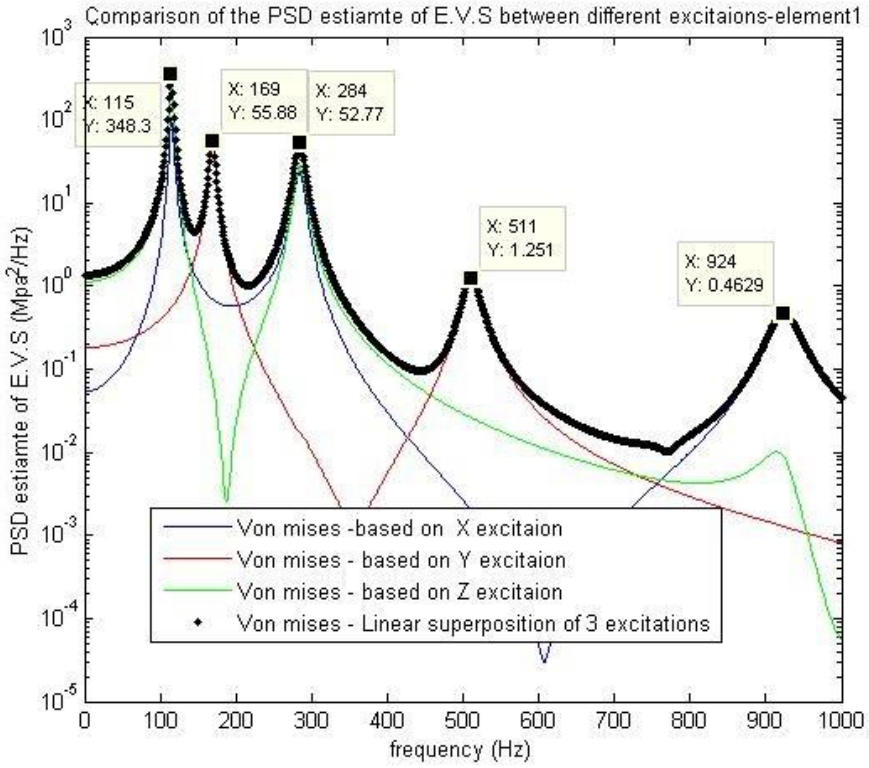

Figure 4.30 *Comparison of the PSD estimates of E.V.S under uniaxial and multiaxial excitations for element 107534.*

As it is apparent from the above figure, the multiaxial response of E.V.S can be estimated by linearly superposing the PSD of the responses of all contributing uniaxial excitations.

According to above mentioned results for the first hot spot, element 107534 which was specified at Figure 4.9, the following table can be represented to show the whole information obtained in this section. This table shows the comparison of the RMS value of the PSD estimate of E.V.S as well as the M.P.S for different excitations. Moreover, the direction of the M.P.S has

been shown by looking at the RMS values in addition to different modes of vibration.

Table 4.17 Comparison of the results for four excitations-Hot spot 1, 107534.

Hot Spot (1) - 107534 - Element(CTETRA)in YZ plane					
X Ex.	Y Ex.	Z Ex.	Mult.	Calculated Quantities	
38.44	19.71	53.89	66.64	RMS of M.P.S - Formula	RMS value of M.P.S and E.V.S (MPa)
38.49	12.31	53.89	66.66	RMS of M.P.S – Ansa	
38.44	28.04	53.91	71.73	RMS of E.V.S	
90	130	90	90	Based on RMS value- Ansa	$\theta\ of\ M.P.S$ (Degree)
90	128	90	91	Based on RMS value of transformation formula	
90	127	90	90	1st Mode	$\theta\ of\ M.P.S$ At different modes (Degree)
90	127	87	126	2nd Mode	
90	123	88	35	3rd Mode	
90	47	90	49	4th Mode	

The RMS value produced based on PSD estimate of stress components under different excitations can be compared easily with the RMS value for multiaxial excitations. The values have been verified by RMS value of M.P.S for each corresponding excitation. Moreover, the direction of the

principal stress can also be investigated by two methods; first by looking at the plane in which the RMS value is maximum and the second by looking at the direction at different modes of the vibration. Variation of values within each excitation shows the rotation of the principal stress at different modes. The red values show the dominating mode with the maximum RMS value of the PSD estimate of the M.P.S.

In total 17 different elements have been analyzed for the first bracket to statistically estimate the direction which has the most damage on the bracket. The following figures and tables show the results for the other 3 specified hot spots in Figure 4.9.

- For second hot spot, 106734:

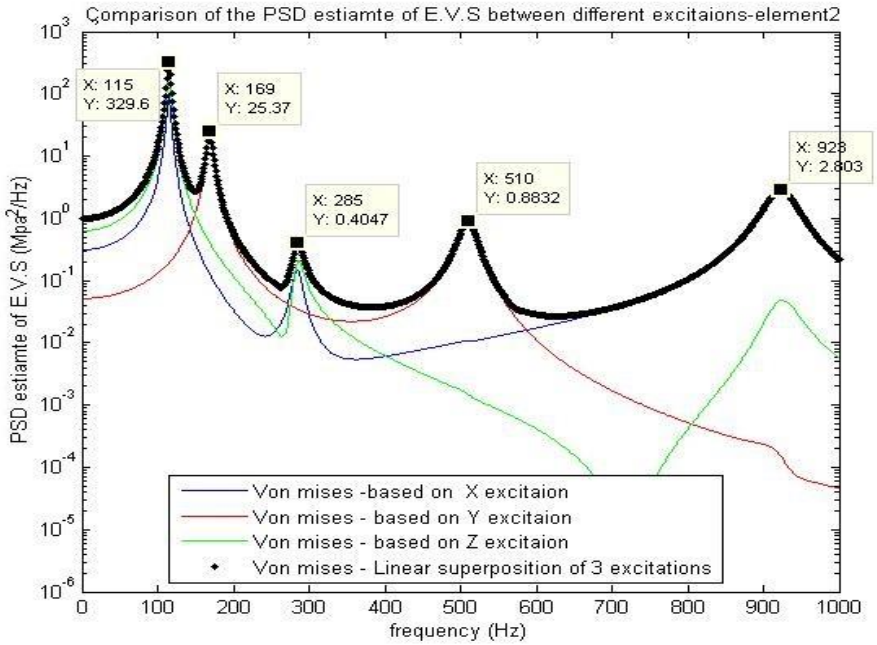

Figure 4.31 *Comparison of the PSD estimates of E.V.S under uniaxial and multiaxial excitations for hot spot 106734.*

Table 4.18 Comparison of the results for four excitations-Hot spot 2, 106734.

Hot Spot (2) - 106734 - Volume Element(CTETRA) in XY plane					
X Ex.	Y Ex.	Z Ex.	Mult.	Calculated Quantities	
32.41	11.27	46.34	56.70	RMS of M.P.S - Formula	RMS value of M.P.S and E.V.S (MPa)
			56.85	RMS of M.P.S – Ansa	
32.41	19.27	46.33	59.63	RMS of E.V.S	
88	133	88	90	Based on RMS value of transformation formula	$\theta\ of\ M.P.S$ (Degree)
87	44	86	87	1st Mode	$\theta\ of\ M.P.S$ At different modes (Degree)
87	134	86	130	2nd Mode	
109	51	86	118	3rd Mode	
89	107	86	116	4th Mode	

- For third hot spot, 113632:

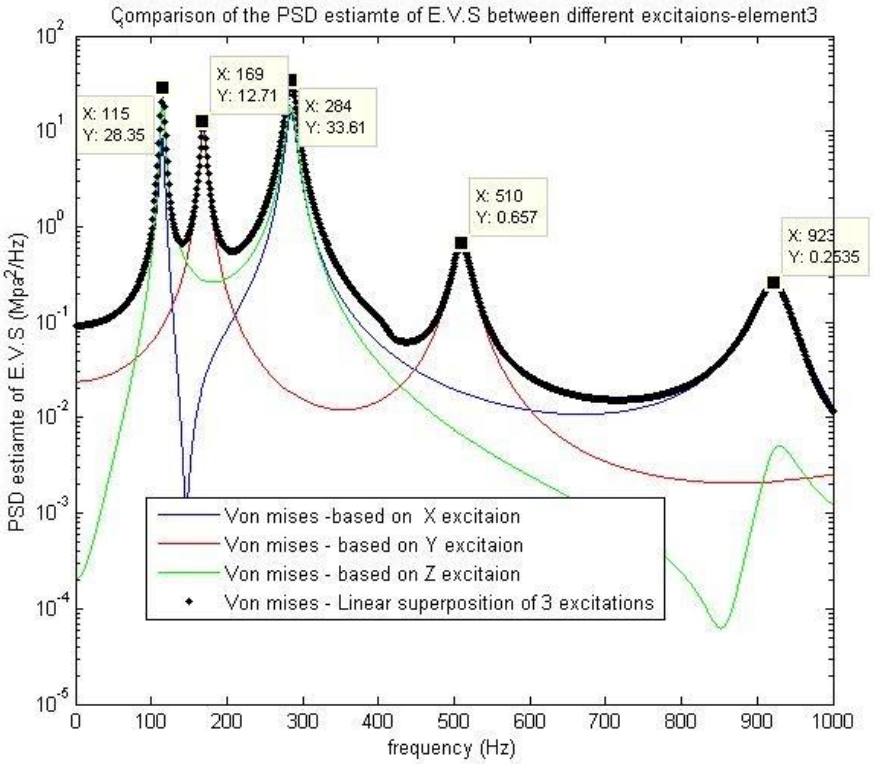

Figure 4.32 *Comparison of the PSD estimates of E.V.S under uniaxial and multiaxial excitations for hot spot 113632.*

Table 4.19 Comparison of the results for four excitations-Hot spot 3, 113632.

Hot Spot (3) - 113632 - Volume Element(CTETRA) in YZ plane					
X Ex.	Y Ex.	Z Ex.	Mult.	Calculated Quantities	
19.66	8.327	22.84	29.95	RMS of M.P.S - Formula	RMS value of M.P.S and E.V.S (MPa)
18.36	8.436	21.29	28.18	RMS of M.P.S – Ansa	
20.95	13.84	24.36	34.55	RMS of E.V.S	
160	40	160	160	Based on RMS value-Ansa	$\theta\ of\ M.P.S$ (Degree)
160	40	160	160	Based on RMS value of transformation formula	
160	40	160	167	1st Mode	$\theta\ of\ M.P.S$ At different modes (Degree)
160	39	17	37	2nd Mode	
160	130	160	160	3rd Mode	
160	130	160	36	4th Mode	

- For forth hot spot, 112781:

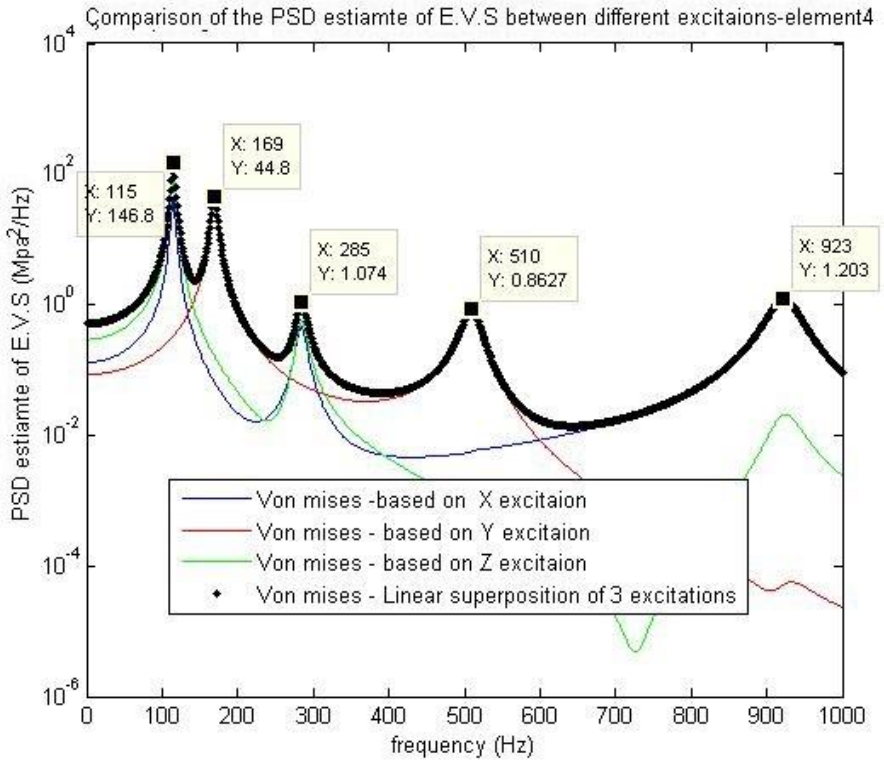

Figure 4.33 *Comparison of the PSD estimate of E.V.S under uniaxial excitations with multiaxial excitation for hot spot 112781.*

Table 4.20 Comparison of the results for four excitations-Hot spot 4, 112781.

Hot Spot (4) - 112781 - Volume Element(CTETRA) in XZ plane					
X Ex.	Y Ex.	Z Ex.	Mult.	Calculated Quantities	
21.53	15.35	30.82	37.81	RMS of M.P.S - Formula	RMS value of M.P.S and E.V.S (MPa)
21.61	15.31	30.70	37.70	RMS of M.P.S – Ansa	
21.74	25.01	31.04	45.40	RMS of E.V.S	
180	40	180		Based on RMS value-Ansa	$\theta\ of\ M.P.S$ (Degree)
175	43	175	175	Based on RMS value of transformation formula	
175	43	173	175	1st Mode	$\theta\ of\ M.P.S$ At different modes (Degree)
175	43	171	42	2nd Mode	
24	39	25	25	3rd Mode	
175	29	0	29	4th Mode	

4.4 Statistical Analysis Results

In both swept sinusoidal and random analysis the aim is to find in which uniaxial excitation we have the safety quotient closest to one. Or in other words which uniaxial excitation has the most similar damage impact as the real excitations during the component service life.

For the swept sinusoidal excitations this quotient has been calculated for maximum von Mises stress responses in different multiaxial combinations. In the random excitation it has been calculated for the RMS value of the Equivalent von Mises PSD estimation for the multiaxial excitation with uncorrelated components.

4.4.1 Statistical Assessment of the Swept Sinusoidal Analysis Results

In swept sinusoidal results for each hot spot, maximum stress response in each of the three orthogonal uniaxial excitations has been compared to the largest maximum stress response between four different multiaxial excitations with different phase combinations between directions. Then the frequency of the maximum stress response was considered to identify the component's natural mode that contributes the most to the maximum stress response value. It is observed that in different components, for the hot spots with high stress response, the maximum stress response appears in certain combinations of the multiaxial loads[2]. The maximum stress response under the uniaxial excitation also occurs in certain directions and more over the quotient between these two values at the corresponding frequency remains the same for all mentioned hot spots despite that the stress response values change from one hot spot to another.

Beside the hot spots this method has been applied to few other randomly chosen elements of each component. It has been observed that different pairs of uniaxial and multiaxial max-response combinations will appear but the quotient for each of such pairs will remain the same. This means if for

[2] Multiaxial Sinusoidal loads with different phase difference combination, $C = (C_{xy}, C_{xz}, C_{yz})$ is described more in Chapter 3.3.2 .

one hotspot in a component maximum uniaxial stresses occur in the X direction and the multiaxial load with $C = (+1, +1, -1)$ has the largest maximum stress response with the quotient $K = 1.5$, in all other elements of the component with the same pair of uniaxial direction and multiaxial combination that result in maximum stress response, the quotient will be the same (K=1.5) .

Table 4.21 Summary of Sinusoidal analysis results.

component	Uniaxial Max-response direction	Multiaxial Phase –difference combination	Frequency (Hz) mode	Safety margin Quotient
1	Vertical (Z)	(1 , 1 , -1)	115 (Hz) 1st mode	1.64
2	Vertical (Z)	(1 , 1 , -1)	97 (Hz) 1st mode	1.82
3	Lateral (Y)	(1 , -1, 1)	35 (Hz) 1st mode	1.4
4	Lateral (Y)	(1 , -1 , 1)	31 (Hz) 1st mode	1.5

4.4.2 Statistical Assessment of the Random Analysis Results

In Random analysis a uniaxial random load with Gaussian distribution has been applied in three orthogonal directions and RMS value of the Equivalent von Mises stress PSD has been calculated for each uniaxial load. This value has been compared to the RMS value of the Equivalent von Mises PSD of the multiaxial load with uncorrelated components.

This analysis has been done for different components and different hot spots in each component. Summary of the all results has been presented in the tables in the Appendix.

For all components that have been analyzed in this thesis work the interested quotient has remained in the interval$(1.1 \leq K \leq 1.65)$.

It has been observed that in some components such as Component 3 and 4 in all hot spots, the highest stress response level occurs under the excitation in a certain direction. This implies that this particular excitation direction and the sensitivity direction of the component are close to each other. But in some other components such as Component 1 and 2, the highest stress response occurs in different directions for different hotspots under applied uniaxial random loads. The stress response value is different as well so the safety margin quotient will be different in each of these hot spots. This could happen due to the several reasons such as, component does not have sensitive direction or it has the same level of sensitivity in all directions or all selected directions that uniaxial load has been applied in that direction are far from the sensitive direction of the component. In this group it is difficult to introduce a single direction as the direction with highest stress response for the component in general or to calculate the unique quotient K.

4.4.3 Statistical Assessment of the Effect of Correlation in Random Excitation Load

In the case of multiaxial excitation the most challenging is to find effective direction of the uniaxial excitation. This direction is important in fatigue analysis when uniaxial tests are used to simulate the stress response of the multiaxial loads. If such a direction can be determined, testing direction can be adjusted in such a way that the uniaxial excitation will be applied in that direction and the stress response of the component will be the most similar compared to the stress response that is present in multiaxial excitation.

As it is described in Section 3.3.1 if the load is an uncorrelated multiaxial excitation, then this effective uniaxial direction will mostly depend on the sensitive direction of the component. But if the load is a correlated multiaxial excitation then beside the sensitive direction of the component the effective direction of the load will affect the direction with the highest stress response.

Sensitive direction is a property of the component and it is not easy to define a general method to find this direction. However for each correlated random multiaxial load it is possible to find the effective direction. In this

thesis work we proposed a method to find such a direction. This method has been described in Chapter 3.3.

In Chapter 3.3, beside the method of finding the effective direction, it has been described how to calculate the equivalent uniaxial random load from the correlated multiaxial random load.

It can be assumed that applying this uniaxial load in effective direction will yield the stress response that is the closest to the stress response present under the multiaxial load. Thus for the component that has the same sensitivity in all directions, quotient between responses to uniaxial load in this direction and multiaxial load, will be the smallest. However, if the component which has some sensitive direction, further investigation and tests is required to have clearer view about the relation between the effective direction of the load and the sensitive direction of the component and their interaction in terms of stress response. This can be subject to further studies.

4.5 Fixture Assembly Results

As it was mentioned in Chapter 3.4, the same random analysis was performed on an assembly of the bracket and the fixture. By doing this analysis the behavior of the bracket was studied when it is attached to flexible fixtures. In this chapter the results obtained from the fixture assembly analysis have been presented. The calculation procedure is exactly the same as for the bracket. The difference is to perform modal analyses for the fixture, bracket and the assembly. The results are categorized in the following categories:

- Modal Analysis of the Fixture and Assembly

- Calculating the Equivalent von Mises stress and the maximum principal stress

4.5.1 Modal Analysis of the Fixture and the Assembly

The result of modal analysis and the mode shapes for the bracket (Component 1) has already been shown in Chapter 4.1.

The results of the modal analysis of the fixture are presented below.

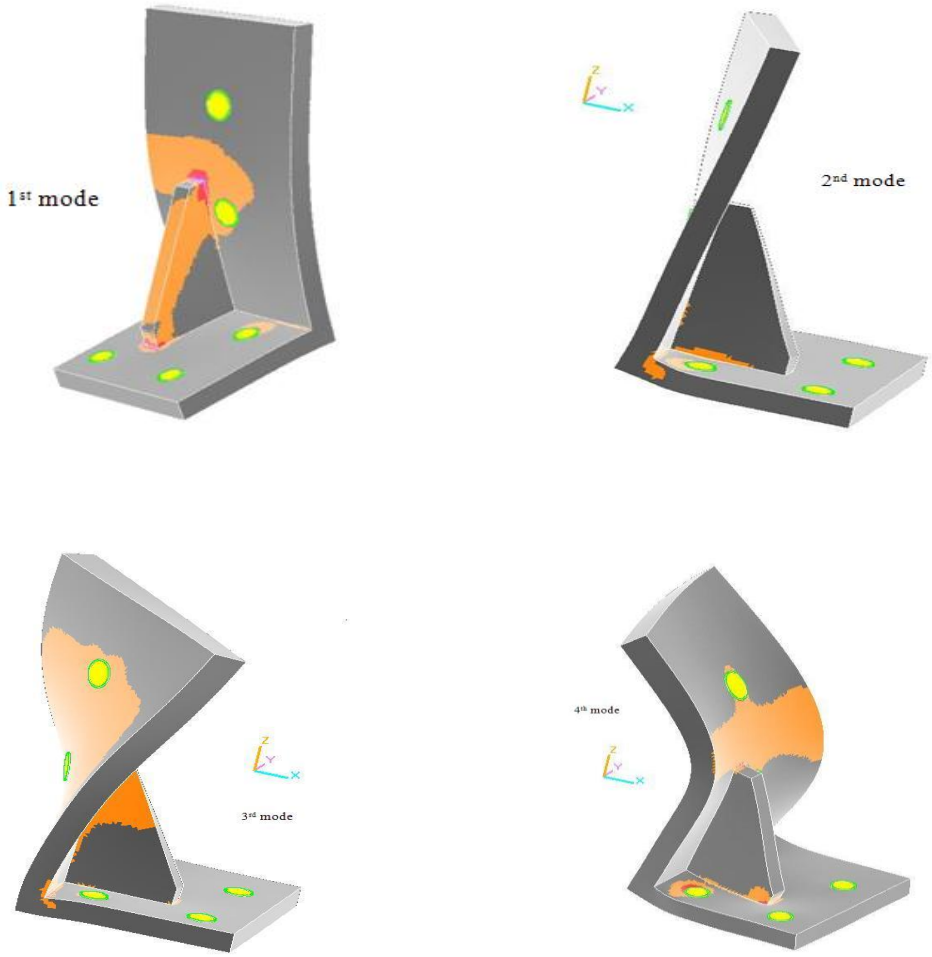

Figure 4.34 *The first 4 modes of the fixture.*

The result of the modal analysis of the Assembly has been presented below.

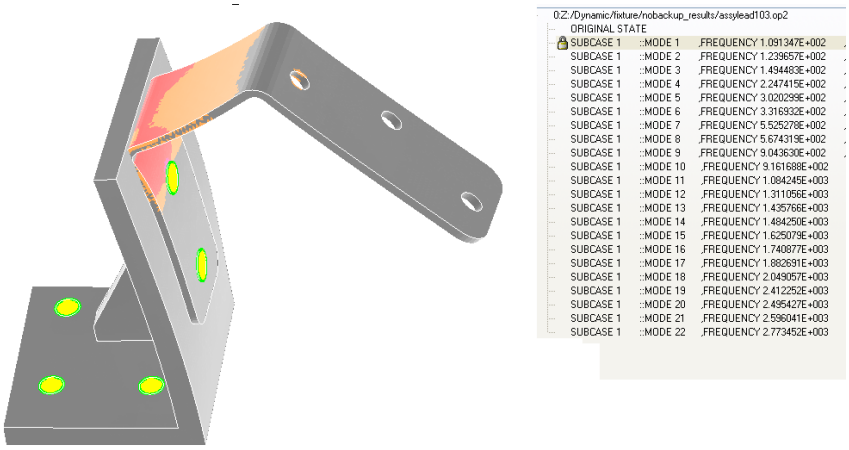

Figure 4.35 *The first mode of the assembly.*

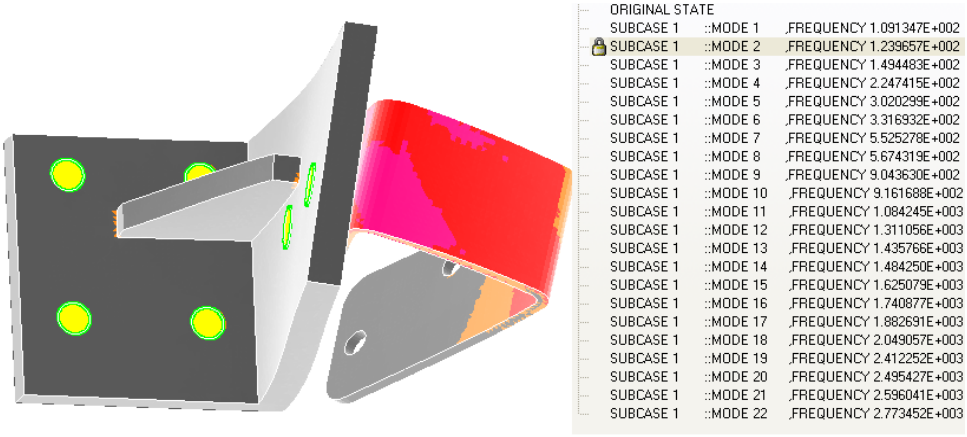

Figure 4.36 *The second mode of the assembly.*

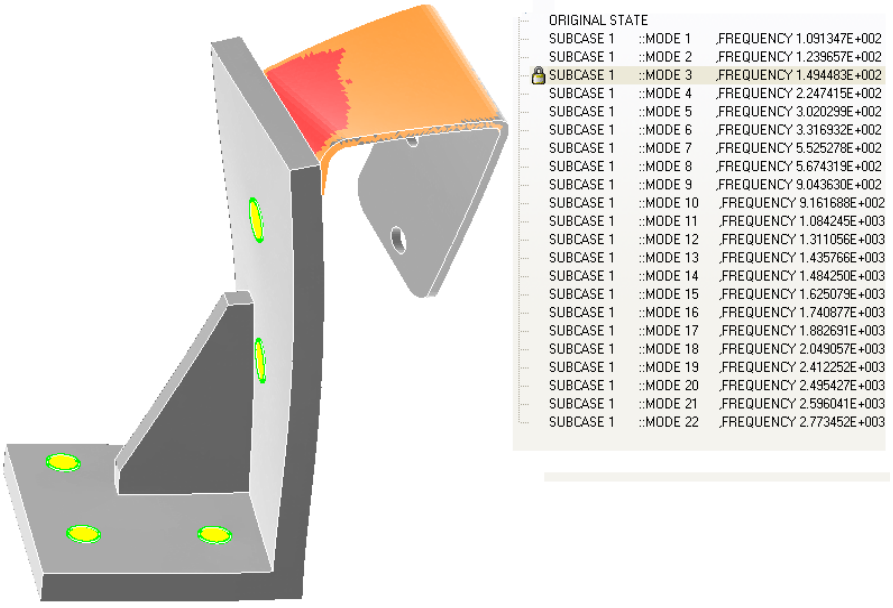

Figure 4.37 *The third mode of the assembly.*

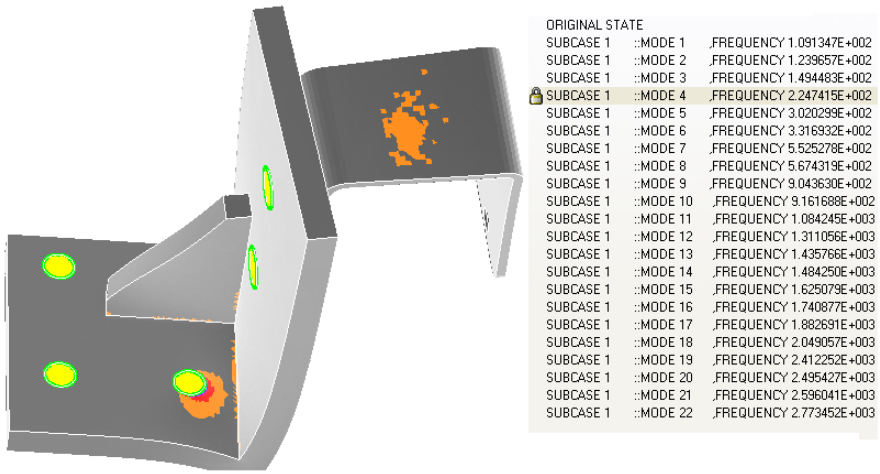

Figure 4.38 *The fourth mode of the assembly.*

The following table shows the natural frequencies of the system:

Table 4.22 Natural Frequencies of the bracket and the fixture.

Structure	**Natural Frequencies (Hz)**					
	1st	2nd	3rd	4th	5th	6th
Bracket	115	169	284	510	924	
Fixture	140	239	313	501	897	
Assembly	109	124	149	225	302	331

As it is apparent from the above figure, the values of natural frequencies of the assembly have been decreased due to the fact that the structural dynamic properties of the fixture and the bracket are affecting each other in the assembly.

4.5.2 Calculating the Equivalent von Mises Stress

In this section the results of the excitation of the base of the fixture in X,Y,Z directions uniaxially and the results of the multiaxial excitation are presented.

- For uniaxial excitation of the bracket under X direction:

The following figure compares the Equivalent von Mises stress [2] with the maximum principal stress obtained for the X direction excitation of the base of the fixture.

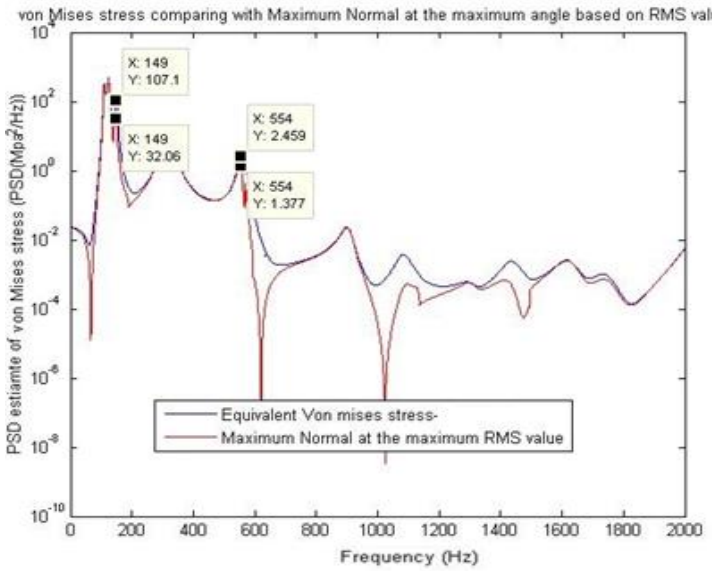

Figure 4.39 *Comparing the Equivalent von Mises stress with the maximum principal stress due to X excitation of the assembly.*

The maximum principal stress shown in the above figure has been plotted at the angle in which the RMS value is maximum. However, as it appears from the above figure, it doesn't follow the Equivalent von Mises stress at some modes which is due to the rotation of the principal stress at those modes of vibration. The same can be observed for Y and Z directions,see Figure 4.40 and Figure 4.41. Thus each uniaxial excitation of the base of the flexible fixture provides the multiaxial stress response on a mounted bracket.

- For uniaxial excitation of the bracket under Y direction:

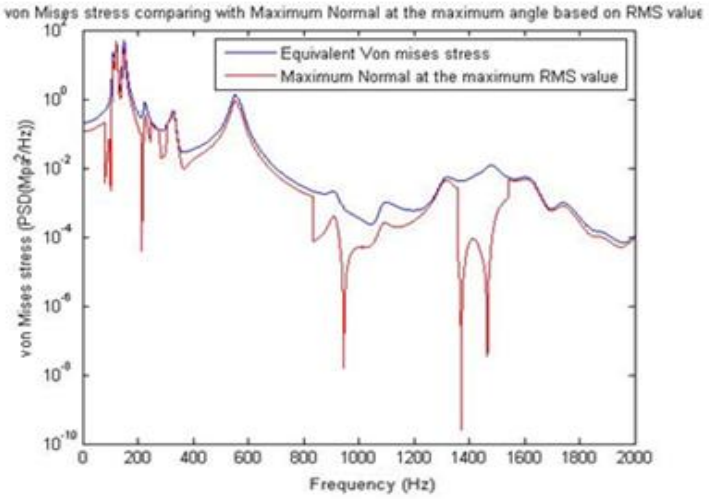

Figure 4.40 *Comparison of the E.V.S with M.PS- Y direction excitation.*

- For uniaxial excitation of the bracket under Z direction:

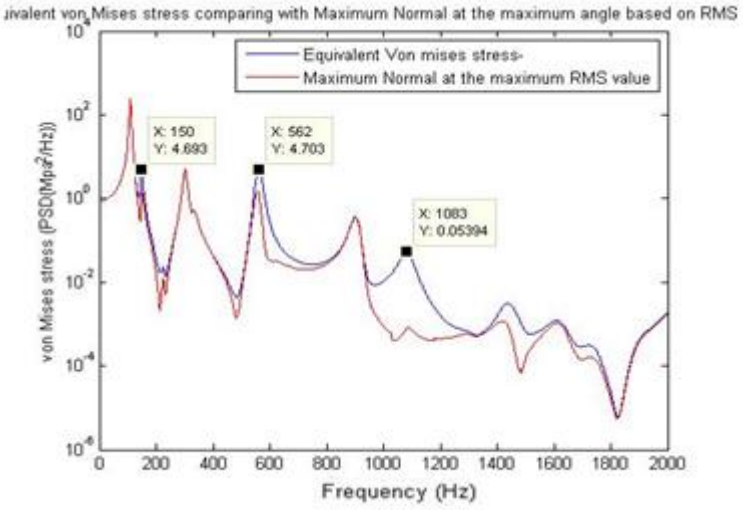

Figure 4.41 *Comparing the E.V.S with M.P.S – Z direction excitation.*

- For multiaxial excitation of the bracket:

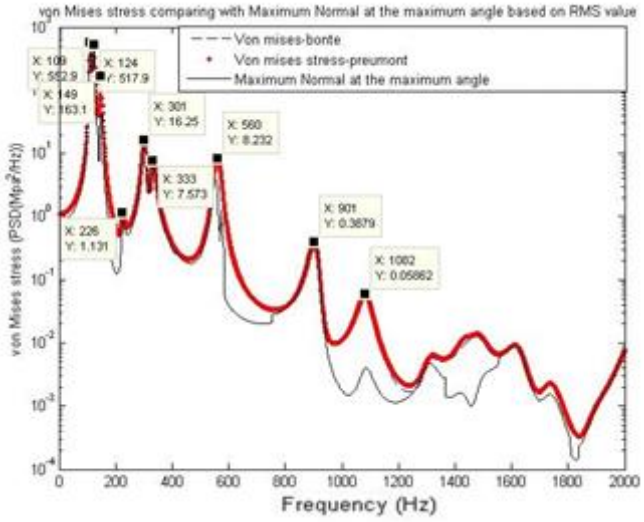

Figure 4.42 *Comparison of the PSD estimate of E.V.S with M.P.S- multiaxial excitation.*

The above figure compares the E.V.S introduced by Preumont [1], with the M.P.S at the angle in which its RMS value is maximum for the case of multiaxial excitation. According to this figure, there is a considerable difference at some modes of vibrations between the Equivalent von Mises stress and the maximum principal stress. Another comparison will be presented in the following figure which compares the E.V.S of all uniaxial excitations with the multiaxial excitation:

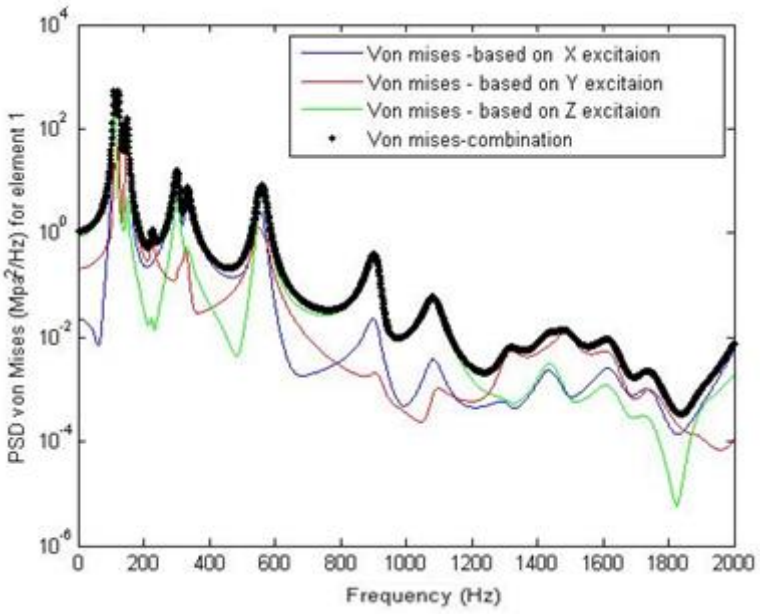

Figure 4.43 *Comparing the E.V.S of all excitations in the assembly.*

As it is apparent from the above figure, the curve that corresponds to the multiaxial excitation covers all responses due to the uniaxial excitations which are identical by analyzing the bracket only.

The following table can be presented as the full result of the analysis on element 106760 on the bracket:

Table 4.23 Results for four excitations applied to the assembly-Element 106760.

Hot Spot (3) - 106760 - Volume Element(CTETRA)- in YZ plane					
X Ex.	Y Ex.	Z Ex.	Mult.	Calculated Quantities	
81,67	28,00	47,46	97,27	RMS of M.P.S - Formula	RMS value of M.P.S and E.V.S (MPa)
90,17	35,33	49,07	108,6	RMS of E.V.S	
98	112	89	96	Based on RMS value of transformation formula	$\theta\ of\ M.P.S$ (Degree)
86	103	86	86	1st Mode	
102	103	86	102	2nd Mode	$\theta\ of\ M.P.S$ At different modes (Degree)
123	123	119	123	3rd Mode	
86	75	85	84	4th Mode	

According to the above table, the maximum RMS value occurs in a plane which is different from those obtained in different modes. This result is different when analyzing only the bracket. The reason might be due to the flexibility of the fixture that causes influence on the bracket. The following tables compare the RMS value of the E.V.S of each excitation of the base of the fixture with that of the bracket only. In this case, the base of the fixture has been firstly excited by four different excitations, X, Y, Z and linear superposition of the uniaxial excitations. Then, the bracket has been

excited by three orthogonal accelerations which have been generated at the interface with the fixture in the first analysis.

Table 4.24 Comparison of the RMS values of E.V.S estimated for the assembly and for the bracket under the X-excitation of the Base.

X Excitation of the base-RMS values of the PSD of E.V.S (MPa) requested output on element 106760			
acce in X dir.	acce in Y dir.	acce in Z dir.	
81,79	6,379	17,5628	Bracket only
90,171			Assembly
1,103	14,136	5,134	Quotient

Table 4.25 Comparison of the RMS values of E.V.S estimated for the assembly and for the bracket under the Y-excitation of the Base.

Y Excitation of the base-RMS values of the PSD of E.V.S (MPa) requested output on element 106760			
acce in X dir.	acce in Y dir.	acce in Z dir.	
23,103	22,883	5,007	Bracket only
35,332			Assembly
1,529	1,544	7,056	Quotient

Table 4.26 Comparison of the RMS values of E.V.S estimated for the assembly and for the bracket under the Z-excitation of the Base.

Z Excitation of the base-RMS values of the PSD of E.V.S (MPa) requested output on element 106760			
acce in X dir.	acce in Y dir.	acce in Z dir.	
24,892	3,707	7,193	Bracket only
49,067			Assembly
1,971	13,236	6,8216	Quotient

Table 4.27 Comparison of the RMS values of E.V.S estimated for the assembly and for the bracket under multiaxial excitation of the Base.

Multiaxial Excitation of base-RMS value of PSD of E.V.S(MPa) requested output on element 106760			
acce in X dir.	acce in Y dir.	acce in Z dir.	
84,399	26,5838	39,4266	Bracket only
108,567			Assembly
1,2869	4,084	2,7536308	Quotient

In the above tables, the 'Assembly' row shows the RMS value of the E.V.S on the specified element when the bracket is excited multiaxially from the base. Since we always have multiaxial loading in the interface of the fixture and the bracket we have only one RMS value for the assembly obtained from this multiaxial excitation. The values in 'Bracket only' show the RMS value of the E.V.S when only the bracket is excited by generated accelerations in either X, Y or Z directions. Then the ratio between two analyses has been shown in the last row of the table. In order to deal with different correlated inputs it is required to use Eq. (3.12) to consider the correlation which hasn't been performed in this report.

As it is apparent from all the tables, the least quotient belongs to the X direction excitation. In other words, stress response of a certain hot spot on the surface of the bracket when it excited through the base of the fixture is very close to the stress response of the same hot spot when it is excited by the generated acceleration in X direction. In fact it shows that the bracket has become more sensitive to X direction. This result of assembly analysis is different from the result of exciting the bracket in Chapter 3 when the bracket was subjected to three independent accelerations. The following table presents the RMS value of the E.V.S of a hot spot on a bracket when it is excited by four independent excitations as it was done in Chapter 3.

Table 4.28 RMS value of the E.V.S of the bracket for different excitations.

Bracket only (MPa)			
x	y	z	xyz
36,9828	29,1388	48,6406	67,6953
1,830453616	2,323201367	1,391744756	: quotient

The above table represents the result of the exciting the bracket with four different excitations. As it was mentioned earlier the inputs for all excitations have the value of g=9810 mm/s^2 and they are uncorrelated. By comparing Table 4.28 and tables 4.24-4.27 the following conclusion can be made:

- When the fixture is rigid enough and there is no influence of the vibrating of the fixture on the bracket, the component is very sensitive to the Z direction excitation and stronger towards the X excitation.

- The bracket is more sensitive to the X direction excitation due to effect of the fixture. Comparing the RMS values of the E.V.S given in the tables above shows that the power in the X direction has been amplified more than twice, which indicates that the bracket is more sensitive to excitation in the X direction while it is more flexible in the Z direction.

5 CONCLUSIONS

In this work safety margins between uniaxial testing and multiaxial testing has been investigated. As a result safety margins for several components have been obtained for swept sinusoidal and random testing. It can be concluded that the safety margins depend on the excitation direction as well as the location of the hotspot on the component and the structural properties of the component. For the analyzed components the safety margin has been found to be in the interval [1.1-1.8].

It has been seen that in the multiaxial swept sinusoidal excitation cancelation between different directions can occur. Therefore it is possible to get less stress levels compared to any uniaxial excitation. In random testing case this is not possible. Stress levels obtained from multiaxial excitation is always higher than stress levels obtained from any uniaxial excitation.

It has been seen that quantifying the stress in random vibration analysis is problematic. The maximum principle stress has been found inadequate due to rotation of the principal stress directions. As a result the Equivalent von Mises stress suggested by Preumont and Pitoiset [1] has been found as a suitable scalar used to quantify the resulting stress in random vibration analysis.

It was found that for correlated random signals it is possible to obtain an effective direction for the excitation. Then the components of the multiaxial excitation can be projected to the effective direction to form an effective uniaxial excitation. It has been seen that in some cases this effective direction gives very close results to the multiaxial excitation of the correlated random signals. By aligning the uniaxial test direction with the effective direction multiaxial effects can be accounted for.

Finally, the influence of the fixture on the sensitive direction of the component and the safety margin has been considered. It has been found out, that the fixture with a relatively low stiffness affects the

sensitive direction of the component. More investigation should be done concerning the fixture influence on the safety margin.

6 REFERENCES

1. Lalanne C. , Author and Jonathan D. Kemp, Reviewer, *Random Vibration, Vol. 3 of Mechanical Vibration & Shock*
2. Preumont A. and Pitoiset X., (2000), Spectral Methods for Multiaxial Random Fatigue Analysis of Metallic Structures, International Journal of Fatigue , Vol. 22
3. Moon S. et al. ,(2011), Fatigue Life Evaluation of Mechanical Components Using Vibration Fatigue Analysis Technique , Journal of Mechanical Science and Technology, Vol. 25(3)
4. MD Nastran 2011 & MSC Nastran 2011 Dynamic Analysis User's Guide
5. MSC Fatigue 2011 User's Guide
6. Brandt A. ,2011, Noise and Vibration Analysis
7. Guide to load analysis for Automotive Applications, FCC Report 347- 091210-332, Pär Johannsesson, Sara Loren, Michael speckert, Nikolaus Ruf, Thomas Svensson, Igor Rychlic, Jacques De Mare
8. MD Nastran 2010 Quick Reference Guide
9. Calculation of Linear System Response to Ergodic Random Excitation, MSC Software Corporation
10. Mechanics of Materials, Ferdinand P. Beer, E. Russell Johnston, Jr. John T. Dewolf
11. An Efficient Method for Calculating RMS von Mises Stress in a Random Vibration Environment, SANDIA REPORT
12. LMS TecWare User Manual Volume 3, "Mathematical Background System", Version 2.9.

13. Bonte M.H.A et al. ,(2004) , Prediction of Mechanical Fatigue Caused by Multiple Random Excitations , Proceedings of ISMA 2004

14. Bonte M.H.A et al. ,(2007) , Determining the Von Mises Stress Power Spectral Density for Frequency Domain Fatigue Analysis Including Out-of-phase Stress Components, Journal of Sound and Vibration, Vol. 302

15. Da Y. et al. ,(2011), High-cycle Fatigue Life Prediction for Pb-free BGA Under Random Vibration Loading, Microelectronics Reliability, Vol. 51

16. Preumont A. et al., Tools for A Multiaxial Fatigue Analysis of Structures Submitted to Random Vibrations

17. Segalman D.J. et al.,(1998), An Efficient Method for Calculating RMS von Mises Stress in a Random Vibration Environment, Sandia National Laboratories Report

18. Halfpenny A., A Frequency Domain Approach for Fatigue Life Estimation from Finite Element Analysis, International Conference on Damage Assessment of Structures (DAMAS 99), Dublin

19. Kurt Pötter, Farhad Yousefi and Harold Zenner, Experiences with lifetime Prediction under multiaxial random loading.

7 APPENDICES

Appendix A
Swept Sine Results

Component 1

Element No:111978	**Max. Peak Amplitude**		**XYZ/X**	**X'YZ/X**	**Y'XZ/X**	**Z'XY/X**
Located at yz-plane	MPa	Freq [Hz]	1.63	2.57	1.62	2.57
X-direction	9.34	115	XYZ/Y	X'YZ/Y	Y'XZ/Y	Z'XY/Y
Y-direction	**15.17**	**169**	1.0	1.58	1.0	1.58
Z-direction	14.64	115	XYZ/Z	X'YZ/Z	Y'XZ/Z	Z'XY/Z
XYZ-in-phase	15.22	169	1.04	1.64	1.04	1.64
X-out of phase, YZ-in-phase (X'YZ)	23.99	115	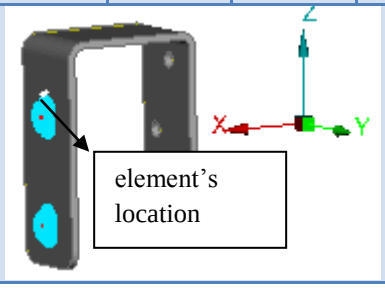			
Y-out of phase, XZ-in-phase (Y'XZ)	15.15	169				
Z-out of phase, XY-in-phase (Z'XY)	**24.02**	**115**				

Element No:108300 Located at yz-plane	Max. Peak Amplitude		XYZ/X	X'YZ/X	Y'XZ/X	Z'XY/X
	MPa	Freq [Hz]	1.04	2.57	1.04	2.57
X-direction	9.97	115	XYZ/Y	X'YZ/Y	Y'XZ/Y	Z'XY/Y
Y-direction	5.23	169	1.97	4.9	1.98	4.9
Z-direction	**15.68**	**115**	XYZ/Z	X'YZ/Z	Y'XZ/Z	Z'XY/Z
XYZ-in-phase	10.32	284	0.66	1.63	0.66	1.64
X-out of phase, YZ-in-phase (X'YZ)	25.63	115	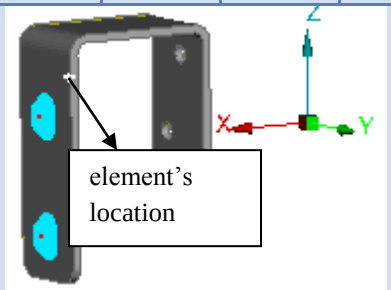			
Y-out of phase, XZ-in-phase (Y'XZ)	10.35	284				
Z-out of phase, XY-in-phase (Z'XY)	**25.66**	**115**				

Element No:113780 Located at yz-plane	Max. Peak Amplitude		XYZ/X	X'YZ/X	Y'XZ/X	Z'XY/X
	MPa	Freq [Hz]	2.08	1.89	2.09	1.87
X-direction	3.27	284	XYZ/Y	X'YZ/Y	Y'XZ/Y	Z'XY/Y
Y-direction	0.42	169	16.19	14.74	16.26	14.76
Z-direction	**3.8**	**115**	XYZ/Z	X'YZ/Z	Y'XZ/Z	Z'XY/Z
XYZ-in-phase	6.8	284	1.79	1.63	1.80	1.63
X-out of phase, YZ-in-phase (X'YZ)	6.19	115	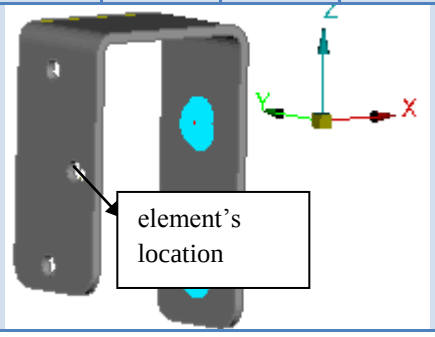			
Y-out of phase, XZ-in-phase (Y'XZ)	**6.83**	**284**				
Z-out of phase, XY-in-phase (Z'XY)	6.2	115				

Element No:109986 Located at yz-plane	Max. Peak Amplitude		XYZ/X	X'YZ/X	Y'XZ/X	Z'XY/X
	MPa	Freq [Hz]	1.80	2.57	1.80	2.58
X-direction	8.66	115	XYZ/Y	X'YZ/Y	Y'XZ/Y	Z'XY/Y
Y-direction	**15.59**	169	1.0	1.43	1.0	1.43
Z-direction	13.59	115	XYZ/Z	X'YZ/Z	Y'XZ/Z	Z'XY/Z
XYZ-in-phase	15.64	169	1.15	1.64	1.14	1.64
X-out of phase, YZ-in-phase (X'YZ)	22.28	115	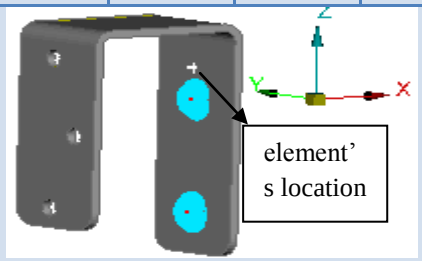			
Y-out of phase, XZ-in-phase (Y'XZ)	15.56	169				
Z-out of phase, XY-in-phase (Z'XY)	**22.3**	**115**				

Element No:111710 Located at xy-plane	Max. Peak Amplitude		XYZ/X	X'YZ/X	Y'XZ/X	Z'XY/X
	MPa	Freq [Hz]	1.49	2.58	1.49	2.58
X-direction	8.98	115	XYZ/Y	X'YZ/Y	Y'XZ/Y	Z'XY/Y
Y-direction	13.38	169	1.00	1.58	1.00	1.73
Z-direction	**14.16**	**115**	XYZ/Z	X'YZ/Z	Y'XZ/Z	Z'XY/Z
XYZ-in-phase	13.41	169	0.95	1.64	0.94	1.64
X-out of phase, YZ-in-phase (X'YZ)	23.17	115	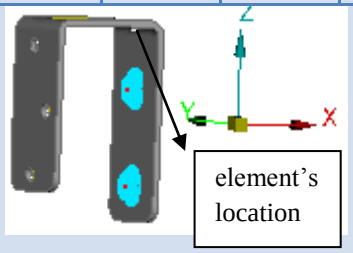			
Y-out of phase, XZ-in-phase (Y'XZ)	13.34	169				
Z-out of phase, XY-in-phase (Z'XY)	**23.19**	**115**				

Element No:105016 Located at yz-plane	Max. Peak Amplitude		XYZ/X	X'YZ/X	Y'XZ/X	Z'XY/X
	MPa	Freq [Hz]	2.09	1.82	2.09	1.82
X-direction	5.56	284	XYZ/Y	X'YZ/Y	Y'XZ/Y	Z'XY/Y
Y-direction	2.66	169	4.36	3.81	4.37	3.81
Z-direction	**6.22**	**115**	XYZ/Z	X'YZ/Z	Y'XZ/Z	Z'XY/Z
XYZ-in-phase	11.6	284	1.86	1.63	1.87	1.63
X-out of phase, YZ-in-phase (X'YZ)	10.13	115	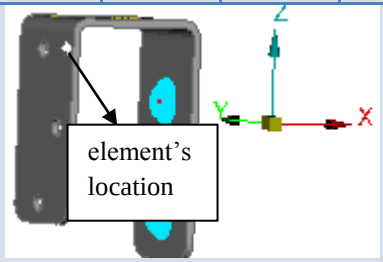			
Y-out of phase, XZ-in-phase (Y'XZ)	**11.62**	**284**				
Z-out of phase, XY-in-phase (Z'XY)	10.14	115				

Element No:111076 Located at yz-plane	Max. Peak Amplitude		XYZ/X	X'YZ/X	Y'XZ/X	Z'XY/X
	MPa	Freq [Hz]	2.08	1.79	2.09	1.79
X-direction	8.16	284	XYZ/Y	X'YZ/Y	Y'XZ/Y	Z'XY/Y
Y-direction	2.01	169	8.46	7.25	8.49	7.26
Z-direction	**8.96**	**115**	XYZ/Z	X'YZ/Z	Y'XZ/Z	Z'XY/Z
XYZ-in-phase	17.0	284	1.90	1.63	1.90	1.63
X-out of phase, YZ-in-phase (X'YZ)	14.58	115	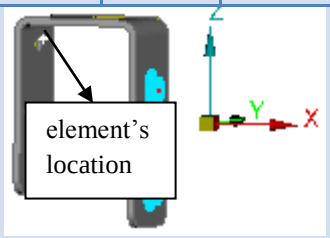			
Y-out of phase, XZ-in-phase (Y'XZ)	**17.06**	**284**				
Z-out of phase, XY-in-phase (Z'XY)	14.59	115				

Element No:104333 Located at yz-plane	Max. Peak Amplitude		XYZ/X	X'YZ/X	Y'XZ/X	Z'XY/X
	MPa	Freq [Hz]	1.14	2.57	1.15	2.57
X-direction	9.03	115	XYZ/Y	X'YZ/Y	Y'XZ/Y	Z'XY/Y
Y-direction	9.42	169	1.1	2.46	1.1	2.47
Z-direction	**14.18**	**115**	XYZ/Z	X'YZ/Z	Y'XZ/Z	Z'XY/Z
XYZ-in-phase	10.32	284	0.73	1.64	0.73	1.64
X-out of phase, YZ-in-phase (X'YZ)	23.21	115	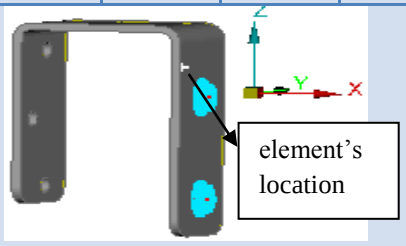			
Y-out of phase, XZ-in-phase (Y'XZ)	10.36	284				
Z-out of phase, XY-in-phase (Z'XY)	**23.23**	**115**				

Component 2

Element No:94980 **Located at xy-plane**	**Max. Peak Amplitude**		**XYZ/X**	**X'YZ/X**	**Y'XZ/X**	**Z'XY/X**
	MPa	Freq [Hz]	0.73	1.92	5.02	6.29
X-direction	9.88	164	XYZ/Y	X'YZ/Y	Y'XZ/Y	Z'XY/Y
Y-direction	21.64	97	0.33	0.87	2.29	2.87
Z-direction	**34.21**	**97**	XYZ/Z	X'YZ/Z	Y'XZ/Z	Z'XY/Z
XYZ-in-phase	7.23	368	0.21	0.55	1.45	1.82
X-out of phase, YZ-in-phase (X'YZ)	18.93	97	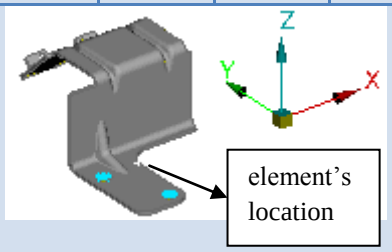			
Y-out of phase, XZ-in-phase (Y'XZ)	49.55	97				
Z-out of phase, XY-in-phase (Z'XY)	**62.16**	**97**				

Element No:257760 **Located at xz-plane**	**Max. Peak Amplitude**		**XYZ/X**	**X'YZ/X**	**Y'XZ/X**	**Z'XY/X**
	MPa	Freq [Hz]	0.68	1.64	1.29	1.62
X-direction	**12.82**	**164**	XYZ/Y	X'YZ/Y	Y'XZ/Y	Z'XY/Y
Y-direction	7.23	97	1.20	2.91	2.28	2.87
Z-direction	11.38	97	XYZ/Z	X'YZ/Z	Y'XZ/Z	Z'XY/Z
XYZ-in-phase	8.68	368	0.76	1.85	1.45	1.83
X-out of phase, YZ-in-phase (X'YZ)	**21.07**	**164**	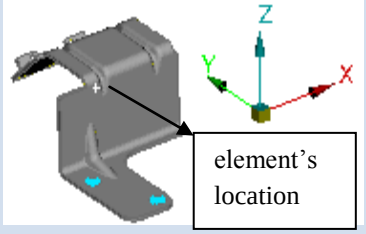			
Y-out of phase, XZ-in-phase (Y'XZ)	16.48	97				
Z-out of phase, XY-in-phase (Z'XY)	20.77	97				

Element No:92202 **Located at xy-plane**	**Max. Peak Amplitude**		**XYZ/X**	**X'YZ/X**	**Y'XZ/X**	**Z'XY/X**
	MPa	Freq [Hz]	0.39	1.65	3.09	3.86
X-direction	18.52	164	XYZ/Y	X'YZ/Y	Y'XZ/Y	Z'XY/Y
Y-direction	24.96	97	0.29	1.22	2.29	2.87
Z-direction	**39.37**	**97**	XYZ/Z	X'YZ/Z	Y'XZ/Z	Z'XY/Z
XYZ-in-phase	7.24	97	0.18	0.77	1.45	1.82
X-out of phase, YZ-in-phase (X'YZ)	30.5	164	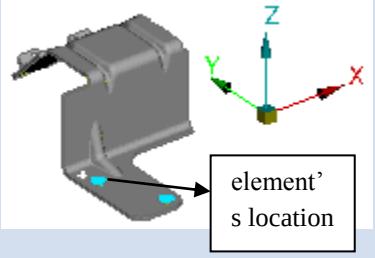			
Y-out of phase, XZ-in-phase (Y'XZ)	57.15	97				
Z-out of phase, XY-in-phase (Z'XY)	**71.53**	**97**				

Element No:351092 **Located at xy-plane**	**Max. Peak Amplitude**		**XYZ/X**	**X'YZ/X**	**Y'XZ/X**	**Z'XY/X**
	MPa	Freq [Hz]	2.06	1.67	1.43	1.79
X-direction	1.6	164	XYZ/Y	X'YZ/Y	Y'XZ/Y	Z'XY/Y
Y-direction	**2.35**	**368**	1.40	1.14	0.97	1.22
Z-direction	1.57	97	XYZ/Z	X'YZ/Z	Y'XZ/Z	Z'XY/Z
XYZ-in-phase	**3.29**	**368**	2.10	1.70	1.45	1.83
X-out of phase, YZ-in-phase (X'YZ)	2.67	368	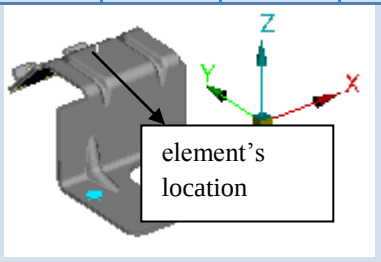			
Y-out of phase, XZ-in-phase (Y'XZ)	2.28	97				
Z-out of phase, XY-in-phase (Z'XY)	2.87	**97**				

Element No:271781 **Located at yz-plane**	**Max. Peak Amplitude**		**XYZ/X**	**X'YZ/X**	**Y'XZ/X**	**Z'XY/X**
	MPa	Freq [Hz]	0.42	1.64	1.08	1.23
X-direction	**23.54**	**164**	XYZ/Y	X'YZ/Y	Y'XZ/Y	Z'XY/Y
Y-direction	10.09	97	0.98	3.84	2.51	2.87
Z-direction	15.86	97	XYZ/Z	X'YZ/Z	Y'XZ/Z	Z'XY/Z
XYZ-in-phase	9.84	368	0.62	2.44	1.60	1.82
X-out of phase, YZ-in-phase (X'YZ)	**38.71**	**164**	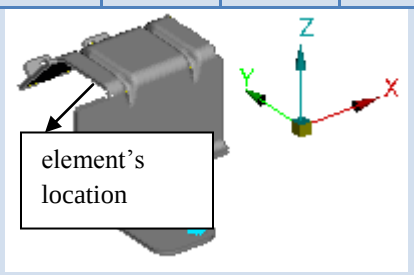			
Y-out of phase, XZ-in-phase (Y'XZ)	25.33	164				
Z-out of phase, XY-in-phase (Z'XY)	28.91	**97**				

Element No:93637 **Located at xy-plane**	**Max. Peak Amplitude**		**XYZ/X**	**X'YZ/X**	**Y'XZ/X**	**Z'XY/X**
	MPa	Freq [Hz]	0.62	1.65	3.29	4.13
X-direction	12.35	164	XYZ/Y	X'YZ/Y	Y'XZ/Y	Z'XY/Y
Y-direction	17.73	97	0.43	1.15	2.29	2.87
Z-direction	**28.06**	**97**	XYZ/Z	X'YZ/Z	Y'XZ/Z	Z'XY/Z
XYZ-in-phase	7.70	368	0.27	0.73	1.45	1.82
X-out of phase, YZ-in-phase (X'YZ)	20.38	164	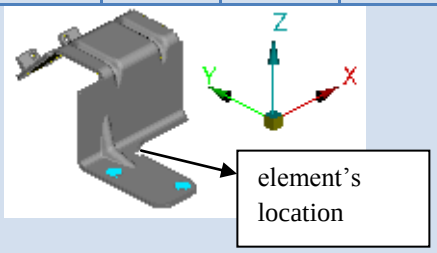			
Y-out of phase, XZ-in-phase (Y'XZ)	**40.6**	**97**				
Z-out of phase, XY-in-phase (Z'XY)						

Element No:189785 **Located at xz-plane**	**Max. Peak Amplitude**		**XYZ/X**	**X'YZ/X**	**Y'XZ/X**	**Z'XY/X**
	MPa	Freq [Hz]	0.35	1.65	1.88	2.36
X-direction	10.31	164	XYZ/Y	X'YZ/Y	Y'XZ/Y	Z'XY/Y
Y-direction	8.45	97	0.43	2.01	2.29	2.88
Z-direction	**13.36**	**97**	XYZ/Z	X'YZ/Z	Y'XZ/Z	Z'XY/Z
XYZ-in-phase	3.65	164	0.27	1.27	1.45	1.82
X-out of phase, YZ-in-phase (X'YZ)	16.97	164	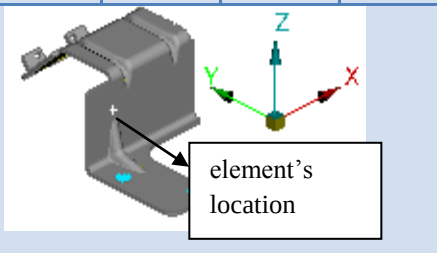			
Y-out of phase, XZ-in-phase (Y'XZ)	**19.34**	**97**				
Z-out of phase, XY-in-phase (Z'XY)						

Component 3

Element No:3296 **Located at xz-plane**	**Max. Peak Amplitude**		**XYZ/X**	**X'YZ/X**	**Y'XZ/X**	**Z'XY/X**
	MPa	Freq [Hz]	1.01	1.00	0.88	1.13
X-direction	**3.1**	**110**	XYZ/Y	X'YZ/Y	Y'XZ/Y	Z'XY/Y
Y-direction	1.8	35	1.73	1.72	1.51	1.94
Z-direction	0.65	237	XYZ/Z	X'YZ/Z	Y'XZ/Z	Z'XY/Z
XYZ-in-phase	3.12	110	4.80	4.75	4.18	5.37
X-out of phase, YZ-in-phase (X'YZ)	3.09	110	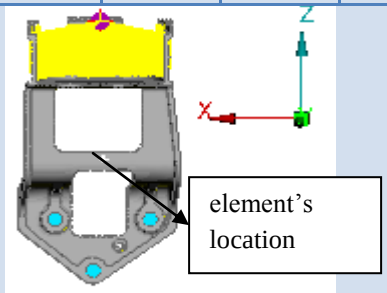			
Y-out of phase, XZ-in-phase (Y'XZ)	2.72	110				
Z-out of phase, XY-in-phase (Z'XY)	**3.49**	**110**				

Element No:17848 Located at xz-plane	Max. Peak Amplitude		XYZ/X	X'YZ/X	Y'XZ/X	Z'XY/X
	MPa	Freq [Hz]	2.51	3.18	5.80	5.13
X-direction	8.55	110	XYZ/Y	X'YZ/Y	Y'XZ/Y	Z'XY/Y
Y-direction	**35.52**	**35**	0.60	0.77	1.40	1.23
Z-direction	11.21	35	XYZ/Z	X'YZ/Z	Y'XZ/Z	Z'XY/Z
XYZ-in-phase	21.43	35	1.91	2.43	4.43	3.91
X-out of phase, YZ-in-phase (X'YZ)	27.21	35	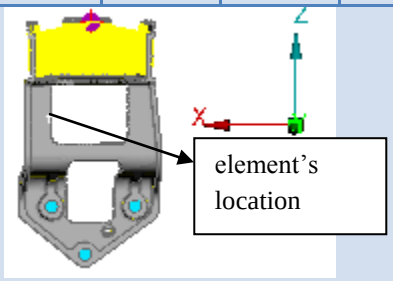			
Y-out of phase, XZ-in-phase (Y'XZ)	**49.61**	**35**				
Z-out of phase, XY-in-phase (Z'XY)	43.84	35				

Element No:18144 Located at xz-plane	Max. Peak Amplitude		XYZ/X	X'YZ/X	Y'XZ/X	Z'XY/X
	MPa	Freq [Hz]	1.84	2.32	4.24	3.76
X-direction	20.17	110	XYZ/Y	X'YZ/Y	Y'XZ/Y	Z'XY/Y
Y-direction	**61.33**	**35**	0.60	0.76	1.40	1.24
Z-direction	19.42	35	XYZ/Z	X'YZ/Z	Y'XZ/Z	Z'XY/Z
XYZ-in-phase	37.09	35	1.91	2.41	4.41	3.91
X-out of phase, YZ-in-phase (X'YZ)	46.78	35	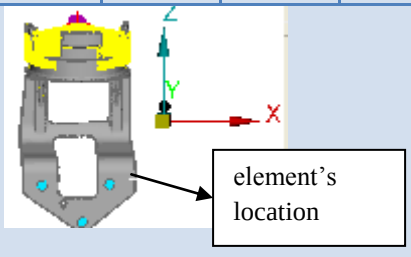			
Y-out of phase, XZ-in-phase (Y'XZ)	**85.58**	**35**				
Z-out of phase, XY-in-phase (Z'XY)	75.93	35				

Element No:22746 **Located at xz-plane**	**Max. Peak Amplitude**		**XYZ/X**	**X'YZ/X**	**Y'XZ/X**	**Z'XY/X**
	MPa	Freq [Hz]	1.39	1.76	3.20	2.84
X-direction	10.44	110	XYZ/Y	X'YZ/Y	Y'XZ/Y	Z'XY/Y
Y-direction	**24**	**35**	0.61	0.76	1.39	1.24
Z-direction	7.57	35	XYZ/Z	X'YZ/Z	Y'XZ/Z	Z'XY/Z
XYZ-in-phase	14.55	35	1.92	2.42	4.42	3.92
X-out of phase, YZ-in-phase (X'YZ)	18.33	35	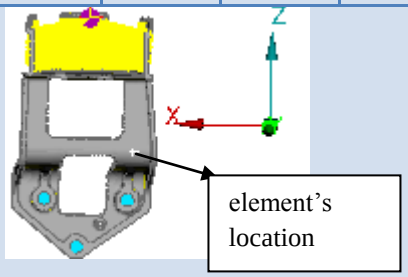			
Y-out of phase, XZ-in-phase (Y'XZ)	**33.46**	**35**				
Z-out of phase, XY-in-phase (Z'XY)	29.66	35				

Element No:35134 **Located at xz-plane**	**Max. Peak Amplitude**		**XYZ/X**	**X'YZ/X**	**Y'XZ/X**	**Z'XY/X**
	MPa	Freq [Hz]	1.43	1.82	3.33	2.94
X-direction	38.43	110	XYZ/Y	X'YZ/Y	Y'XZ/Y	Z'XY/Y
Y-direction	**91.47**	**35**	0.60	0.77	1.40	1.23
Z-direction	28.97	35	XYZ/Z	X'YZ/Z	Y'XZ/Z	Z'XY/Z
XYZ-in-phase	55.08	35	1.90	2.42	4.42	3.90
X-out of phase, YZ-in-phase (X'YZ)	70.04	35	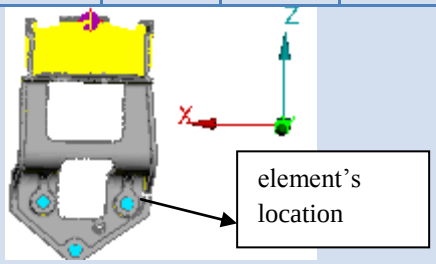			
Y-out of phase, XZ-in-phase (Y'XZ)	**128**	**35**				
Z-out of phase, XY-in-phase (Z'XY)	112.9	35				

Element No:29942 Located at xz-plane	Max. Peak Amplitude		XYZ/X	X'YZ/X	Y'XZ/X	Z'XY/X
	MPa	Freq [Hz]	2.36	3.00	5.47	4.83
X-direction	9.44	110	XYZ/Y	X'YZ/Y	Y'XZ/Y	Z'XY/Y
Y-direction	**36.95**	**35**	0.60	0.77	1.40	1.23
Z-direction	11.66	35	XYZ/Z	X'YZ/Z	Y'XZ/Z	Z'XY/Z
XYZ-in-phase	22.3	35	1.91	2.43	4.43	3.91
X-out of phase, YZ-in-phase (X'YZ)	28.32	35	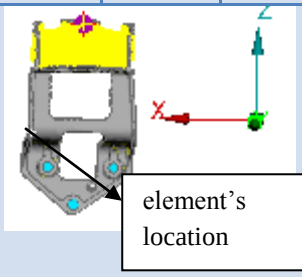			
Y-out of phase, XZ-in-phase (Y'XZ)	**51.61**	**35**				
Z-out of phase, XY-in-phase (Z'XY)	45.6	35				

Element No:34761 Located at xz-plane	Max. Peak Amplitude		XYZ/X	X'YZ/X	Y'XZ/X	Z'XY/X
	MPa	Freq [Hz]	3.50	4.41	8.06	7.14
X-direction	9.74	110	XYZ/Y	X'YZ/Y	Y'XZ/Y	Z'XY/Y
Y-direction	**56.28**	35	0.61	0.76	1.39	1.24
Z-direction	17.75	35	XYZ/Z	X'YZ/Z	Y'XZ/Z	Z'XY/Z
XYZ-in-phase	34.08	35	1.92	2.42	4.42	3.92
X-out of phase, YZ-in-phase (X'YZ)	43	35	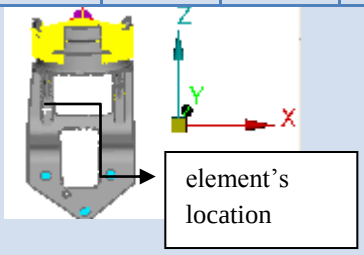			
Y-out of phase, XZ-in-phase (Y'XZ)	**78.5**	**35**				
Z-out of phase, XY-in-phase (Z'XY)	69.55	35				

Element No:46445 Located at yz-plane	Max. Peak Amplitude		XYZ/X	X'YZ/X	Y'XZ/X	Z'XY/X
	MPa	Freq [Hz]	6.70	8.48	15.47	13.70
X-direction	2.5	110	XYZ/Y	X'YZ/Y	Y'XZ/Y	Z'XY/Y
Y-direction	**27.72**	**35**	0.60	0.76	1.40	1.24
Z-direction	8.75	35	XYZ/Z	X'YZ/Z	Y'XZ/Z	Z'XY/Z
XYZ-in-phase	16.76	35	1.92	2.42	4.42	3.91
X-out of phase, YZ-in-phase (X'YZ)	21.19	35	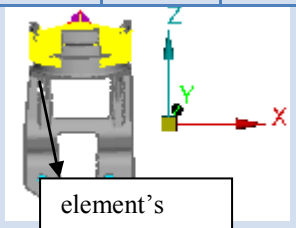			
Y-out of phase, XZ-in-phase (Y'XZ)	**38.68**	**35**				
Z-out of phase, XY-in-phase (Z'XY)	34.25	35				

Element No:55196 Located at xy-plane	Max. Peak Amplitude		XYZ/X	X'YZ/X	Y'XZ/X	Z'XY/X
	MPa	Freq [Hz]	3.71	4.68	8.53	7.56
X-direction	1.43	110	XYZ/Y	X'YZ/Y	Y'XZ/Y	Z'XY/Y
Y-direction	**8.75**	**35**	0.61	0.76	1.39	1.24
Z-direction	2.76	35	XYZ/Z	X'YZ/Z	Y'XZ/Z	Z'XY/Z
XYZ-in-phase	5.3	35	1.92	2.42	4.42	3.92
X-out of phase, YZ-in-phase (X'YZ)	6.69	35	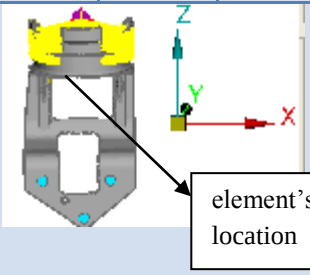			
Y-out of phase, XZ-in-phase (Y'XZ)	**12.2**	**35**				
Z-out of phase, XY-in-phase (Z'XY)	10.81	35				

Component 4

Element No:52883 Located at xz-plane	Max. Peak Amplitude		XYZ/X	X'YZ/X	Y'XZ/X	Z'XY/X
	MPa	Freq [Hz]	2.51	4.13	7.74	6.11
X-direction	9.87	107	XYZ/Y	X'YZ/Y	Y'XZ/Y	Z'XY/Y
Y-direction	**50.54**	**31**	0.49	0.81	1.51	1.19
Z-direction	17.8	31	XYZ/Z	X'YZ/Z	Y'XZ/Z	Z'XY/Z
XYZ-in-phase	24.73	31	1.39	2.29	4.29	3.39
X-out of phase, YZ-in-phase (X'YZ)	40.77	31	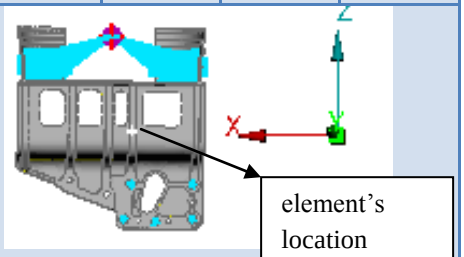			
Y-out of phase, XZ-in-phase (Y'XZ)	**76.37**	**31**				
Z-out of phase, XY-in-phase (Z'XY)	60.3	31				

Element No:71795 Located at xz-plane	Max. Peak Amplitude		XYZ/X	X'YZ/X	Y'XZ/X	Z'XY/X
	MPa	Freq [Hz]	1.41	2.32	4.39	3.48
X-direction	15.25	107	XYZ/Y	X'YZ/Y	Y'XZ/Y	Z'XY/Y
Y-direction	**44.22**	**31**	0.49	0.80	1.51	1.20
Z-direction	15.77	31	XYZ/Z	X'YZ/Z	Y'XZ/Z	Z'XY/Z
XYZ-in-phase	21.55	31	1.37	2.24	4.24	3.37
X-out of phase, YZ-in-phase (X'YZ)	35.38	31	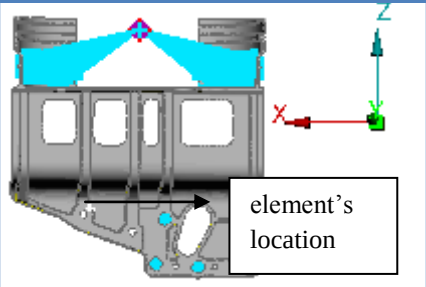			
Y-out of phase, XZ-in-phase (Y'XZ)	**66.91**	**31**				
Z-out of phase, XY-in-phase (Z'XY)	53.1	31				

Element No:17542 Located at xy-plane	Max. Peak Amplitude		XYZ/X	X'YZ/X	Y'XZ/X	Z'XY/X
	MPa	Freq [Hz]	2.19	3.66	6.89	5.42
X-direction	8.07	107	XYZ/Y	X'YZ/Y	Y'XZ/Y	Z'XY/Y
Y-direction	**36.6**	**31**	0.48	0.81	1.52	1.19
Z-direction	13.03	31	XYZ/Z	X'YZ/Z	Y'XZ/Z	Z'XY/Z
XYZ-in-phase	17.64	31	1.35	2.27	4.27	3.35
X-out of phase, YZ-in-phase (X'YZ)	29.55	31	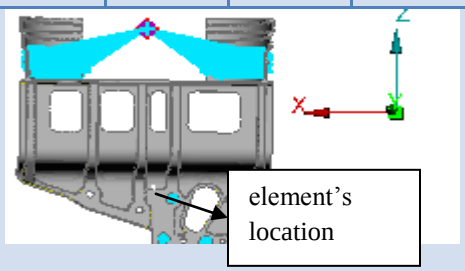			
Y-out of phase, XZ-in-phase (Y'XZ)	**55.58**	**31**				
Z-out of phase, XY-in-phase (Z'XY)	43.7	31				

Element No:98257 Located at yz-plane	Max. Peak Amplitude		XYZ/X	X'YZ/X	Y'XZ/X	Z'XY/X
	MPa	Freq [Hz]	2.94	4.92	9.19	7.21
X-direction	6.57	107	XYZ/Y	X'YZ/Y	Y'XZ/Y	Z'XY/Y
Y-direction	**39.85**	**31**	0.48	0.81	1.52	1.19
Z-direction	14.05	31	XYZ/Z	X'YZ/Z	Y'XZ/Z	Z'XY/Z
XYZ-in-phase	19.3	31	1.37	2.30	4.30	3.37
X-out of phase, YZ-in-phase (X'YZ)	32.31	31	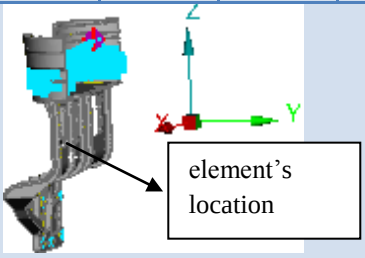			
Y-out of phase, XZ-in-phase (Y'XZ)	**60.39**	**31**				
Z-out of phase, XY-in-phase (Z'XY)	47.39	31				

Element No:148059 Located at xz-plane	Max. Peak Amplitude		XYZ/X	X'YZ/X	Y'XZ/X	Z'XY/X
	MPa	Freq [Hz]	1.17	1.66	3.12	2.43
X-direction	46.71	107	XYZ/Y	X'YZ/Y	Y'XZ/Y	Z'XY/Y
Y-direction	**95.41**	**31**	0.57	0.81	1.53	1.19
Z-direction	34.13	31	XYZ/Z	X'YZ/Z	Y'XZ/Z	Z'XY/Z
XYZ-in-phase	54.7	31	1.60	2.27	4.27	3.32
X-out of phase, YZ-in-phase (X'YZ)	77.41	31	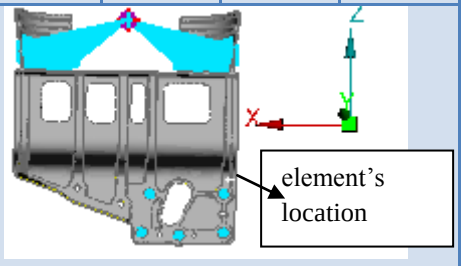			
Y-out of phase, XZ-in-phase (Y'XZ)	**145.7**	**31**				
Z-out of phase, XY-in-phase (Z'XY)	113.4	31				

Element No:125353 Located at xy-plane	Max. Peak Amplitude		XYZ/X	X'YZ/X	Y'XZ/X	Z'XY/X
	MPa	Freq [Hz]	1.47	2.49	4.67	3.65
X-direction	17.79	107	XYZ/Y	X'YZ/Y	Y'XZ/Y	Z'XY/Y
Y-direction	**54.55**	**31**	0.48	0.81	1.52	1.19
Z-direction	19.4	31	XYZ/Z	X'YZ/Z	Y'XZ/Z	Z'XY/Z
XYZ-in-phase	26.07	31	1.34	2.28	4.28	3.34
X-out of phase, YZ-in-phase (X'YZ)	44.25	31	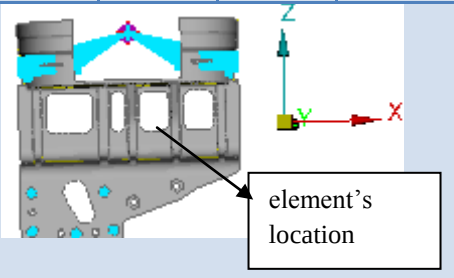			
Y-out of phase, XZ-in-phase (Y'XZ)	**83.05**	**31**				
Z-out of phase, XY-in-phase (Z'XY)	64.85	31				

Element No:4787 **Located at xz-plane**	**Max. Peak Amplitude**		**XYZ/X**	**X'YZ/X**	**Y'XZ/X**	**Z'XY/X**
	MPa	Freq [Hz]	2.97	4.97	9.38	7.38
X-direction	13.44	31	XYZ/Y	X'YZ/Y	Y'XZ/Y	Z'XY/Y
Y-direction	**82.95**	**31**	0.48	0.80	1.52	1.20
Z-direction	29.62	31	XYZ/Z	X'YZ/Z	Y'XZ/Z	Z'XY/Z
XYZ-in-phase	39.93	31	1.35	2.25	4.25	3.35
X-out of phase, YZ-in-phase (X'YZ)	66.77	31	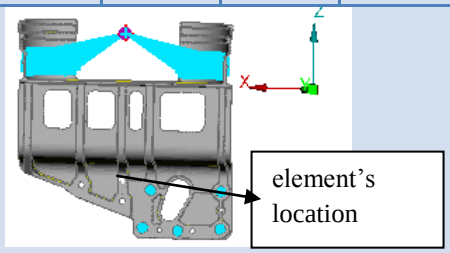			
Y-out of phase, XZ-in-phase (Y'XZ)	**126**	**31**				
Z-out of phase, XY-in-phase (Z'XY)	99.14	31				

Appendix B

Comparison of E.V.S in Different Components.

- Component 1

Component 1		Eq. von Mises RMS(MPa)				Safety Margin Qoutient		
Plane	El.No.	X-dir	Y-dir	Z-dir	Multi-dir	Kx	Ky	Kz
y-z	107534	38,360	28,004	53,781	71,751	1,87	2,56	1,33
y-z	105337	33,856	43,822	47,335	72,852	2,15	1,66	1,54
y-z	111978	50,327	57,855	56,621	95,320	1,89	1,65	1,68
y-z	109986	39,704	59,532	49,794	87,178	2,20	1,46	1,75
y-z	111076	43,967	7,993	49,777	66,894	1,52	8,37	1,34
y-z	113632	20,952	13,840	24,357	34,546	1,65	2,50	1,42
y-z	113651	4,064	0,750	3,423	5,37	1,32	7,15	1,57
y-z	108300	38,495	19,620	53,756	68,85	1,79	3,51	1,28
x-y	108891	28,918	46,833	40,959	68,610	2,37	1,46	1,68
x-y	111710	30,989	49,221	42,959	72,310	2,33	1,47	1,68
x-y	102828	25,034	40,091	33,997	58,226	2,33	1,45	1,71
x-y	106734	32,410	19,273	46,330	59,626	1,84	3,09	1,29
x-y	109413	27,546	25,612	39,430	54,37	1,97	2,12	1,38
x-y	108262	27,546	25,612	39,430	54,37	1,97	2,12	1,38
x-z	113273	9,801	35,470	12,811	38,970	3,98	1,10	3,04
x-z	111695	18,216	8,718	19,540	28,09	1,54	3,22	1,44
x-z	112781	21,739	25,011	31,040	45,395	2,09	1,81	1,46

- Component 2

Component 2		Eq. von Mises RMS(Mpa)				Safety Margin Quotient		
Plane	El.No.	X-Dir	Y-Dir	Z-Dir	multi-Dir	Kx	Ky	Kz
y-z	87178	49,627	48,100	64,000	94,169	1,90	1,96	1,47
y-z	271781	86,355	57,114	51,872	115,800	1,34	2,03	2,23
x-y	351092	7,930	13,622	6,506	17,052	2,15	1,25	2,62
x-y	92202	70,296	77,920	111,511	153,126	2,18	1,97	1,37
x-z	88125	55,440	27,100	27,580	67,590	1,22	2,49	2,45
x-z	257760	47,200	42,800	35,530	72,951	1,55	1,70	2,05
x-z	94980	40,080	67,675	95,864	124,000	3,09	1,83	1,29

- Component 3

Component 3		Eq. von Mises RMS(Mpa)				Safety Margin Quotient		
Plane	El.No.	X-Dir	Y-Dir	Z-Dir	multi-Dir	Kx	Ky	Kz
y-z	25941	102,470	145,540	68,230	190,620	1,86	1,31	2,79
y-z	46445	14,870	47,020	23,540	54,650	3,68	1,16	2,32
x-y	5521	17,370	16,150	12,630	26,870	1,55	1,66	2,13
x-y	55196	8,870	14,700	10,730	20,250	2,28	1,38	1,89
x-z	3296	10,676	3,220	3,090	11,570	1,08	3,59	3,74
x-z	17848	26,270	59,860	30,610	72,180	2,75	1,21	2,36
x-z	22746	31,150	40,190	21,470	55,200	1,77	1,37	2,57
x-z	18144	59,970	102,440	47,540	127,870	2,13	1,25	2,69
x-z	28366	112,510	150,050	87,230	206,840	1,84	1,38	2,37
x-z	29942	28,530	61,900	31,840	75,230	2,64	1,22	2,36
x-z	34761	29,970	94,080	52,150	111,670	3,73	1,19	2,14
x-z	35134	113,870	153,080	87,450	209,880	1,84	1,37	2,40

- Component 4

Component 4		Eq. von Mises RMS(MPa)				Safety Margin Quotient		
Plane	El.No.	X-Dir	Y-Dir	Z-Dir	multi-Dir	Kx	Ky	Kz
y-z	98257	22,480	64,900	39,050	79,010	3,51	1,22	2,02
y-z	33081	35,290	64,660	35,690	81,850	2,32	1,27	2,29
x-y	121014	36,260	77,520	27,470	89,880	2,48	1,16	3,27
x-y	125353	54,100	88,530	32,250	108,660	2,01	1,23	3,37
x-z	12666	46,700	91,330	52,420	115,190	2,47	1,26	2,20
x-z	52883	31,980	82,180	47,590	100,210	3,13	1,22	2,11
x-z	71795	46,120	72,000	36,520	92,970	2,02	1,29	2,55
x-z	17542	26,280	59,560	27,900	70,820	2,69	1,19	2,54
x-z	148059	139,680	156,680	83,460	225,890	1,62	1,44	2,71
x-z	4787	41,220	134,660	69,080	156,860	3,81	1,16	2,27

Appendix C

Static Formula of Transformation of Stress Tensor

According to the solid mechanics, for a certain static load and a given biaxial stress tensor, it is possible to transform the stress state from the current plane into a new plane and evaluate the value of stress state at the new transformed coordinate system. As it is apparent from Mohr Circle [10], the value of Normal X stress is maximum, maximum principal stress, when there is no shear stress. One approach is to determine the maximum principal stress by looking for a plane in which the stress component is maximum which was performed for this analysis. The following transformation formula is used for each uniaxial excitation as well as the multiaxial excitation [10].

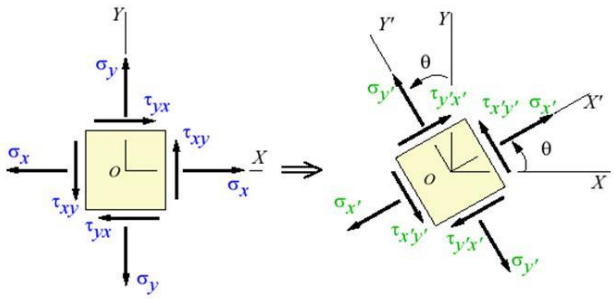

***C.1** Transformation of stresses into new coordinate system.*

$$\sigma_{x'} = \frac{\sigma_x+\sigma_y}{2} + \frac{\sigma_x-\sigma_y}{2}\cos(2\theta) + \tau_{xy}\sin(2\theta) \qquad \text{(C.1)}$$

Where σ_x and σ_y are *normal stresses* in X and Y directions and τ_{xy} is the *shear stress* at the plane of the element. The angle 'θ' is the swept angle for each transformation.

According to the transformation formula, the normal X stress is transformed over 180 degrees, starting from zero when normal X stress is along with X axis in Figure C.1. The normal X stress value is calculated at each angle increment to obtain the maximum value which will be the

maximum principal stress as well as the rotated angle to reach this value. The value of θ is augmented as 1 degree increment for each transformation in Matlab.

The point of consequence in this analysis is that the sign of the FRF for each stress component should be taken into account. Thus, in order to calculate the signed stress by this method, the magnitude of each stress tensor should be multiplied by the sign of its corresponding FRF. The following formula in Matlab represents how to use the sign of the FRF in calculating the normal X stress response:

$$Sign(\sigma_x) = sign(\text{atan}(\frac{S_{xi}}{S_{xr}})) \quad \text{(C.2)}$$

$$Signed\ stress\ = Sign(\sigma_x) \times |\sigma_x| \quad \text{(C.3)}$$

As it was mentioned earlier by using the real-valued signed stress value, the maximum principal can be calculated by using transformation formula. The following figure demonstrates the normal X stress caused by uniaxial X excitation at all 180 degrees rotational angles. The peak value demonstrates the maximum principal stress. The figures have been obtained for element 107534 located on the bracket shown in Table 3.1.

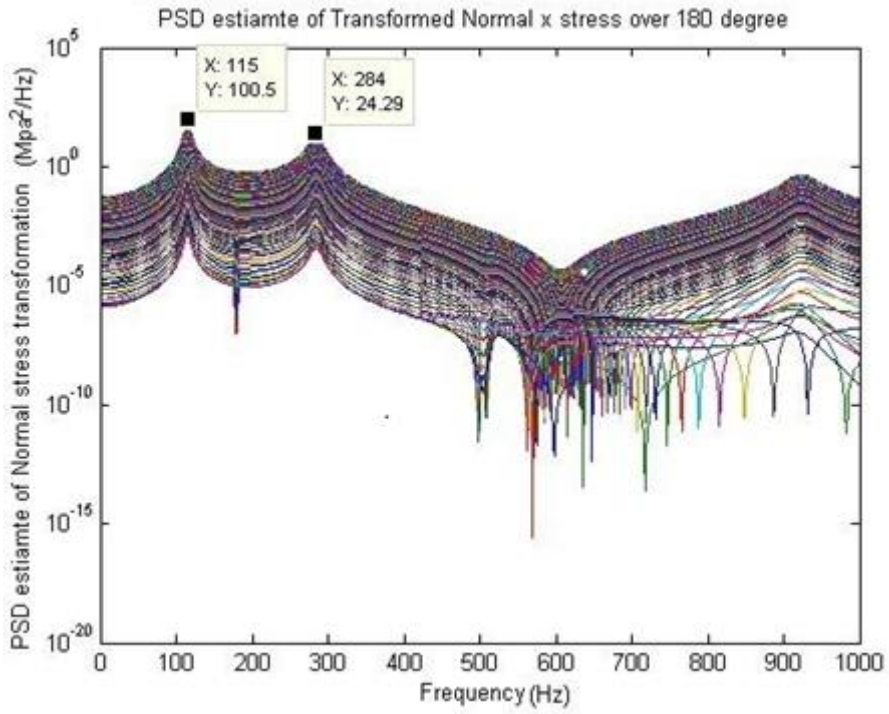

Figure C.2 *Transformed normal X stress at 180 angles for X excitation.*

Such figure can be plotted for each uniaxial as well as the multiaxial excitations to demonstrate the transformed stress at different angles and maximum principal stress for each excitation. However, this figure doesn't give any information about the plane of maximum principal or possibility of its rotation during the excitation. The direction of maximum principal can be observed by the following method:

- Calculating the root mean square of the PSD estimate of normal X stress using Eq.(3.5) at all transformed angles and plotting the RMS value versus its corresponding angle for each excitation [11].

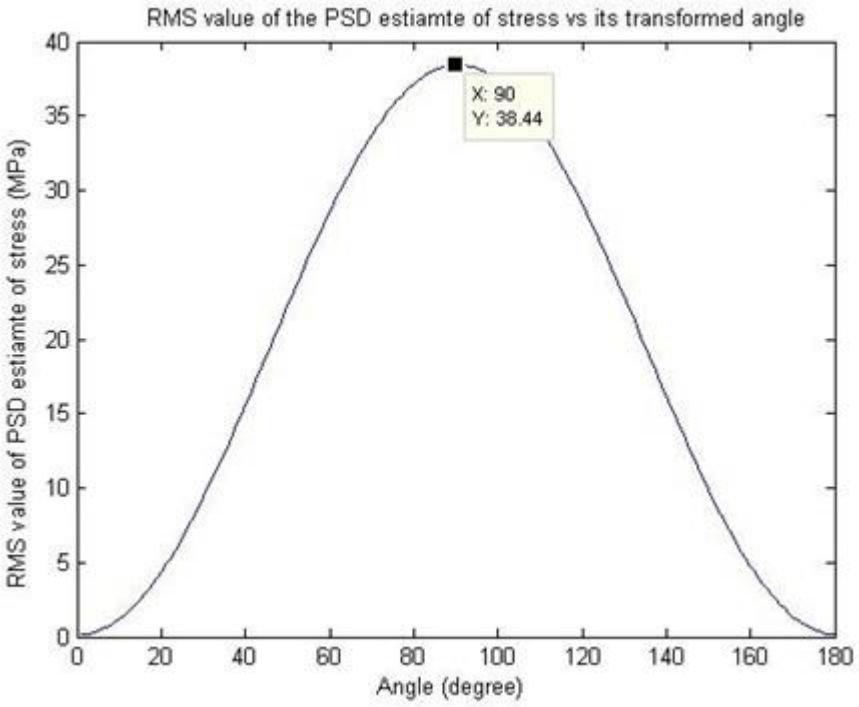

Figure C.3 *RMS value of Normal X at corresponding angle for X excitation.*

The above figure demonstrates the RMS values of the PSD estimates of normal X stress for X excitation versus 180 different angles. This figure simply shows that Normal X stress reaches its maximum value once the angle rotates 90 degrees from zero.

Using the RMS value of the PSD estimate of the normal stress has the advantage of the simplicity and provides a good scalar to compare the RMS value of the principal stress and its direction for different excitations. Therefore, RMS value of the principal stress is an appropriate tool to clarify the possibility of the rotating principal stress at different excitations. However, it doesn't give any information about the rotation of the principal stress at different modes of one certain excitation. In order to obtain this information it is necessary to study the maximum principal stress at different modes.

Now, in order to observe the plane of maximum principal stress at different modes it is required to plot it versus angle. The following figure demonstrates the result when the bracket is excited by X excitation.

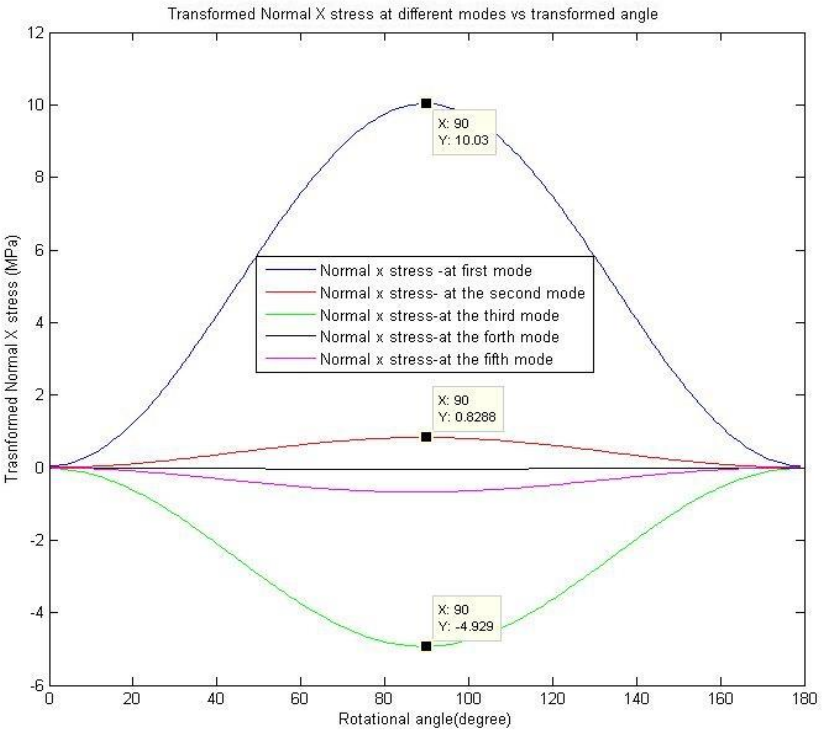

Figure C.4 *Maximum principal stress at different modes for X excitation.*

The same as previous method Figure C.4 shows that for excitation in X direction, the plane of maximum principal stress is located at the angle of 90 degrees which is along with the Z axis. It proves that there are no rotations of principal stress at different modes when the bracket is subjected to only one uniaxial excitation in X direction. However this is not always the case, for Y direction excitation for instance, the maximum principal at each mode takes place at different angle. This is illustrated in the following figure.

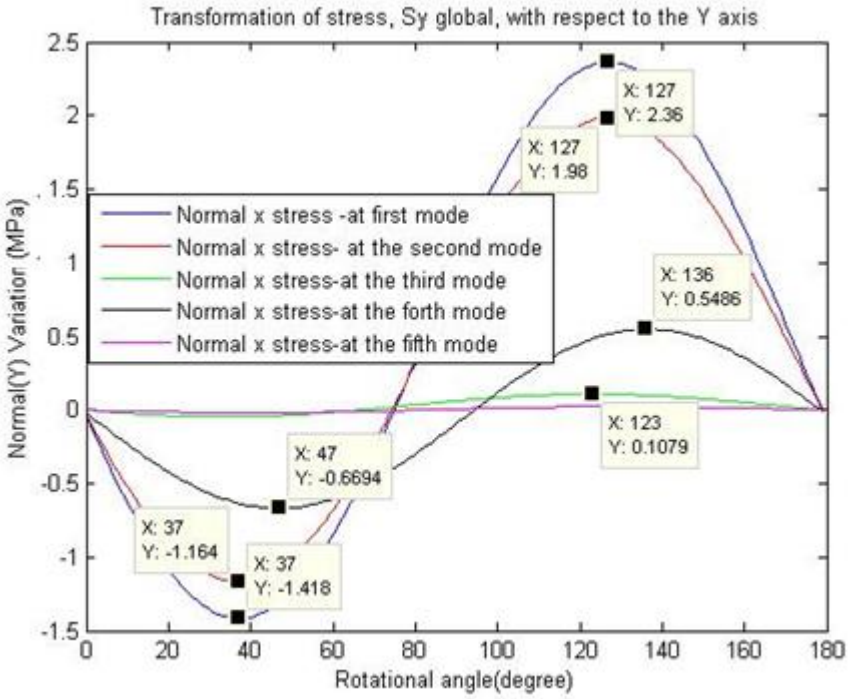

Figure C.5 *Maximum principal stress at different modes for Y excitation.*

As it can be seen from the figure given above the maximum principal stress (Normal X) is present at different angles in different modes.

Transformation of Stress Tensor in Ansa and MD-Nastran

Calculating the principal stress and its direction was deliberately explained in the previous section. In that case, as it was mentioned earlier, the basic static formula was used for transformation. Thus, in order to verify the accuracy of the result for dynamic load, the second type of the analysis was performed to calculate the maximum principal stress and corresponding angle in which the RMS value is maximum. The procedure is the same as the previous section except that transformation is performed in Ansa by changing the local coordinate system for each analysis. In this case, as it is apparent from the following figure, the PSD estimates of stress components

are requested at 18 different local coordinate systems. In fact, the orientation of the planes is varied by 10 degrees increment over 180 degrees range of transformation and the FRA is performed in each coordinate system.

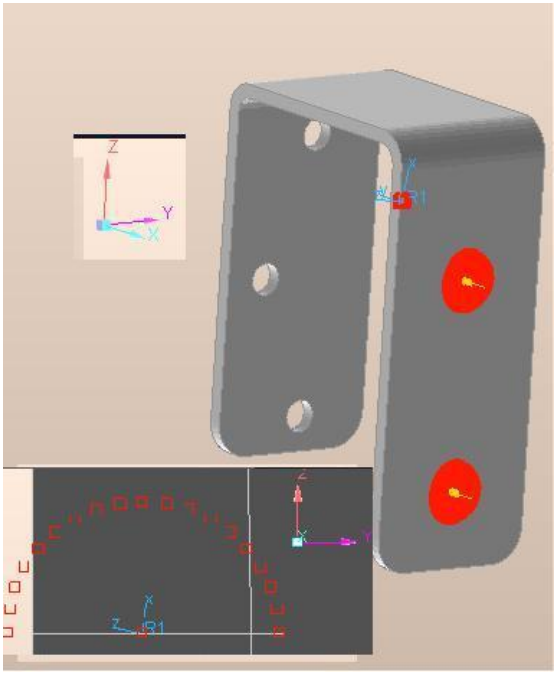

Figure C.6 *Changing the local coordinate system to perform transformation.*

The RMS value of the maximum principal stress will be calculated for each excitation and the result will be compared with those transformations in Matlab. This type of analysis was performed for 8 hot spots and in total of 800 different analyses has been done to verify the previous method. The following figures demonstrate the transformed normal X stress, RMS value of the PSD estimates of the maximum principal stress over 18 (or sometimes 9 orientations in 90 degrees) transformed angles with 10 degrees increment.

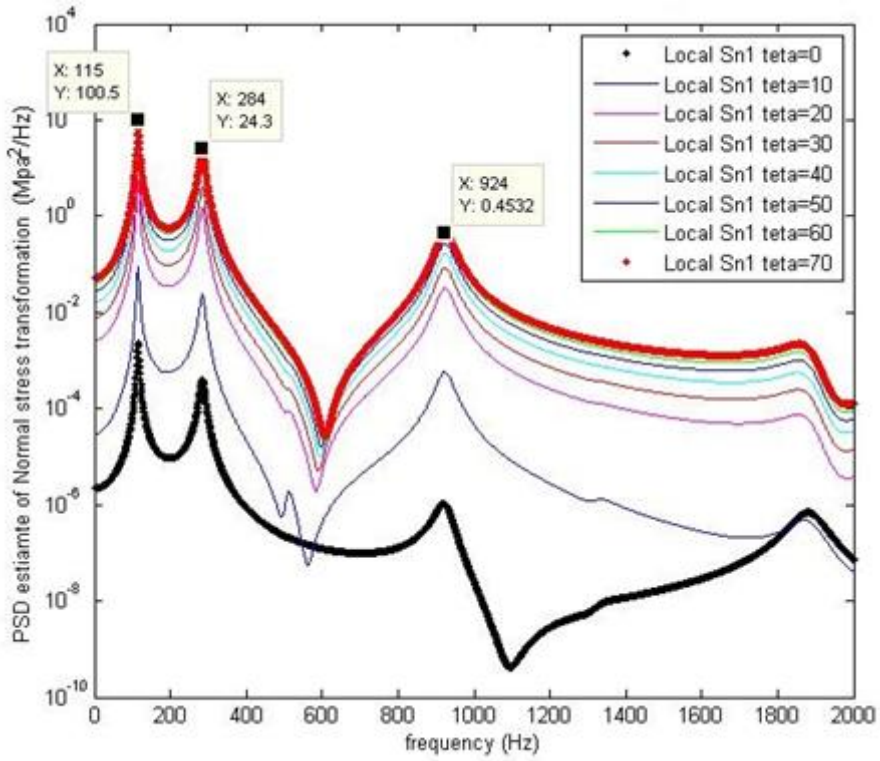

Figure C.7 *Transformed normal X stress for X excitation.*

Each curve in the above figure has been obtained by changing the coordinate system in Ansa and performing analysis in MD-Nastran. It can be observed that, the resonance peak magnitudes in Figure C.7 are very close to the resonance peak magnitudes in Figure C.2. But this figure has been obtained by less transformations and large degree increments. The following figure demonstrates the RMS value of the maximum principal stress versus the angle increments from 1 to 8 and each one shows 10 degrees increment. The RMS value at 20 degrees has been omitted, thus RMS value at 8 means at 90 degrees.

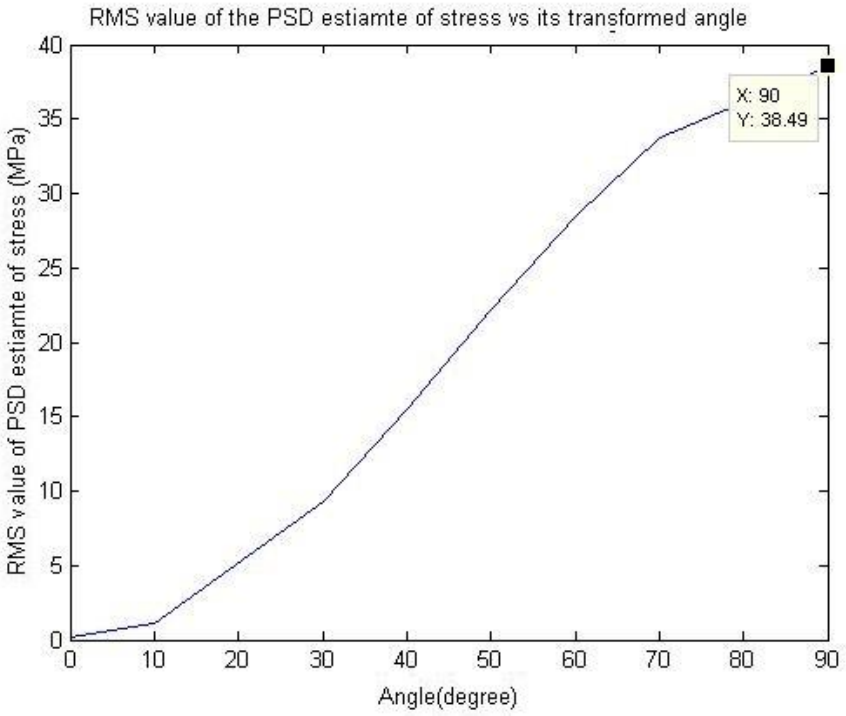

Figure C.8 *RMS value of the Transformed Normal X stress versus angle.*

When the peak value at 90 degrees, 38.49 MPa, is compared with the value presented in Figure C.3, it will be clear that they are very close to each other. It can be said that transforming the stress tensor using the formula given in Eq. (C.1) and transforming the coordinate system using Ansa and MD-Nastran gives the same results.

Eight different elements were studied on the bracket shown in Table 3.1 to check the selected methods and more than 80 analyses have been performed for each excitation in order to prove the accuracy of the selected methods. The two subsections mentioned above explain the methods by studying only one element, 107534, for one uniaxial excitation.

Another way to verify the direction of the maximum principal stress is to use Metapost. To do so, the bracket was meshed by shell elements and the directions of the maximum principal stress were evaluated on it. The

following figure, illustrates the direction of the maximum principal stress at the first mode of vibration when the bracket is excited in X direction.

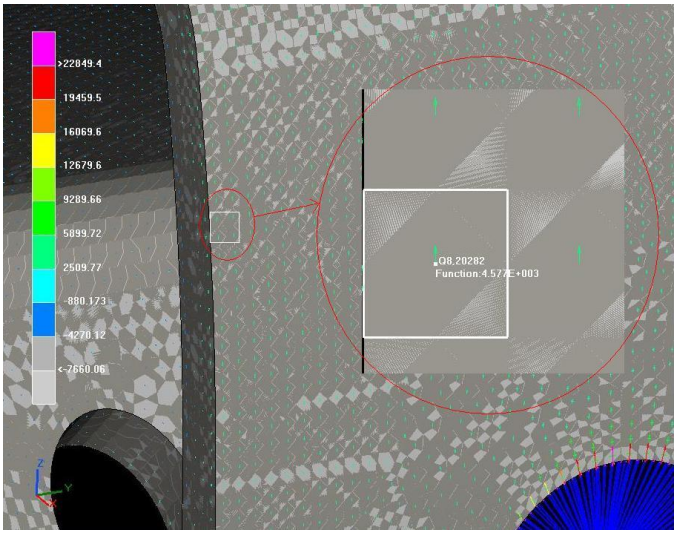

Figure C.9 *Direction of the maximum principal stress at the first mode-element 107534.*

As it is apparent from Figure C.9, the direction of the maximum principal stress is 90 degrees from the horizontal axis. As it is apparent from the global coordinate system on the figure, this means that for this excitation, the direction of the principal stress is along with the Z axis. This figure verifies the result shown in Figure C.8.

The following figure shows the direction of the maximum principal stress at the second mode of vibration when the bracket is excited in Y direction.

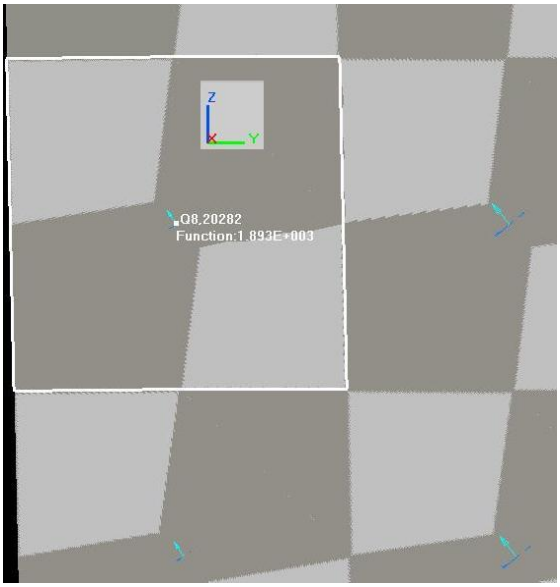

Figure C.10 *Direction of the maximum principal stress at the second mode-element 107534.*

The figure shows that the maximum principal stress occurs at the angle around 130 degrees with respect to horizontal axis which is in compliance with the results shown in Figure C.5. The reason is that the second mode is torsion and the bracket is very sensitive to torsion when it is excited in Y direction. Thus, the M.P.S at the second mode of vibration occurs at 127 degrees when the bracket is excited in Y direction which can be understood by the above figure either.

Appendix D

The Results of the M.P.S of Fixture Analysis under Y and Z excitations

- For excitation of the bracket in Y direction:

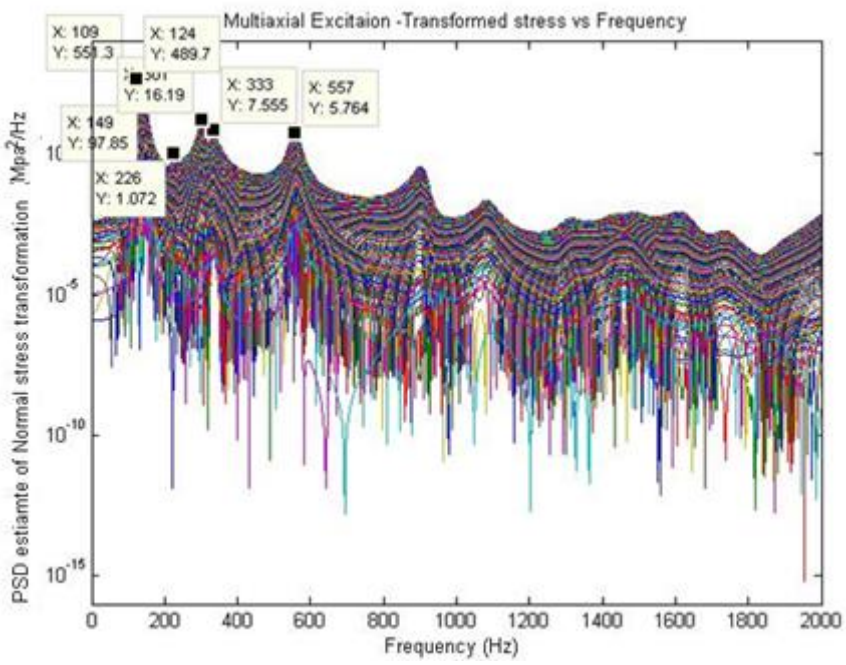

Figure D.1 *Transformed stress by Eq. (C.1)-excitation in Y direction.*

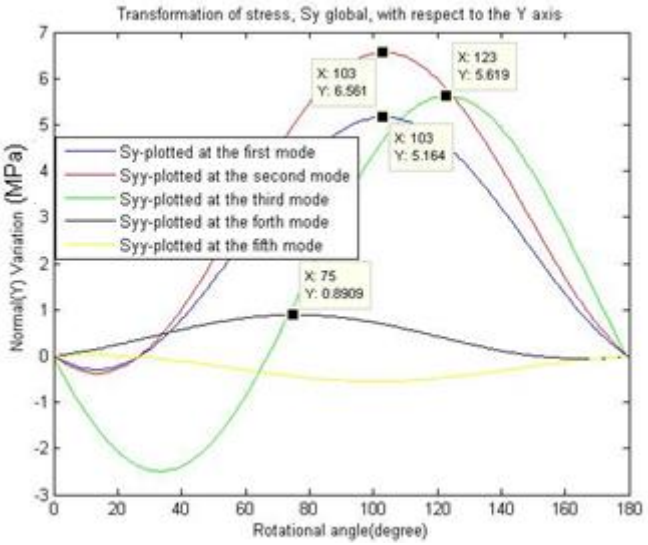

Figure D.2 *Transformed stress at different modes of vibration-excitation in Y direction.*

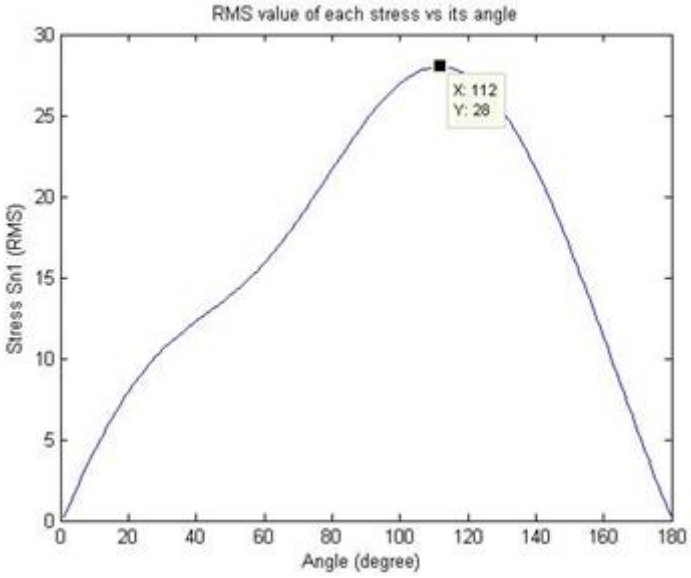

Figure D.3 *The RMS value of the transformed stress- Y excitation.*

- For excitation of the bracket in Z direction:

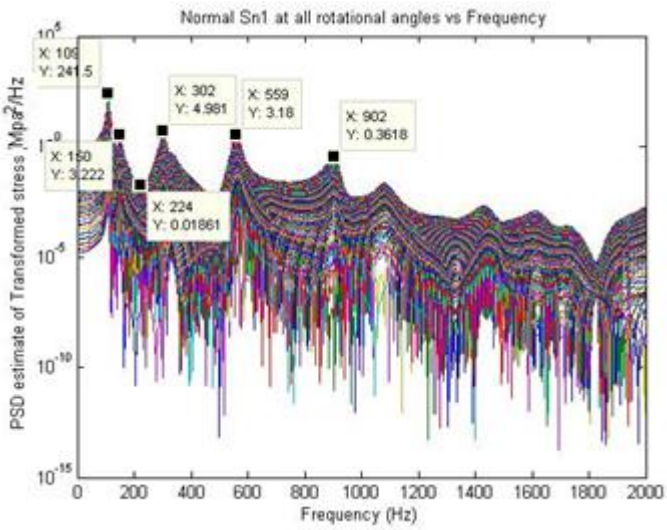

Figure D.4 *Transformed stress by Eq. (C.1) over 180 degrees-excitation in Z direction.*

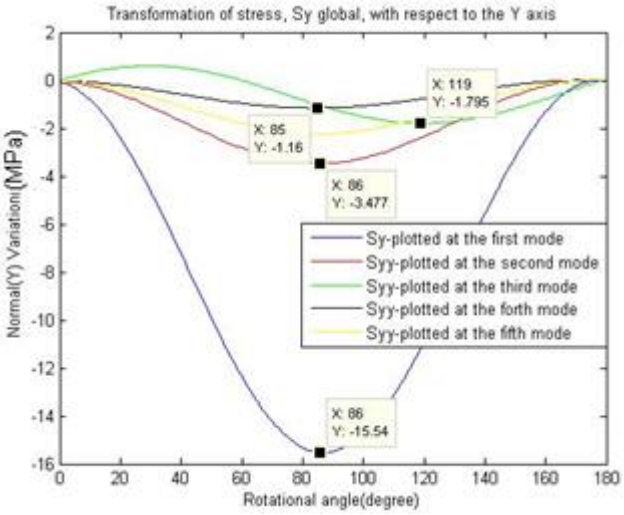

Figure D.5 *Transformed stress at different modes of vibration-excitation in Z direction.*

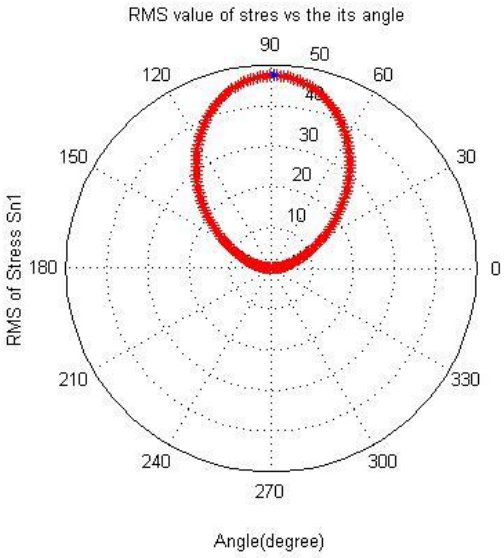

Figure D.6 *The RMS value of the transformed stress- Z excitation.*

- For multiaxial excitation of the bracket:

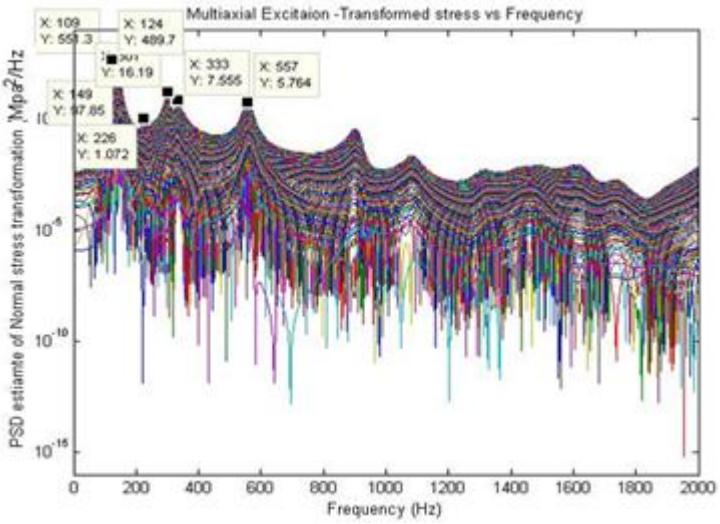

Figure D.7 *Transformed stress by Eq. (C.1)-Multiaxial Excitation.*

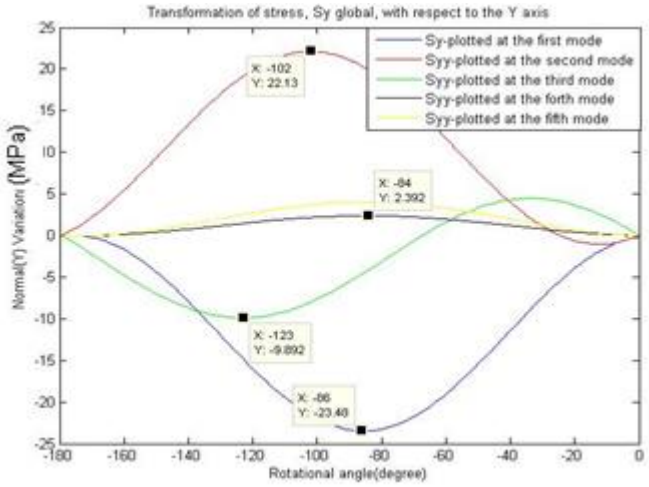

Figure D.8 *Transformed stress at different modes of vibration- multiaxial excitation.*

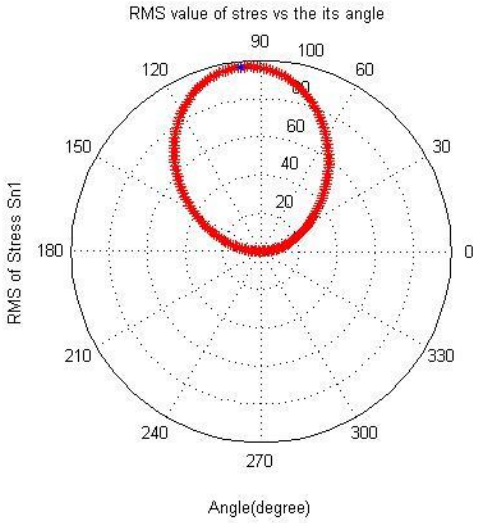

Figure D.9 *The RMS value of the transformed stress- multiaxial excitation.*

Appendix E

Generation of Random Signals

For investigation of the effect of correlated loads in vibration fatigue analysis first step is to produce correct random signals with specific correlation between them. A time domain set of load samples can be easily generated in Matlab and tailored to have a desired power. To introduce the correlation between two or more random signals we can make a linear combination of different uncorrelated random signals and then find out what is the correlation coefficient for each pair of those signals. Another alternative is to generate the signals in such a way that they will have the desired correlation.

- **Generating Correlated Random Signal Using Combination of the Pre-known Random Signals.**

In this method first a random signal with uncorrelated components is generated ,$X = [x_1, x_2, x_3]$ .Then this signal is used to produce the signal Y with correlated components, where each component of signal Y is a linear combination of X .For instance $Y = [y_1, y_2, y_3]$ Such that $y_1 = 2x_1$, $y_2 = x_1 + x_2$ and $y_2 = x_1 + x_3 + {}^{x_2}/_2$.

With this combination signal Y's correlation matrix will be

$$C(Y) = \begin{bmatrix} 1 & 0.50 & 0.41 \\ 0.50 & 1 & 0.52 \\ 0.41 & 0.52 & 1 \end{bmatrix}.$$

This method will be useful when it is known that interested signals are made of certain combinations of the pre-known random signals.

- **Generating Random Signal with Desired Correlation.**

It may be desired to generate a signal with certain correlation given the matrix $C = \begin{bmatrix} 1 & C_{xy} & C_{xz} \\ C_{xy} & 1 & C_{yz} \\ C_{xz} & C_{yz} & 1 \end{bmatrix}$. Here C is a Hermitian, positive-definite matrix. For generating a signal Y with this correlation first one should generate the uncorrelated random signal $X = [x_1, x_2, x_3]$ and then Y will be obtained from the following equation.

$$Y = X \times C'$$

Here C' is the Cholesky decomposition of the matrix C. Resulting signal Y will be a random signal with standard Gaussian distribution meaning that they will have unit power level. For adjusting the power of the signals to a certain power P ($g^2/_{Hz}$) the signal should be multiplied by ($\sqrt{P} \times g$) .

- **Determining the Effective Direction of a Random Signal with Correlated Components.**

In first step 29 different directions (d_i) which are evenly distributed on the upper half of the unit sphere have been determined. These 29 directions have been suggested in LMS manual [12].Then the multiaxial signal with correlated components is constructed and can be described in each time instant as a vector, L=(x_t , y_t , z_t).

In the second step signal vectors L(t) and directions d_i will be compared and signal vectors with direction deviation less or equal to 30 degrees from each direction d_i will be projected on that direction. The magnitudes of these projected vectors will be summed.

Step two will result in 29 values corresponding to 29 directions. These values have been illustrated in Figure 3.14.

In the third step these values will be compared and the maximum value will be determined. The direction corresponding to the maximum value will be selected as the effective direction of the multiaxial random signal.

If all the random vectors of the multiaxial signal are projected on to the effective direction, the resulting random signal can be used as a uniaxial representative of the original multiaxial signal.

School of Engineering, Department of Mechanical Engineering
Blekinge Institute of Technology
SE-371 79 Karlskrona, SWEDEN

Telephone: +46 455-38 50 00
E-mail: info@bth.se